INFORMATION TO USERS

This manuscript has been reproduced from the microfilm master. UMI films the text directly from the original or copy submitted. Thus, some thesis and dissertation copies are in typewriter face, while others may be from any type of computer printer.

The quality of this reproduction is dependent upon the quality of the copy submitted. Broken or indistinct print, colored or poor quality illustrations and photographs, print bleedthrough, substandard margins, and improper alignment can adversely affect reproduction.

In the unlikely event that the author did not send UMI a complete manuscript and there are missing pages, these will be noted. Also, if unauthorized copyright material had to be removed, a note will indicate the deletion.

Oversize materials (e.g., maps, drawings, charts) are reproduced by sectioning the original, beginning at the upper left-hand corner and continuing from left to right in equal sections with small overlaps. Each original is also photographed in one exposure and is included in reduced form at the back of the book.

Photographs included in the original manuscript have been reproduced xerographically in this copy. Higher quality 6" x 9" black and white photographic prints are available for any photographs or illustrations appearing in this copy for an additional charge. Contact UMI directly to order.

UMI®

Bell & Howell Information and Learning
300 North Zeeb Road, Ann Arbor, MI 48106-1346 USA
800-521-0600

A STUDY OF TWO DIMENSIONAL BRAIDED COMPOSITES

Yong Yan

A Thesis

in

Department of Mechanical Engineering

Presented in Partial Fulfillment of the Requirements
for the Degree of Master of Applied Science
at Concordia University
Montreal, Quebec, Canada

December 1998

ABSTRACT

A Study of Two-Dimensional Braided Composites

Yong Yan

A microstructure model of 2-D braided composite is developed. The fiber volume and crimp angle are evaluated by this model and are compared with experimental results. The maximum fiber volume fraction is also obtained. Effective stiffness of 2-D braided composite is obtained in a close form by the analysis of elastic deformation energy in repeat-unit-cell of braided composites. Effective stiffness consists of contributions of axial yarn, braiding yarn, and matrix material. Each of them takes a different weight in the effective stiffness. The weights of contribution of axial yarn, braiding yarn, and matrix material are $\chi V_f/k$, $(1-\chi)V_f/k$, and $(1-V_f/k)$ respectively, where V_f is the fiber volume fraction, χ is the axial yarn content in a braided composite, and k is the filament packing fraction. The results of effective stiffness from theoretical prediction are very good as compared with test data from experiments. Effective coefficients of thermal and hygro expansion are analyzed by virtual energy method. The independent parameters in design and analysis of braided composites are successfully separated from all other parameters. This greatly reduces the difficulties of design and analysis of 2-D braided composites. Objected-oriented Matlab programs are built for the parameter analysis.

ACKNOWLEDGEMENT

The author wishes to express his warmest gratitude to Dr. Suong Van Hoa for his supervision, guidance, encouragement and financial support throughout the course of this study.

The author is indebted to his wife Ziwen for her understanding and support. His 6 years old son Weidi who has been fighting bravely with a strange disease is always a source of inspiration to him.

Finally, the support of the FCAR (Fonds pour la Formation de Chercheur et l'Aide à la Recherche) awarded to the author is gratefully acknowledged.

TABLE OF CONTENTS

LIST OF FIGURES

LIST OF TABLES

NOMENCLATURE

k	Filament packing fraction
m_a	The count number of axial yarns
m_b	The count number of braiding yarns
d_f	The diameter of filament
t_a	Thickness of axial yarn
t_b	Thickness of braiding yarn
A_a	Cross sectional area of axial yarn
A_b	Cross sectional area of braiding yarn
W_a	Width of axial yarn
W_b	Width of braiding yarn
ξ	Thickness to width ratio
ω	Speed ratio of braiding machine
D	Diameter of mandrel
V_f	Fiber volume fraction
χ	Axial yarn content of braided preform
γ	Yarn crimp angle
θ	Braiding angle
L	Yarn space
E_1	Young's modulus along axis 1 (axial direction) of straight yarn

E_2 Young's modulus along axis 2 (transverse direction) of straight yarn

G_{12} Shear modulus according to 1,2 direction of straight yarn

ν_{12} Possion ratio according to 1,2 direction

ν_{23} Possion ratio according to 2,3 direction

E Young's modulus of resin

ν Possion ratio of resin

α Coefficient of thermal expansion of resin

α_1 Coefficient of thermal expansion of yarn along 1 direction

α_2 Coefficient of thermal expansion of yarn along 2 direction

β Coefficient of hygro expansion of resin

β_1 Coefficient of hygro expansion of yarn along 1 direction

β_2 Coefficient of hygro expansion of yarn along 2 direction

$[\overline{C}]$ Effective stiffness matrix of braided composite

$[\overline{\alpha}]$ Effective coefficients of thermal expansion of braided composite.

$[\overline{\beta}]$ Effective coefficients of hydric expansion of braided composite.

Chapter 1 Introduction

Braiding is a simple and versatile textile process in which two or more systems of yarns are intertwined in the bias direction to form an integrated structure(which is called braided fabric preform). Braided composite is manufactured by applying resin to the braided fabric preform.

Braided composites promise to have low cost manufacturing and improved damage resistance as compared to traditional laminated composites. Tension and compression stiffness and tension strength of braided composite are comparable to that of laminated composites. Improved resistance to delamination and damage containment appear to far outweigh the compression strength degradation. Because of the thickness reinforcement and uneven surfaces of preform, the braided composites appear to have better through-the-thickness and interlaminar(for 2-D braided composites) strength than laminated composites. Through-the-thickness tension is an important parameter in design of structures subjected to out of plane loads, structural joints, attachments, etc.

Perhaps the most important feature of the braiding process is the possibility of fabricating a wide range of complex shapes ranging from solid rods to I-beam and thick-wall rocket nozzles. Making these shapes integrally, eliminates the need for cutting fibers to form joints, splices or overlaps with the associated local strength loss. Direct formation of integral shapes also offers the possibility of greatly simplifying the composite's manufacturing process.

Other methods of reinforcing composite, such as filament winding, also provide near net shapes. However, only braided fabric preform fully interconnects the

fibrous array to provide both through-thickness properties and stand alone structure that is stable without a matrix [1, 2].

Braiding can form shapes either by over-braiding mandrels on conventional machine (2-D) or by using new braiding processes to form solid shapes directly(3-D).

Two dimensional braided laminate of a certain desired thickness is formed by over-braiding layers of the desired architecture on top of each other. This leads to a two dimensional material as there are no interlayer yarns through the laminate thickness.

Three dimensional braided fabrics have been produced on traditional horn-gear machines for ropes and packings in solid with circular, or square cross-sections. Now. a number of new machines without the traditional horn gears have been developed to create complex shapes. The new braiding processes included: two-step[3]. AYPEX[4], interlock twiner[5], four-steps[6], multistep[7,8].

Composite materials reinforced with braided fabric preforms are being considered for potential structural applications in the aircraft and automotive industries. Braided fabric preforms can be built by automated and efficient manufacturing techniques. The architecture of a braided fabric preform is complex. The main controlling parameters for the strength of braided composites properties are (1) Braiding parameters, such as yarn sizes, yarn spacing, braiding angles. (2) Material parameters, such as yarn and resin stiffness and strength properties and overall fiber volume fraction. (3) Impregnation parameters, such as the process by which the resin is applied, curing temperature and pressure.

Although three dimensional braiding processes have many advantages, they also have many shortcomings as compared to two-dimensional braiding processes. To braid even a very thin prefrom, the number of yarn carriers is large for three dimensional braiding machine. The thicker the braided preform, the larger is the three dimensional machine. Additionally, the impregnation of three dimensional braided preform is difficult, especially for thick preform.

Because braided composites are new, very little material data has been reported in literature. It is necessary to do many experimental and theoretical research works on them.

The purpose of this research is to study the struture and properties of two-dimensional braided composite. This includes microstructure model, effective stiffness. effective coefficients of hygrothermal expansion, parameter analysis.

For the analysis of effective stiffness and effective coefficients of hygrothermal expansion of 2-D braided composite, Naik, R. A. [17] first discretized each yarn in the repeat unit cell (RUC) into yarn slices and then transformed yarn slice stresses to the global RUC coordinates, finally computed the volume average of stresses in all the yarn slices. Hamada, H. et al. [9], developed a numerical analysis method by using finite element analysis.

In this research an energy approach was used to analyze the effective stiffness and effective coefficients of hygrothermal expansion of 2-D braided composite.

Chapter 2 Braiding processes

The dimensions of the braided structures are used as the criteria for categorizing braiding. A braided structure having two braiding yarn systems with or without a third laid-in yarn is considered as two-dimensional braiding. A braided structure involving three or more systems of braiding yarns to form an integrally braided structure is three dimensional braiding process.

2.1 Two dimensional braiding process

Fig 2.1 shows the conventional vertical braiding mechanism, the spindle movement performs the intertwining of the yarn, and the braiding structure is formed. The braiding mechanism consists of a taking-up mechanism and spindle movement. Spindles move along the circle, so that the spindle movement is restricted to a one-directional movement. The fabric is taken up in the vertical direction. The taking-up of the braided fabric is also a one-directional movement. Shapes, such as tubular braid and flat braid , can be fabricated by combination of these two one-directional movements.

When longitudinal reinforcement is required, a third yarn can be inserted between the braiding yarns to produce a triaxial braid with $0/\pm 6$ fiber orientation. If there is a need for structures having more then three yarn thickness , several layers of fabric can be braided over each other to produce the required thickness.

Figure 2.2 illustrates a 144-horizontal braider that is capable of biaxial or triaxial braiding.

The versatility of braiding for forming complex structural shape is illustrated in Figure 2.3 which shows a fiber glass preform for a composite coupling shaft.

2.2 Three dimensional braiding process

The recently developed three-dimensional braiding techniques have greatly improved the design of preforms for advanced composites. Different three different dimensional processes have be built, such as horn-gear braiding process, two step braiding process, four step braiding process, multi-step process.

2.2.1 Horn-gear braiding process

Fig 2.4 shows an example of the manufacturing of an integrated braid (I-beam) by a horn-gear braiding machine. When the spindles move in two dimensions according to the shape of the cross section, the integrated braid can be fabricated. However, the configuration of the track is so complex that it is difficult to decide an initial spindle setting pattern. The spindle which is caught by a horn-dog moves along the track according to the rotation of a horn-gear, is shown in Figure 2.5. At the crossing point of two tracks , the spindle is transferred from the right horn-gear to the left horn-gear. If an inadequate initial spindle setting pattern is adopted, collision of the spindles occurs at the crossing point of the track as shown in the right-hand case and then braiding cannot proceed. Even if collision of the spindles does not occur, there is a possibility to fabricate an irregular braiding structure under specific initial

setting patterns. Consequently, the braiding structure depends on the initial spindle setting pattern on the track.

Some initial carrier setting patterns have been developed by Hamada et al [9] .

2.2.2 Two step braiding process

The two step braiding proceed is so termed because it involves two distinct motions of each yarn carrier. The braid consists of an array of longitudinal (axial) yarns arranged in a prescribed configuration such as rectangular , circular, box . etc.. and braiding yarns positioned at selected locations on the perimeter of the axial array. The shape of the axial yarn configuration determines the final shape of the preform. The braiding yarns, which move along alternating diagonals of the axial array. inter-link the axial yarns and hold them in the desired shape. Fig 2.6 shows a rectangular arrangement of axial yarns and the locations and paths of the braiding yarns.

Research has been carried out with regards to the two-step braided preform structure and its relation to the braiding process[10, 11]. These studies have effectively characterized the preform structure and identified the key processing parameters.

2.2.3 Four-step braiding process

The four step braiding process involves four distinct Cartesian motions of groups of yarns termed rows and columns. For a given step, alternate rows(or columns) are shifted a prescribed distance relative to each other. The next step involves the alternate shifting of the columns (or rows) a prescribed distance. the

third and fourth steps involve simply the reverse shifting sequence of the first and second steps , respectively. A complete set of four steps is called a machine cycle as shown in Fig. 2.7. It should be noted that after one machine cycle the rows and columns have returned to their original positions. The braid pattern shown is of the 1 $\times$ 1 variety, so termed because the relation between the shifting distance of rows and columns is one to one. Other braid patterns (i. e., 1 $\times$ 3, 1 $\times$ 5,ect.) are possible but they require different machine bed configurations and a specialized machine. Row and column braiding yarn carriers of the type depicted in Figure 2.7 may be used to fabricate preforms of rectangular cross sections such as T-beam, I-beam, and box beam.

The relationship between the processing parameters which are inherent in the four step process and the resulting geometric structure has been independently studied by Pastore et al.[11] and Camponeschi et al.[12] . The unit cell approach to the analysis of 3-D braids was pioneered by Yang et al.[13].

2.2.4 Multi-step braiding process

Recently, a unification of three-dimensional braiding has been suggested[7,8]. This novel braiding scheme, termed multi-step braiding, is an extension to the aforementioned four-step braiding. By allowing for both individual control of a given row/column and the insertion of axial yarns, the range of attainable braid architectures is greatly broadened. It is this general Cartesian braiding which lends itself to the design of the microstructure of three-dimensional braids.

As an example of a multi-braiding scheme, consider the arrangement depicted in the Fig. 2.8. Here, the columns are ultimately moved two units but are moved one unit per step. This leads to a total of eight steps in the multi-step process. This simple variation of the four-step braiding process gives birth to the architecture shown in Fig 2.9. This unique geometry and corresponding grouping of yarns [7] allow for a distinction between inner and outer yarns. Keep in mind that the yarns represented in Fig. 2.9 are idealized as straight lined. Knowledge of such a relation will open the door to tailored design of preform size, fiber volume fraction and micro-structure.

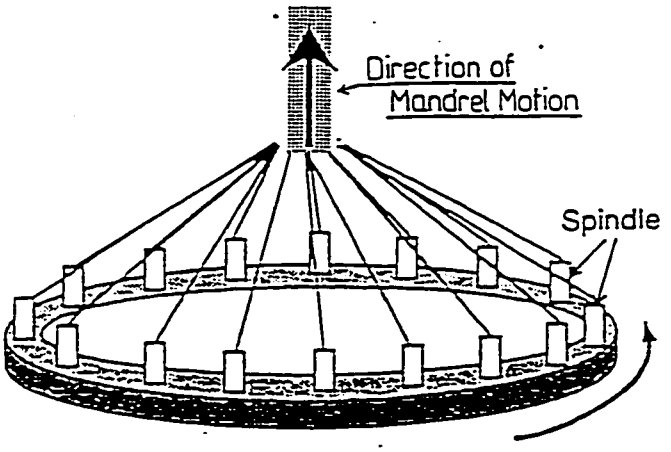

Fig 2.1 Conventional braiding mechanism [9]

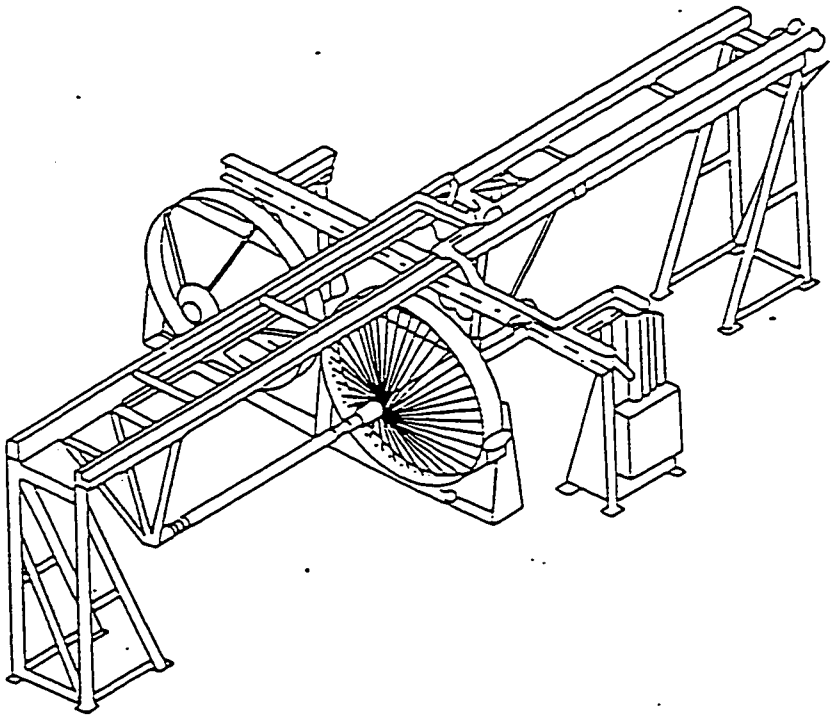

Fig 2.2 Braiding machine (144-carrier horizontal model)

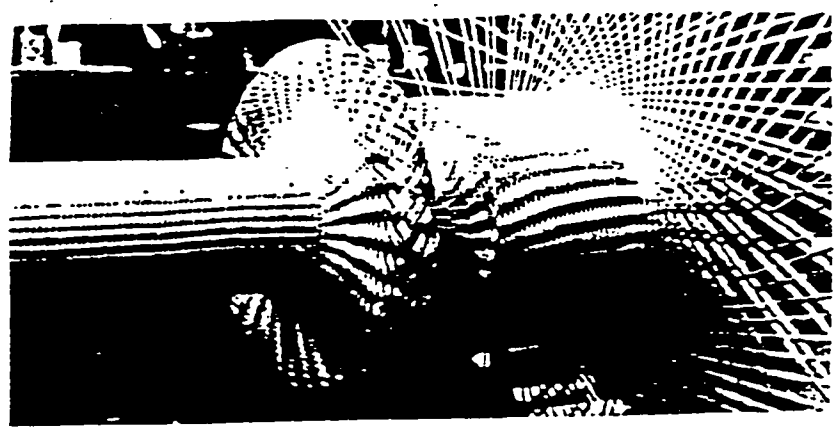

Fig 2.3 Formation of fiber glass preform for composite shaft

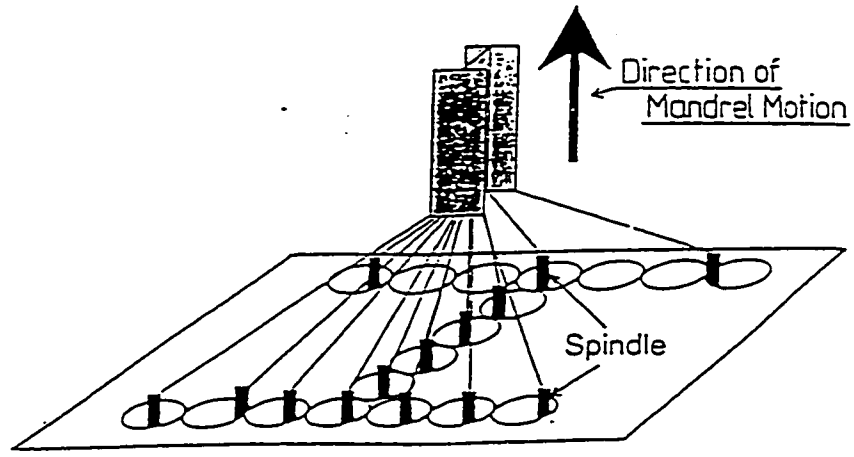

Fig 2.4 Integrated braiding mechanism [9]

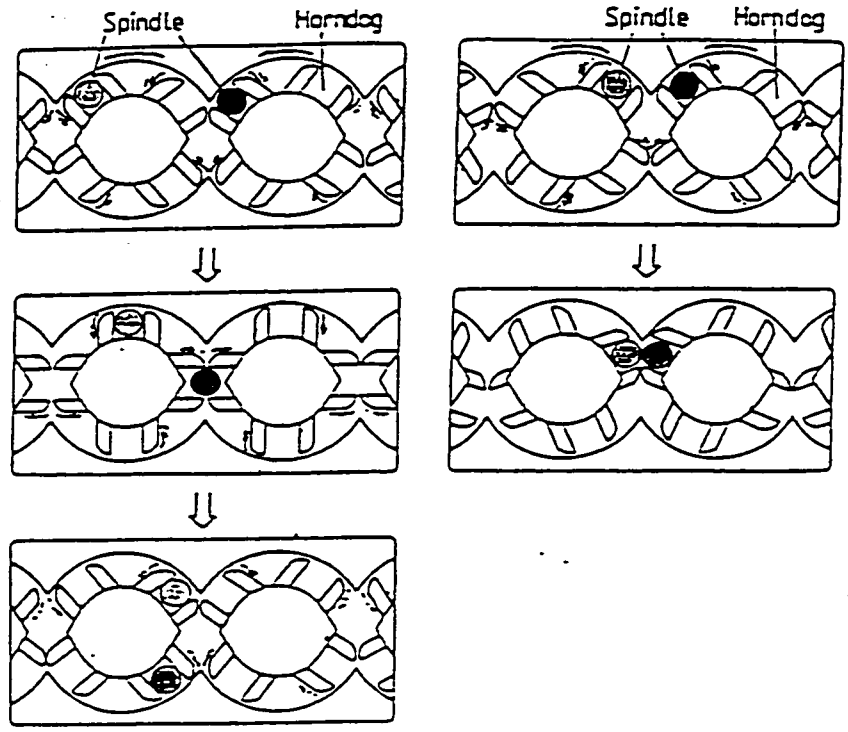

Fig 2.5 Mechanism of spindle movement [9]

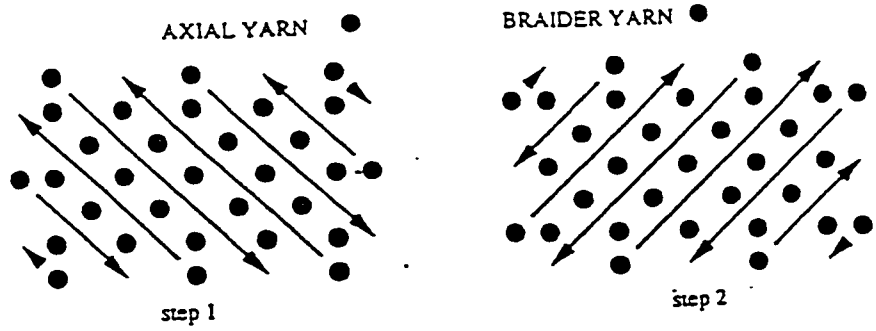

Fig 2.6 The two-step braiding process [8]

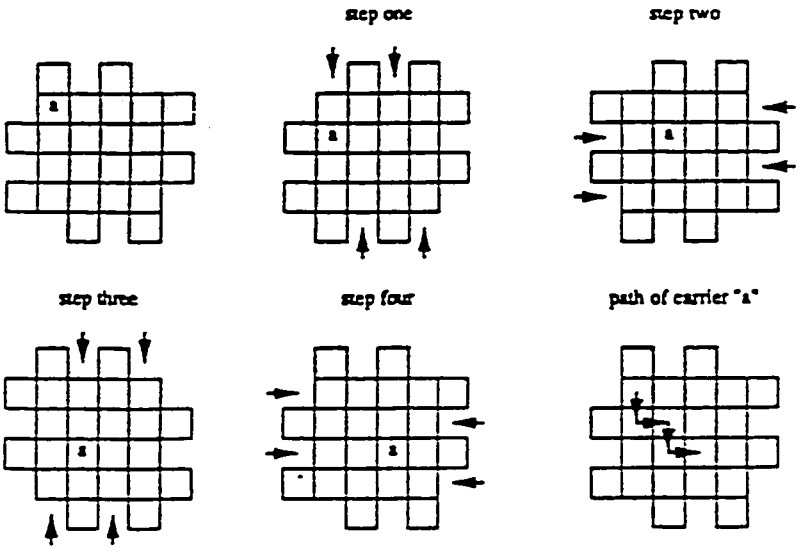

Fig 2.7 The four step braiding process [8]

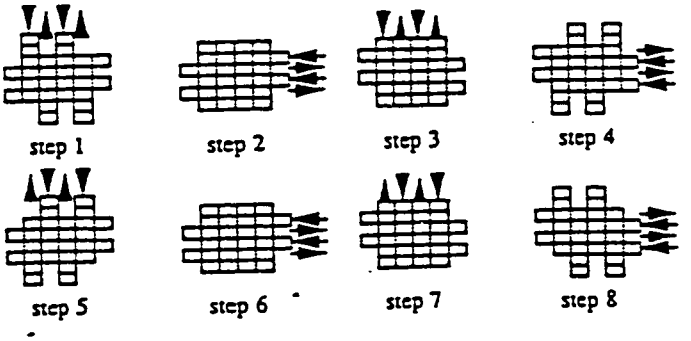

Fig 2.8 An example of multi-step shifting sequence utilizing a total eight steps [8]

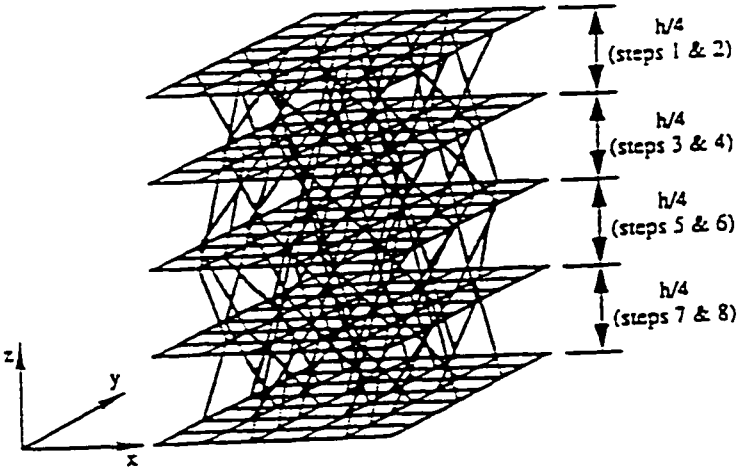

Fig 2.9 An idealized architecture resulting from an eight step shifting sequence [8]

Chapter 3 Two dimensional braiding processes

In the two dimensional braiding process, two and three systems of yarns are intertwined in the bias direction to form an integrated structure. The braiding yarns are in $+\theta$ and $-\theta$ directions and usually interlace in either a 1×1 or a 2×2 pattern, as shown in Fig 3.1. In a 1×1 pattern a $+\theta$ braiding yarn passed over one $-\theta$ braiding yarns and then under one $-\theta$ braiding yarns vice versa, while in a 2×2 pattern a $+\theta$ braiding yarn continuously passed over two $-\theta$ braiding yarns and then under two $-\theta$ braiding yarns vice versa.

A two dimensional biaxial and a two dimensional triaxial braided preform are shown in Fig 3.9a, and Fig 3.13a respectively. There are additional axial yarns in triaxial braided preform. They are inserted between the braiding yarns along the longitudinal direction.

A two dimensional braided composite laminate with a desired thickness can be built by over-braiding layers of the desired architecture on top of each other. The resin can be applied in-situ or after the preform is removed from the mandrel.

A horizontal braiding machine with 72 braiding yarn carriers and 36 axial yarn carriers in our lab is shown in Fig 3.2. This machine can braid both biaxial and triaxial axis-symmetric preforms. It consists of track plate , yarn carriers, former and axial feeding device. The control parameters for braiding are rotational speed of yarn carriers n, the feed rate v_a(m/s), the geometry of braiding and axial yarns, the size of mandrel. Using these control parameters, the geometric parameters of a braided preform, such as braiding angle, yarn space, overall fiber volume fraction, yarn

volume fraction, yarn thickness, yarn cross-sectional area, yarn crimp angle and yarn undulating paths, can be controlled.

3.1 Braid angle θ and speed ratio

The braiding angle is the acute angle between the direction of braiding yarn and the axis of mandrel as shown in Fig 3.3. The rotational speed of braiding yarn carrier and feed rate of the mandrel control the braiding angle θ. The total number of revolutions a yarn carrier rotates around the mandrel axis in one minute is the rotational speed n. The unit of n is revolution per minute (rpm). The total distance of a mandrel moving along its axial direction in one second time is the feed rate v_a. The unit for v_a is meter per second (m/s).

To obtain the relation between braiding angle and v_a and n, the surface of a mandrel is developed to a rectangular area as shown in Fig 3.3. The yarn path can be thought of as a straight line in Fig 3.3.

The time for a braiding yarn carrier to turn one revolution around the mandrel axis is

$$T = 60 \times \frac{1}{n} \qquad (s) \tag{3-1}$$

Thus, the corresponding axial feeding distance p in time T is

$$p = v_a \times T = \frac{60 v_a}{n} \qquad (m) \tag{3-2}$$

So from Fig 3.3

$$\tan\theta = \frac{\pi D}{1000p} = \frac{\pi D}{1000 \times 60 \times \frac{v_a}{n}} = \frac{\pi D n}{60 \times 1000 v_a} \tag{3-3}$$

Where

D is the diameter of mandrel, its unit is mm.

Define the speed ratio of braiding machine

$$\omega = \frac{n}{v_a} \tag{3-4}$$

Then

$$\omega = \frac{60 \times 1000}{\pi D} \tan\theta \tag{3-5}$$

The curves of speed ratio versus braiding angle are shown in Fig 3.4 .

3.2 Filament packing fraction

Both braiding and axial yarns consist of filaments. The yarns will change their shapes as they are braided with each other. The filament packing fraction is the filament area to yarn area ratio. J.W.S. HEARLE, et al studied this in 1969[14]. Open and close packing forms were studied in their paper. If the fibers are arranged in concentric pattern, as in Fig 3.5a, the packing form is called open packing. Otherwise , if the fibers are arranged in a hexagonal pattern, as in Fig 3.5b, the packing form is called close packing.

3.2.1 Open packing fraction

In Fig 3.5a, if each of the rings is completely filled and fiber cross-sections are circular, we can get the radius of a yarn

$$R_y = 2(N_r - 1)r_0 + r_0 = (2N_r - 1)r_0 \tag{3-6}$$

where

N_r is the number of rings

r_0 is the radius of a filament

The number of filaments in a yarn

$$N_f = 1 + \sum_{i=2}^{N_r} \frac{2\pi(i-1)(2r_0)}{2r_0} = 1 + \pi N_r(N_r - 1) \tag{3-7}$$

Thus the filament packing fraction

$$k_0 = \frac{N_f \times \pi r_0^2}{\pi R_y^2} = \frac{1 + \pi N_r(N_r - 1)}{(2N_r - 1)^2} \tag{3-8}$$

Where

the subscript o refers to open packing .

If the number of filaments is large enough,

then

$$k_o = \lim_{N_r \to \infty} \frac{1 + \pi N_r(N_r - 1)}{(2N_r - 1)^2} \approx \frac{\pi}{4} = 0.785 \tag{3-9}$$

So the theoretical maximum filament packing fraction for open packed fiber is 0.785.

3.2.2 Close packing fraction

In Fig 3.5(b), the fibers are packed in a hexagonal pattern . If each of layer is completely occupied, the overall hexagonal area is

$$A = 6 \times [\frac{1}{2}(2N_r - 1)^2 r_0^2 \sin 60^0] = 6\sqrt{3}(N_r - \frac{1}{2})^2 r_0^2 \tag{3-10}$$

The number of filaments in a yarn is

$$N_f = \sum_{i=2}^{N_r} [6(i-1)] + 1 = 3N_r(N_r - 1) + 1 \tag{3-11}$$

Where N_r is the number layers

Thus , the filament packing fraction is

$$k_c = \frac{N_f \times \pi r_0^2}{A} = \frac{\pi[3N_r(N_r - 1) + 1]}{6\sqrt{3}(N_r - \frac{1}{2})^2} \tag{3-12}$$

If N_r is large enough,

$$k_c = \lim_{N_r \to \infty} \frac{\pi[3N_r(N_r - 1) + 1]}{6\sqrt{3}(N_r - \frac{1}{2})^2} = \frac{\pi}{2\sqrt{3}} \approx 0.91 \tag{3-13}$$

The equation (3-8), (3-12) can also be applied to other shapes according to [14]. Actually, the filament packing fraction are 0.6~0.75 from experiment. The diagrams of k_c, k_o versus N_r are shown in Fig 3.7. As can be seen when the number of rings is larger than 5 , the values of k_c, k_o are very close to their limit values.

3.3The geometrical parameters of yarn cross section

The cross sectional area of a yarn is assumed to have the shape illustrated in Fig 3.6. The width and height are w, t respectively. The upper and lower boundary curves are arcs with the same radius.

The radius of these arcs can be calculated from Fig 3.6.

$$\overline{oi} = r - \frac{t}{2} \tag{3-14}$$

$$\overline{ei} = \frac{w}{2} \tag{3-15}$$

So in the triangle Δoei

$$r^2 = \overline{ei}^2 + \overline{oi}^2 \tag{3-16}$$

That is

$$r^2 = (\frac{w}{2})^2 + (r - \frac{t}{2})^2 \tag{3-17}$$

So

$$r = \frac{w^2 + t^2}{4t} \tag{3-18}$$

Let thickness to width ratio

$$\xi = \frac{t}{w} \tag{3-19}$$

Then

$$r = \frac{w^2 + t^2}{4t} = \frac{t[(\frac{w}{t})^2 + 1]}{4} = \frac{t(1+\xi^2)}{4\xi^2} \tag{3-20}$$

$$\sin\psi = \frac{\overline{ei}}{r} = \frac{2\xi}{1+\xi^2} \qquad (0 < \xi \leq 1) \tag{3-21}$$

or

$$\psi = \arcsin(\frac{2\xi}{1+\xi^2}) \tag{3-22}$$

The area of the sector $\overline{oefg}$

$$A_s = \frac{2\psi}{2\pi}(\pi r^2) = \frac{t^2(1+\xi^2)^2}{16\xi^4}\arcsin(\frac{2\xi}{1+\xi^2}) \tag{3-23}$$

The area of the triangle Δoeg is

$$A_\Delta = \frac{1}{2}\overline{eg} \times \overline{oi} = \frac{1}{2}w(r - \frac{t}{2}) = \frac{(1-\xi^2)t^2}{8\xi^3} \tag{3-24}$$

So the cross sectional aera of a yarn is

$$A = 2(A_s - A_\Delta) = \lambda t^2 \tag{3-25}$$

Where

$$\lambda = \left[\frac{(1+\xi^2)^2}{8\xi^4}\arcsin(\frac{2\xi}{1+\xi^2}) - \frac{(1-\xi^2)}{4\xi^3}\right] \tag{3-26}$$

If we assume that the cross sectional area of a yarn is proportional to its filament count number, and the filament cross section is circular shape with a constant diameter d_f.

Then

$$kA = m \times (\frac{\pi}{4}d_f^2) \tag{3-27}$$

Where

A is the cross-section area of a yarn

m is the filament count number

k is the filament packing fraction

d_f is the diameter of filament

Substitute (3- 25) to (3-27)

$$k\lambda t^2 = m \times \frac{\pi d_f^2}{4} \tag{3-28}$$

$$t = \sqrt{\frac{\pi m}{4k\lambda}} \times d_f \tag{3-29}$$

Where

λ is given by Equation (3-26).

k can be chosen in the range of 0.6~0.75.

From Equation (3-29), if we know the values of k, d_f, m, ξ of a yarn, then we can get the width w and thickness t of this yarn. The thickness versus ξ curves are shown in Fig 3.8.

3.4 The geometric parameters of biaxial braided composite

In this section, the fiber volume fraction V_f and its upper limit, yarn volume fraction and its upper limit, yarn jamming angle θ_L, crimp angle γ are studied. The relative equations are given.

3.4.1 Fiber volume fraction and yarn volume fraction

(1) The fiber volume fraction and the yarn volume fraction

The fiber volume fraction is the ratio of the volume of total filaments to the volume of braided composite which consists of these filaments. The yarn volume

fraction is the total volume of yarns to the volume of braided composite which contains these yarns.

As shown in Fig 3.9b

$$t^{\cdot} = t \tag{3-30}$$

$$w^{\cdot} = \frac{w}{\cos\theta} \tag{3-31}$$

$$A^{\cdot} = \frac{A}{\cos\theta} \tag{3-32}$$

Then the fiber volume fraction V_f

$$V_f = \frac{k(NA^{\cdot})}{\pi D(2t)} \tag{3-33}$$

Where

N is the number of braiding yarn carriers

Substitute (3-25), (3-32) to equation (3-33), then the fiber volume fractions is

$$V_f = \frac{kNt\lambda}{2D\pi\cos\theta} \tag{3-34}$$

The yarn volume fraction is

$$V_y = \frac{V_f}{k} = \frac{Nt\lambda}{2D\pi\cos\theta} \tag{3-35}$$

The curves of fiber volume fraction versus thickness to width ratio ξ are shown in Fig 3.10 . The upper limits of fiber volume fraction and yarn volume fraction are given as follows.

(2) The upper limits of fiber volume fraction and yarn volume fraction

In Fig 3.9 , the yarn space is

$$L = \frac{\pi D}{N/2} \tag{3-36}$$

If no overlap occurs between yarns,

then

$$w' \le \frac{\pi D}{N/2} \tag{3-37}$$

From equation (3-31), (3-32),

$$\frac{w'}{A'} = \frac{w}{A} \tag{3-38}$$

$$w' = \frac{A'w}{A} \tag{3-39}$$

Substitute (3-37) to (3-39)

$$w' = \frac{A'}{A} w \le \frac{2\pi D}{N} \tag{3-40}$$

Thus

$$NA' \le \frac{2\pi DA}{w} \tag{3-41}$$

Substitute Equation (3-41) to (3-33)

$$V_f \le \frac{kA}{wt} \tag{3-42}$$

Again substitute (3-19), (3-25) to (3-42)

$$V_f \le \frac{k\lambda t^2}{t \times t/\xi} = k\xi\lambda \tag{3-43}$$

Where

λ is given by Equation (3-26)

Thus the fiber volume fraction is

$$V_f \le k\xi\lambda = k\left[\frac{(1+\xi^2)^2}{8\xi^3}\arcsin(\frac{2\xi}{1+\xi^2}) - \frac{1-\xi^2}{4\xi^2}\right] \tag{3-44}$$

The yarn volume fraction is

$$V_y = \frac{V_f}{k} \le \left[\frac{(1+\xi^2)^2}{8\xi^3}\arcsin(\frac{2\xi}{1+\xi^2}) - \frac{1-\xi^2}{4\xi^2}\right] \tag{3-45}$$

Using Equation (3-44), the curve of maximum fiber volume fraction versa thickness to width ratio can be plotted, as shown in Fig 3.11.

3.4.2 The jamming angle θ_L

When the surface of the mandrel is completely covered by a layer of braiding yarn (and axial yarns in triaxial case) without overlap, the braiding angle θ is called the jamming angle.

When $6 = 6_L$

$$w^{\cdot} = \frac{\pi D}{N/2} \tag{3-46}$$

Substitute Equation (3-31) into it, the jamming angle is

$$\theta_L = \arccos\frac{wN}{2\pi D} \tag{3-47}$$

3.4.3 The crimp angle γ

When the preform is cut along the braiding yarn direction in Fig 3.9, the cross section B-B is shown in Fig 3.12.

The path of the braid yarn axis can be assumed to have the following form

$$z = \frac{t}{2}\sin(\frac{\pi x}{2L'}) \tag{3-48}$$

Where

$$L' = \frac{L}{2\sin\theta} \tag{3-49}$$

Substitute (3-36), (3-49) to (3-48)

then

$$z = \frac{t}{2}\sin(\frac{N\sin\theta}{2D}x) \tag{3-50}$$

So

$$\frac{dz}{dx} = \frac{t}{2}\frac{N\sin\theta}{2D}\cos(\frac{N\sin\theta}{2D}x) \tag{3-51}$$

If the crimp angle is defined as

$$\gamma = \frac{dz}{dx}|_{x=0} \tag{3-52}$$

Then from Equation(3-51),

$$\gamma = \frac{dz}{dx}|_{x=0} = \frac{tN}{4D}\sin\theta \tag{3-53}$$

The crimp angle when $\theta = \theta_L$ is

$$\gamma_c = \frac{dz}{dx}|_{x=0} = \frac{tN}{4D}\sin\theta_c \tag{3-54}$$

3.5 The geometric parameters of triaxial braided composite

The triaxial braided preform and its cross section A-A are shown in Fig 3.13. In this section the subscript a and b are used to denote the axial yarn and braiding yarn respectively.

As in section 3.4, the thickness to width ratios are

$$\xi_a = \frac{t_a}{w_a} \tag{3-55}$$

$$\xi_b = \frac{t_b}{w_b} \tag{3-56}$$

We assume that the thickness to width ratio ξ, the filament diameter d_f and the filament packing ratio k of both axial and braiding yarn are same ,then

$$\xi_a = \xi_b = \xi$$

$$kA_a = m_a(\frac{\pi}{4}d_f^2) \tag{3-57}$$

$$kA_b = m_b(\frac{\pi}{4}d_f^2) \tag{3-58}$$

Thus

$$A_a = \frac{m_a}{m_b}A_b \tag{3-59}$$

From Equation(3-25)

$$A_a = \lambda t_a^2 \tag{3-60}$$

$$A_b = \lambda t_b^2 \tag{3-61}$$

Thus

$$A_a = (\frac{t_a}{t_b})^2 A_b \tag{3-62}$$

Substitute (3-59) to (3-62), get

$$t_a = \sqrt{\frac{m_a}{m_b}}\, t_b \tag{3-63}$$

$$w_a = \sqrt{\frac{m_a}{m_b}}\, w_b \tag{3-64}$$

3.5.1 Fiber volume fraction and yarn volume fraction

(1)The fiber volume fraction and yarn volume fraction

From Equation (3-31), (3-32)

$$w_b^{\cdot} = \frac{w_b}{\cos 6} \tag{3-65}$$

$$A_b^{\cdot} = \frac{A_b}{\cos 6} \tag{3-66}$$

Then the fiber volume V_f

$$V_f = \frac{k(NA_b^{\cdot} + \frac{N}{2} A_a)}{\pi D(2t_b + t_a)} \tag{3-67}$$

Where

N is the number of braiding yarn carrier

Substitute Equation (3-59), (3-63), (3-61), (3-66) to (3-67),

Then

$$V_f = \frac{kN(\frac{A_b}{\cos\theta} + \frac{m_a}{2m_b}A_b)}{\pi D(2t_b + \sqrt{\frac{m_a}{m_b}}t_b)} = \frac{kN(1 + \frac{m_a}{2m_b}\cos\theta)\lambda t_b}{\pi D\cos\theta(2+\sqrt{\frac{m_a}{m_b}})} \tag{3-68}$$

So the yarn volume fraction is

$$V_y = \frac{N(1 + \frac{m_a}{2m_b}\cos\theta)\lambda t_b}{\pi D\cos\theta(2+\sqrt{\frac{m_a}{m_b}})} \tag{3-69}$$

It is seen here, when $m_a=0$, Equation (3-68), (3-69) will be the same as Equation (3-34), (3-35).

(2) The upper limit of fiber volume fraction and yarn volume fraction

Use the same way as in section 3.4, the upper limit of fiber volume fraction and yarn volume fraction can be obtained as follows,

As it is known

$$L = \frac{\pi D}{N/2} \tag{3-70}$$

$$W_b \leq \frac{\pi D}{N/2} \tag{3-71}$$

$$W_a \leq \frac{\pi D}{N/2} \tag{3-72}$$

Where

N is the number of braiding yarn carrier

D is the diameter of mandrel

From Equation (3-65), (3-66)

$$W_b^{\cdot} = \frac{A_b^{\cdot}}{A_b} W_b \tag{3-73}$$

Substitute Equation (3-73) into Equation (3-71)

$$NA_b^{\cdot} \le \frac{2\pi D A_b}{W_b} \tag{3-74}$$

Further substitute Equation (3-61), (3-56) into (3-74), note that we have assumed $\xi_a = \xi_b = \xi$,

Then

$$NA_b^{\cdot} \le 2\pi D t_b \lambda \xi \tag{3-75}$$

Substitute Equation (3-55), (3-60) into (3-72)

$$\frac{NA_a}{2} \le \pi D t_a \lambda \xi \tag{3-76}$$

Add Equation (3-75) and (3-76)

$$NA_b^{'} + \frac{NA_a}{2} \leq \pi D (2t_b + t_a)\lambda\xi \tag{3-77}$$

Substitute the above Equation to Equation (3-67), so the upper limit of the fiber volume fraction is

$$V_f \leq k\xi\lambda \tag{3-78}$$

Thus the upper limit of yarn volume fraction is

$$V_y \leq \xi\lambda \tag{3-79}$$

Equations (3-78), (3-79) are the same as (3-44), (3-45).

3.5.2 The jamming angle θ_L

The jamming angle can be derived from Fig. 3.13a, if no overlap of yarn occurs,

then

$$W_b^{'} + W_a \leq (\frac{i+1}{2})L \tag{3-80}$$

Where

i=1 for 1×1 braided preform

i=2 for 2×2 braided preform

and

$$W_b^{'} \le L \tag{3-81}$$

Where

L is the yarn space

Substitute Equation (3-65) to (3-80)

Then

$$\frac{W_b}{\cos\theta} + W_a \le (\frac{i+1}{2})L \tag{3-82}$$

$$\cos\theta \ge \frac{W_b}{\left(\frac{i+1}{2}\right)L - W_a} \tag{3-83}$$

Or

$$\theta \le \arccos\frac{W_b}{\left(\frac{i+1}{2}\right)L - W_a} \tag{3-84}$$

Substitute Equation (3-65) to (3-81)

Then

$$\frac{W_b}{\cos\theta} \le L \tag{3-85}$$

$$\cos\theta \ge \frac{W_b}{L} \tag{3-86}$$

Or

$$\theta \le \arccos(\frac{W_b}{L}) \tag{3-87}$$

Then the jamming angle is

$$\theta_L = \min\left(\arccos\frac{W_b}{\left(\frac{i+1}{2}\right)L - W_a}, \quad \arccos(\frac{W_b}{L}) \right) \tag{3-88}$$

3.5.3 The yarn crimp angle γ

The yarn path in Fig. 3.14 can be described by following equation

$$z = \frac{t_a + t_b}{2}\sin(\frac{\pi x}{2L'}) \tag{3-89}$$

Where

$$L' = \frac{L}{2\sin\theta} \tag{3-90}$$

Substitute Equation (3-70), (3-90) into (3-89)

Then

$$z = \frac{t_a + t_b}{2} \sin(\frac{N \sin 6}{2D} x) \tag{3-91}$$

So the yarn crimp angle γ is

$$\gamma = \frac{dz}{dx}|_{x=0} = \frac{(t_a + t_b)N}{4D} \sin\theta \tag{3-92}$$

3.6 The procedure for the design of braided preform

The design of braided preform follows the steps as described below,

Step1: Chose the type of yarn and yarn count number m_a, m_b , yarn volume fraction V_y and filament packing fraction k. Calculate the fiber volume fraction V_f.

Step2: In Fig 3.11, choose the thickness to width ratio.

Step3: Using Equation (3-29), find thickness of one layer braided preform, then calculate its width and the total thickness of the braided preform.

Step4: In Fig3.10, using the values of fiber volume fraction and thickness to width, find the value of braiding angle.

Step5: Determine the machine speed ratio from Fig 3.4

3.7 Estimate geometric parameters of braided composite from experiment

If total thickness, number of layers, braiding angle, are tested from a braided composite, the thickness and width of yarns, fiber volume fraction of composite can

be estimated.

Step 1:The thickness of yarn can be obtained as the total thickness divided by the number of layers.

Step 2: In Fig 3.8 find the thickness to width ratio, then calculate the width of the yarn.

Step 3: Use the values of thickness to width ratio and the braiding angle to find the fiber volume fraction in Fig 3.10.

Step 4: Calculate the crimp angle of the yarn.

Because the thickness to width ratio is not easy to be found, a better way for estimating geometric parameters is shown in section 3.8.1.

3.8 The comparison between experimental data and theoretical results

In 1996, John E. Master and Pierre J. Minguet investigated the role of the braid architecture in determining braided laminate mechanical properties [15]. In their research, the braided fibrous preforms were formed on cylindrical mandrels. With the exception of one braid that featured large yarns, all the braids were formed with a 144 braiding yarn carrier New England Butt Triaxial Braiding machine, 72 axial yarns were incorporated into the fabric. The AS4 graphite fibers and Shell's 1895 epoxy matrix are used by them. The filament diameter of AS4 is 7 μm.

They use a shorthand notation to define the braided architecture. It is based in three primary braid parameters (1) braiding angle; (2) the count number of axial and braiding yarns; (3) axial yarn content of braided preform.

The proposed notation is

$$\left[0_{m_a} / \pm\theta_{m_b}\right]\chi\%\ Axial$$

Where

0 indicates the direction of axial yarns, (°)

θ indicates the direction of braiding yarns,(°)

m_a is the count number of axial yarns, the unit for it is K, which means one thousand,

m_b is the count number of braiding yarn, the unit for it is K,

χ is the axial yarn content of braided preform.

χ can be deduced from Fig 3.13 (b) as follows,

$$\chi = \frac{\frac{N}{2}A_a}{NA_b' + \frac{N}{2}A_a} \tag{3-93}$$

Where

N is the number of braiding yarn carriers,

A_a, A_b' are defined in Fig 3.13(b).

Substitute (3-59), (3-66) to (3-93)

$$\chi = \frac{\frac{m_a}{2m_b}}{\frac{1}{\cos\theta} + \frac{m_a}{2m_b}} \times 100\% \tag{3-94}$$

For example,

$[0_{18K} / \pm 66.5_{6K}]$ 37.6% *Axial*

means that the preform has 37.6% axial yarn with an axial yarn count number of 18K, and (100-37.6)% braiding yarn with ±66.5° braiding angle and a braiding yarn count number of 6K.

3.8.1 Comparison with experimental results of reference [15]

For the convenience of discussion, we list the known parameters in [15] as follows,

The number of braiding yarn carrier

$N = 144$

The filament diameter of AS4

$d_f = 0.007$ mm

The count number of axial yarns m_a and braiding yarns m_b, the thickness H of the braided laminates, the diameter of cylindrical mandrel D, the number of layers of laminates N_L, and the braiding angle θ are all listed in table 3-1.

By using the known parameters above, the fiber volume fraction V_f and the crimp angle γ can be predicted by the theory given in this chapter.

In table 3-1, for all the cases

$m_a = 18K, \quad m_b = 6K, \quad N_L = 5$

From Equation (3-63)

$$t_a = \sqrt{\frac{m_a}{m_b}}\, t_b = \sqrt{3}\, t_b$$

Table 3-1 The known parameters in reference [15]

Material type $\left[0_{m_a} / \pm\theta_{m_b}\right]\chi\%$ *Axial*	Yarn space L ,mm	Mandrel diameter D, mm	Number of layers N_L	The thickness of laminates H. mm
$[0_{18K} / \pm 66.5_{6K}]$ 37.6% *Axial*	6.10	140	5	2.87±0.03
$[0_{18K} / \pm 66.5_{6K}]$ 37.6% *Axial*	5.25	120	5	3.28±0.08
$[0_{18K} / \pm 66.5_{6K}]$ 37.6% *Axial*	4.80	110	5	3.68±0.03

We assume

$$(t_a + 2t_b)N_L = H \tag{3-95}$$

So

$$t_b = \frac{H}{(\sqrt{3}+2)N_L} = \frac{H}{18.66} \quad \text{mm} \tag{3-96}$$

From Equation (3-57), (3-58), and choose filament packing fraction k=0.75 [15]

$$A_a = \frac{m_a}{k}(\frac{\pi}{4}d_f^2) = 0.924 \quad \text{mm}^2$$

$$A_b = \frac{m_b}{k}(\frac{\pi}{4}d_f^2) = 0.308 \quad \text{mm}^2$$

From Equation (3-68)

$$V_f = \frac{kN(1 + \frac{m_a}{2m_b}\cos\theta)\lambda t_b}{\pi D\cos\theta(2+\sqrt{\frac{m_a}{m_b}})}$$

Substitute Equation (3-61) to above Equation, get

$$V_f = \frac{kN(1 + \frac{m_a}{2m_b}\cos\theta)A_b / t_b}{\pi D\cos\theta(2+\sqrt{\frac{m_a}{m_b}})} \quad (3\text{-}97)$$

$$= \frac{0.75\times144\times(1 + \frac{18}{2\times6}\cos66.5^\circ)\times0.308/t_b}{\pi D\cos66.5^\circ(2+\sqrt{\frac{18}{6}})} = \frac{11.37}{D\times t_b}$$

From Equation (3-92)

$$\gamma = \frac{(t_a + t_b)N}{4D}\sin\theta$$

$$= \frac{(1+\sqrt{3})\times144\times\sin66.5^\circ}{4}\times\frac{t_b}{D} \qquad (rad)$$

That is

$$\gamma = \frac{180}{\pi}\times90.19\times\frac{t_b}{D} = 5168\frac{t_b}{D} \qquad (^\circ) \quad (3\text{-}98)$$

For the case $[0_{18K} / \pm66.5_{6K}]$ 37.6% $Axial$, D=140 mm.

(1) From Equation (3-96)

$$t_b = \frac{H}{18.66} = \begin{cases} 0.155 & H = 2.87 + 0.03 \\ 0.152 & H = 2.87 - 0.03 \end{cases} \quad (3\text{-}99)$$

(2) From Equation (3-97)

$$V_y = \frac{11.37}{D\times t_b} = \frac{11.37}{140t_b} = \begin{cases} 52.3\% & t_b = 0.155 \\ 53.4\% & t_b = 0.152 \end{cases} \quad (3\text{-}100)$$

(3) From Equation (3-98)

$$\gamma = 5168\frac{t_b}{D} = \begin{cases} 5.74^\circ & t_b = 0.155 \\ 5.62^\circ & t_b = 0.152 \end{cases} \tag{3-101}$$

By the same way, the theoretical values of t_b, V_y, γ can be obtained for the other cases. The theoretical and experimental [15] results of yarn volume fractions and crimp angles are listed in Table 3-2.

Table 3-2 Comparison between the results of theory and experiment [15]

Material type	Braiding yarn thickness t_b mm	Crimp angles γ (°)		Fiber volume fraction V_f (%)	
		Exp. [15]	Theory	Exp. [15]	Theory
$[0_{18K}/\pm 66.5_{6K}]$ 37.6% Axial	0.154±0.002	10.7±3.6	5.69±0.06	51.2±1.9	52.9±0.6
$[0_{18K}/\pm 66.5_{6K}]$ 37.6% Axial	0.176±0.004	13.9±3.8	7.55±0.19	52.8±2.0	53.8±1.3
$[0_{18K}/\pm 66.5_{6K}]$ 37.6% Axial	0.198±0.001	16.8±4.1	9.27±0.08	51.0±2.0	52.4±0.4

From Table 3-2, we can see that the predicted overall fiber volume fractions of our theory meet those of experiment [15] very well. The theoretical crimp angles are lower than the experimental crimp angles. The lower theoretical crimp angles result from the interstitial resin thickness which is neglected in Equation (3-91) and (3-95). The resin thickness depends on many factors , such as the tension of yarns, the type of

resin, the curing process. The interstitial resin thickness is not easy to be controlled and accurately evaluated, so it is neglected in our theoretical models. The in-plane mechanical behavior is the functions of *cos* γ. γ is small as discussed in chapter 4, so the error of it has no significant effect on the in-plane mechanical behaviors. For example, the relative error between cos10.7° and *cos* 5.69° is only 1.24%.

3.8.2 Comparison with the experimental results of reference [16]

The count number of axial yarns m_a and braiding yarns m_b, the yarn space L, the number of layers N_L, the thickness of the braided composite laminates H, are all listed in Table 3-3. The filament diameter of AS4 graphite fiber is 0.007 mm.

Table 3.3 The known parameters in reference [16]

Material type $\left[0_{m_a} / \pm\theta_{m_b}\right]\chi\%$ *Axial*	Yarn space L, mm	Number of layers N_L	The thickness of laminates H, mm
$[0_{30K} / \pm 70_{6K}]$ 46% *Axial*	6.05	8	5.66
$[0_{15K} / \pm 70_{15K}]$ 46% *Axial*	11.04	6	5.61
$[0_{36K} / \pm 45_{15K}]$ 46% *Axial*	5.52	6	5.64
$[0_{6K} / \pm 45_{15K}]$ 12% *Axial*	5.52	10	5.66

The experimental and theoretical results of fiber volume fractions are listed in Table 3-4. The maximum difference between the values of experiment and theory is

about 6% , which happens in the case of $[0_{30K} / \pm 70_{6K}]$ 46% *Axial*, and the case of $[0_{6K} / \pm 45_{15K}]$ 12% *Axial*.

Table 3-4 Comparison between the results of theory and experiment [16]

Material type	Braiding yarn thickness t_b mm	Fiber volume fraction V_f (%)	
		Exp. [16]	Theory
$[0_{30K} / \pm 70_{6K}]$ 46% *Axial*	0.1670	55.3	58.5
$[0_{75K} / \pm 70_{15K}]$ 46% *Axial*	0.2207	59.4	58.9
$[0_{36K} / \pm 45_{15K}]$ 46% *Axial*	0.2648	58.4	58.2
$[0_{6K} / \pm 45_{15K}]$ 12% *Axial*	0.2150	56.4	58.8

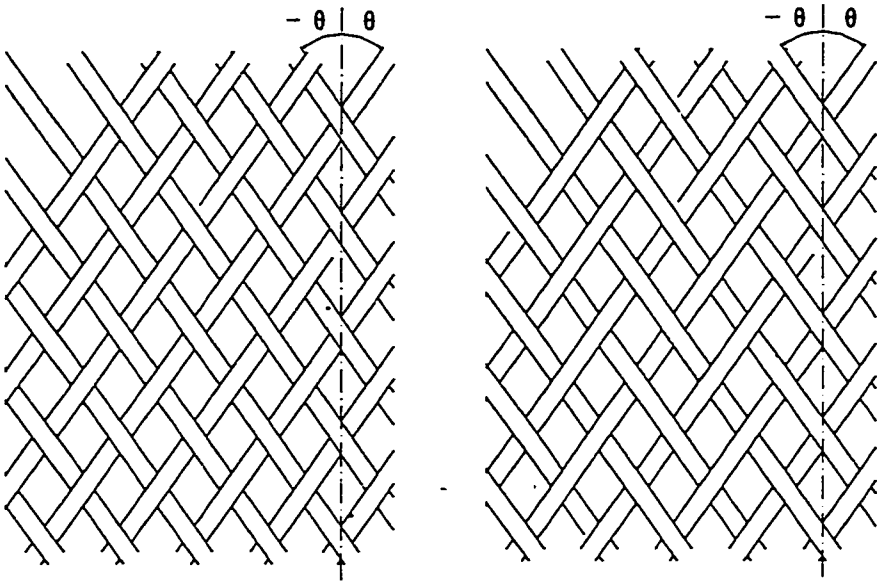

(a) 1×1 braided preform (b) 2×2 braided preform

Fig 3.1 The patterns of braided preform

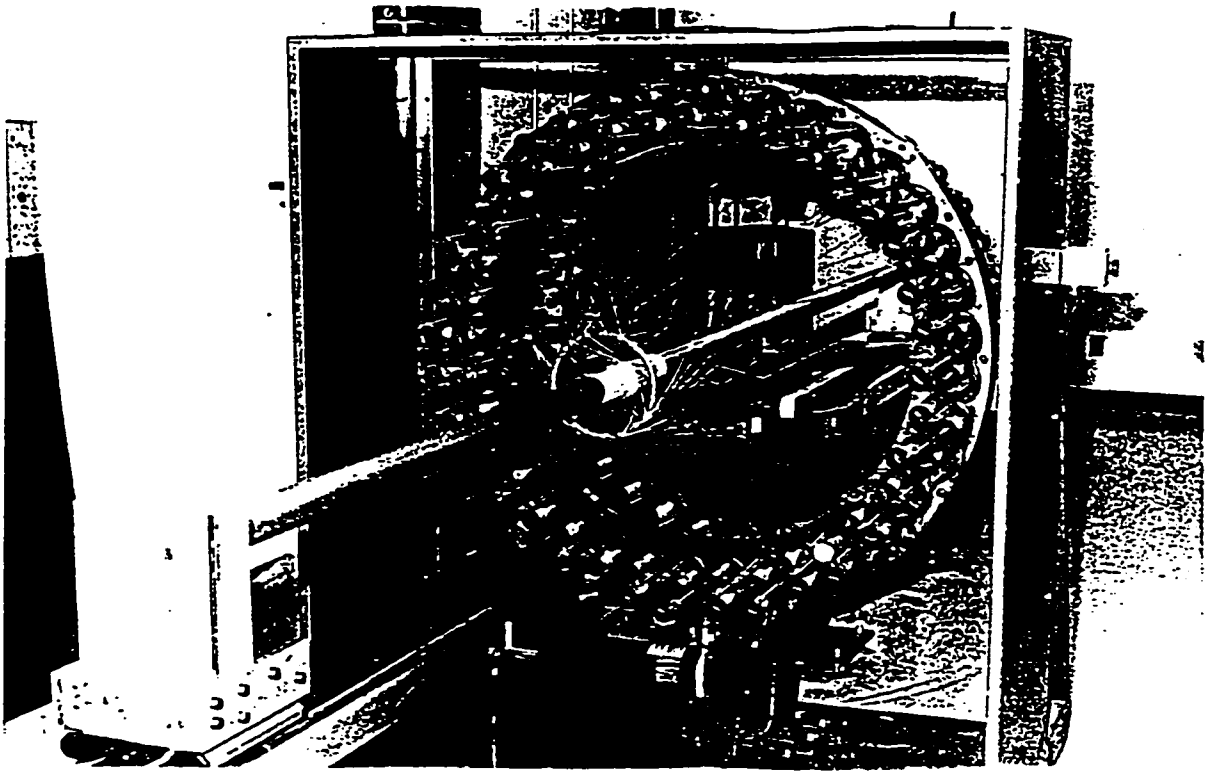

Fig 3.2 A horizontal braiding machine with72-braiding yarn carriers and 36-axial yarn carriers

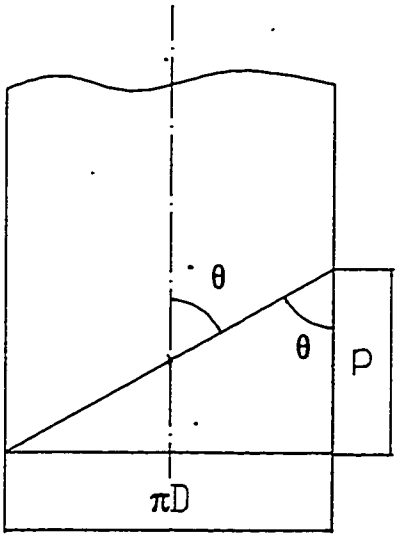

Fig 3.3 Developed surface of braiding mandrel

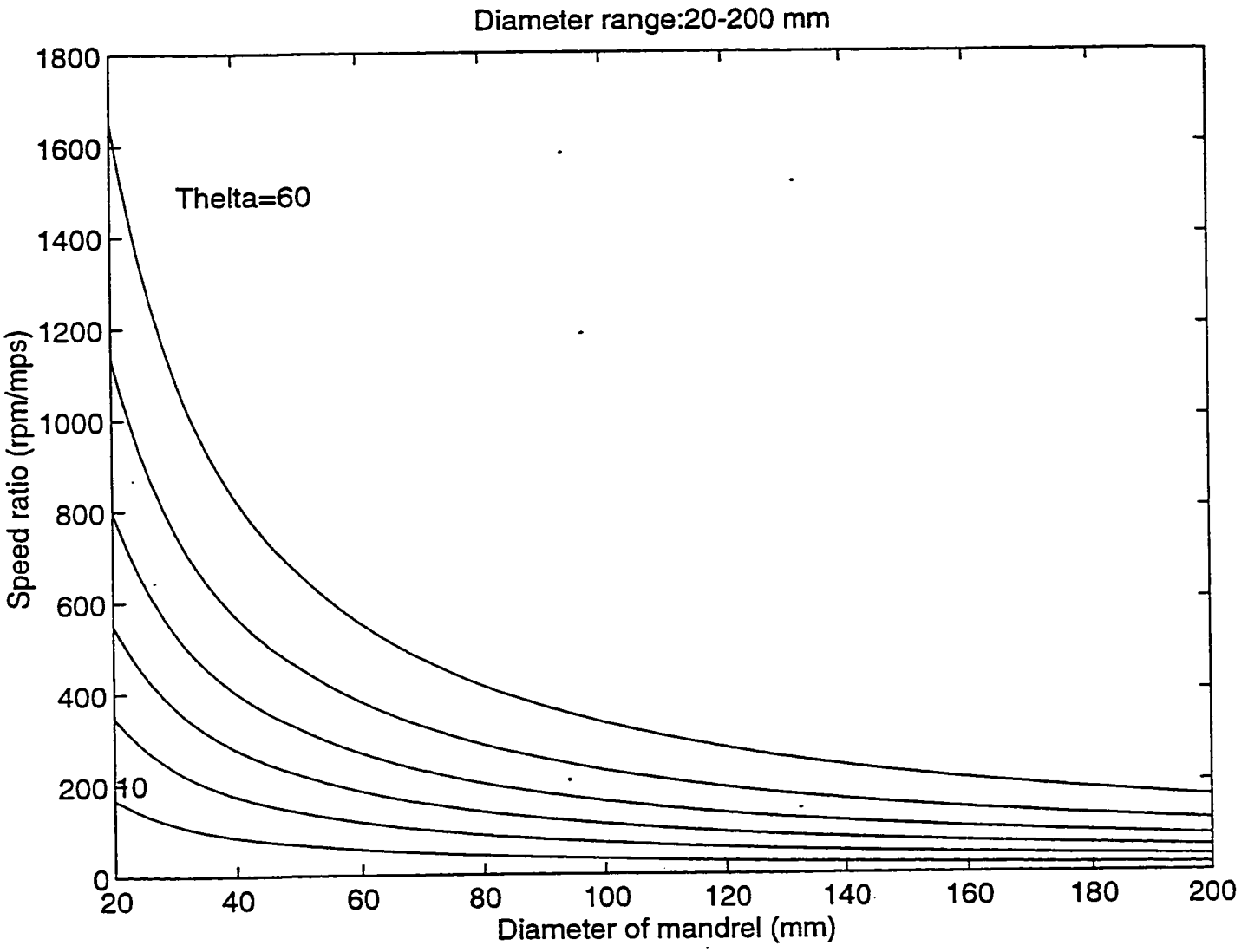

Fig 3.4 Speed ratio versus diameter of mandrel

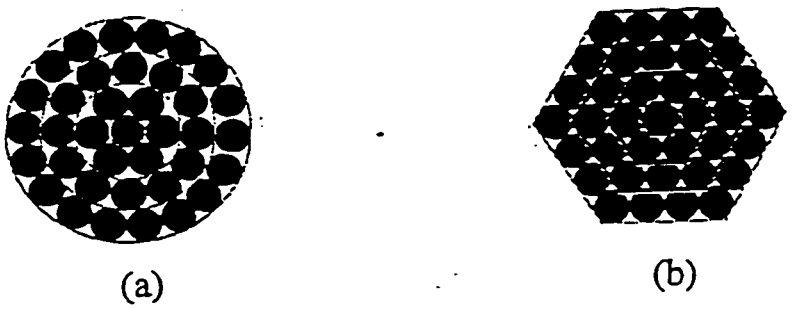

Fig 3.5 Fiber packing in yarns: (a) open-packing in circular yarns; (b) close-packing in hexagonal yarns. [2]

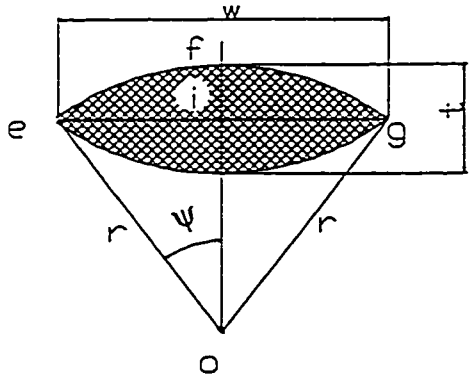

Fig 3.6 The cross sectional area of a yarn

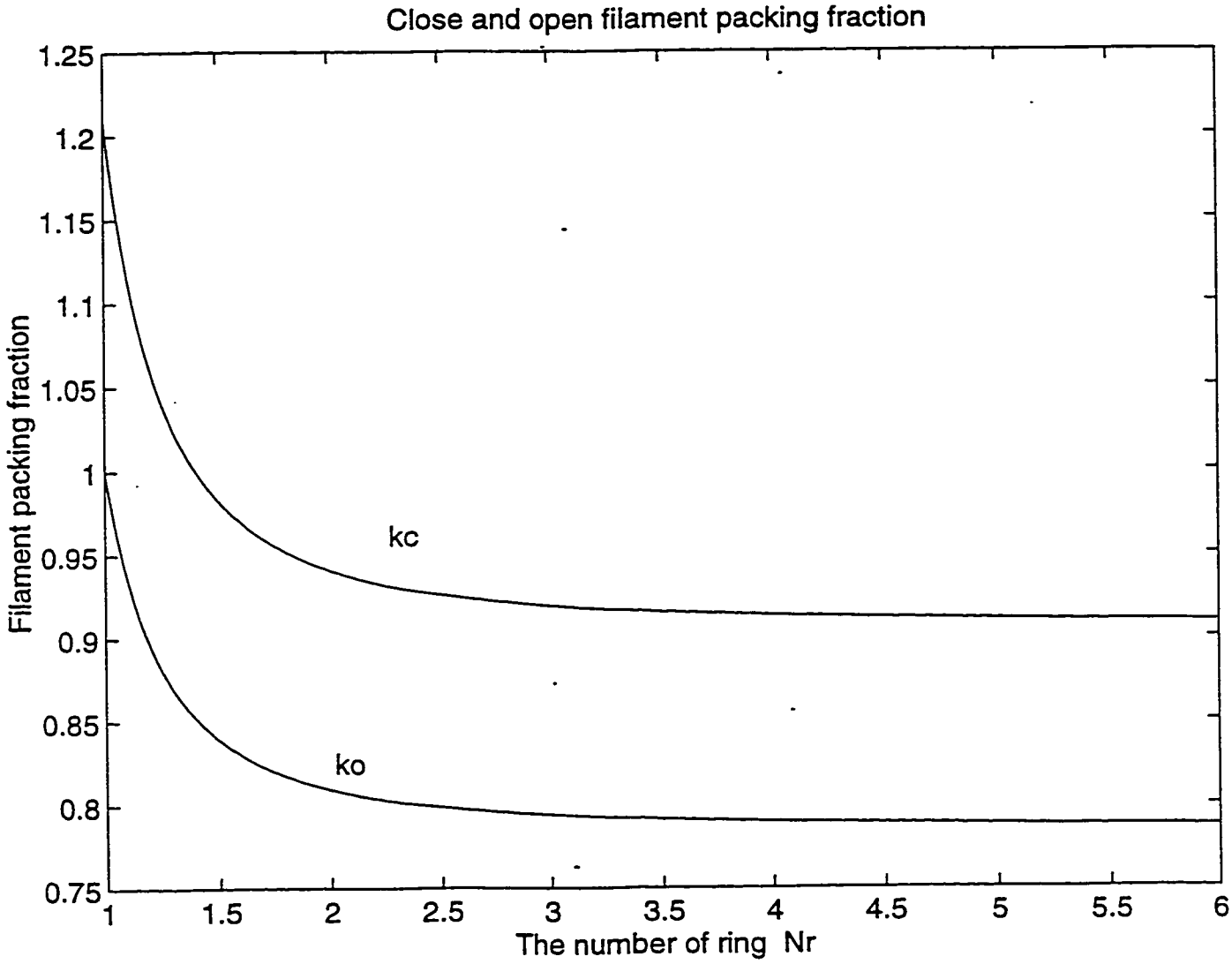

Fig 3.7 Filament packing fraction

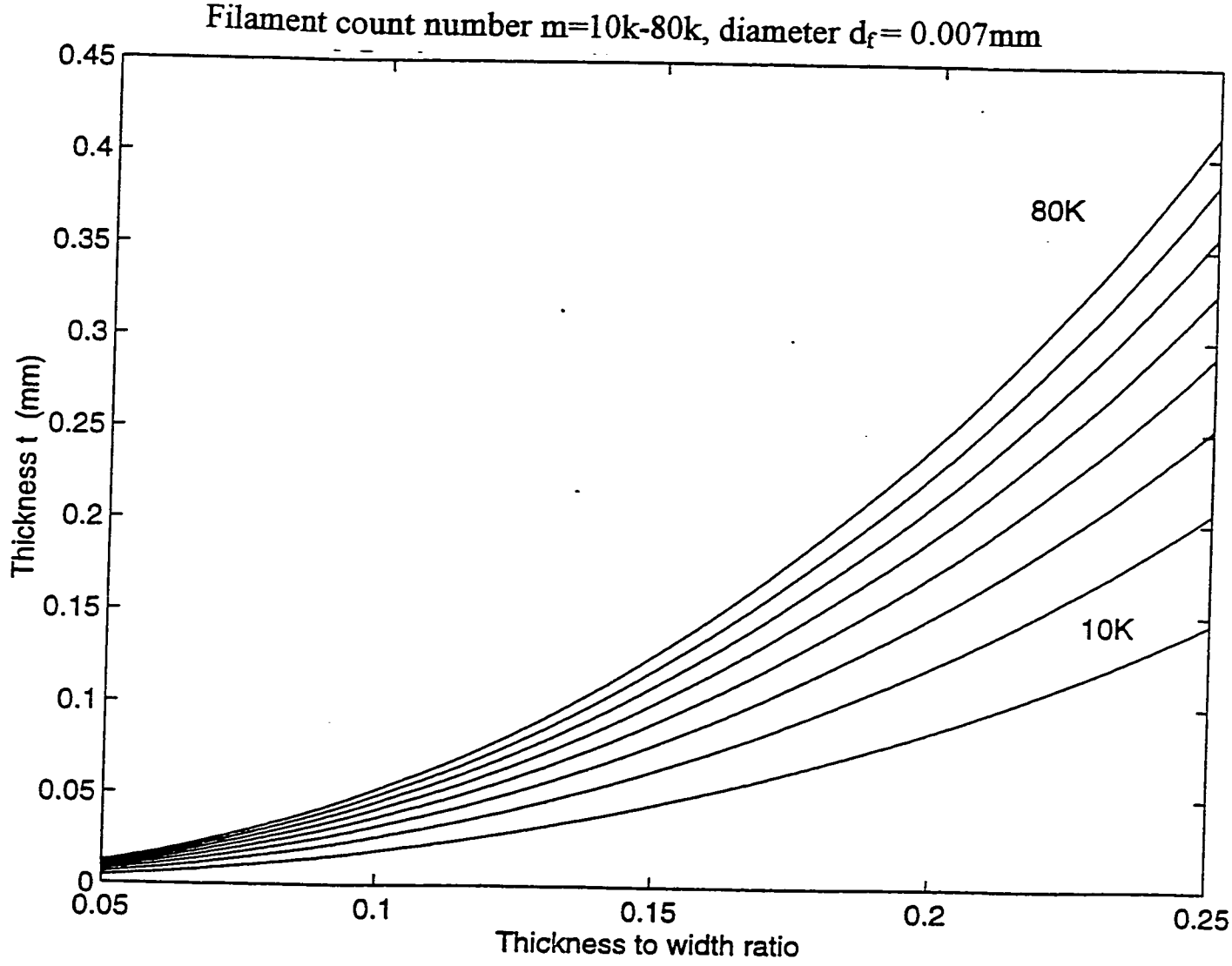

(a) ξ=0.05~0.25

Fig 3.8 Thickness versus ξ

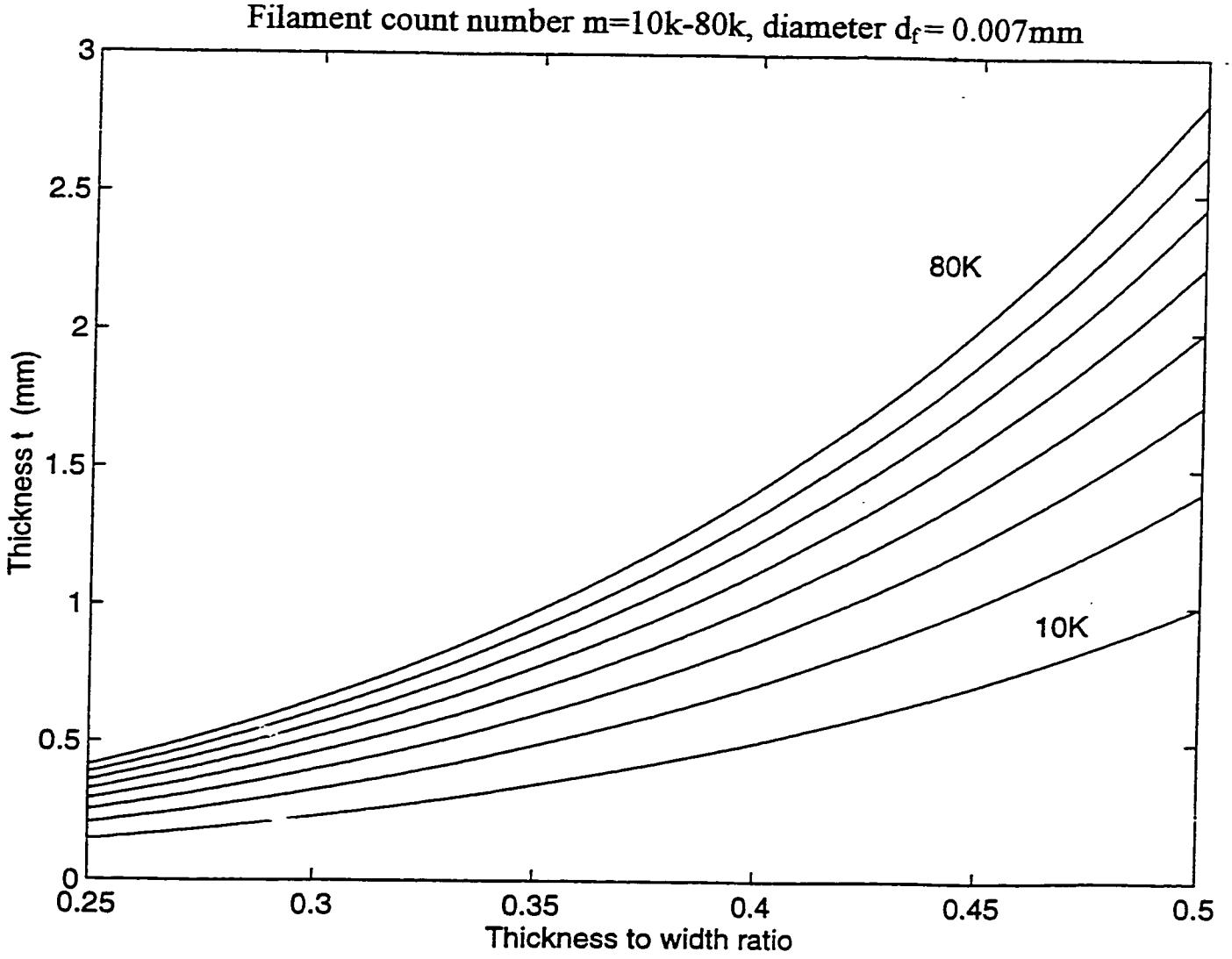

(b) ξ=0.25~0.5

Fig 3.8 Thickness versus ξ

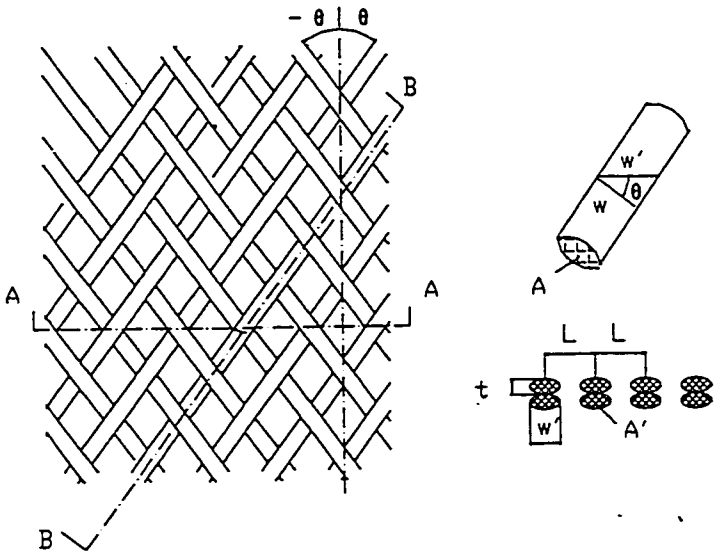

(a) 2×2 Braided preform (b) A-A cross section

Fig 3.9 One layer of biaxial braided preform

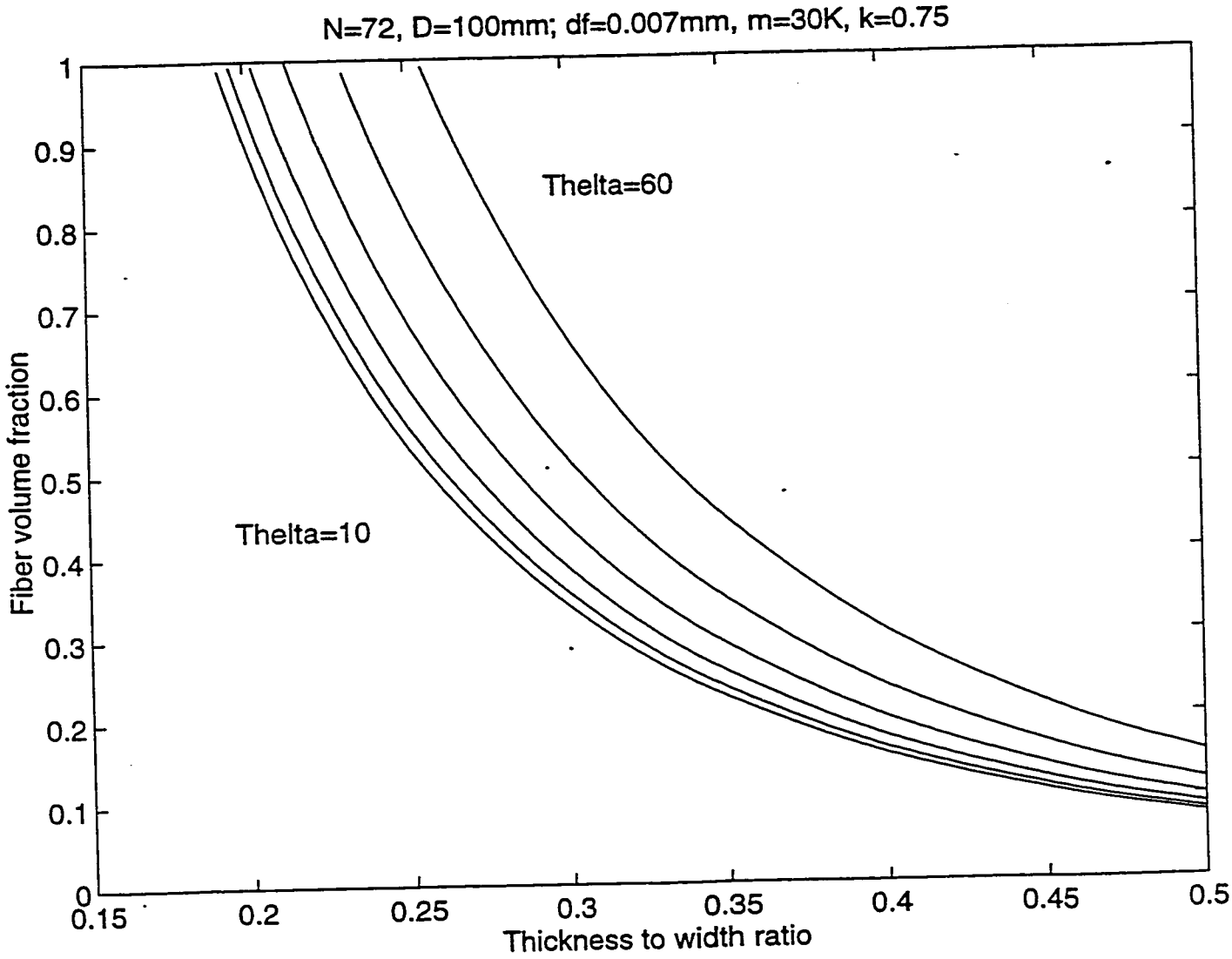

Fig 3.10 Fiber volume fraction versus ξ

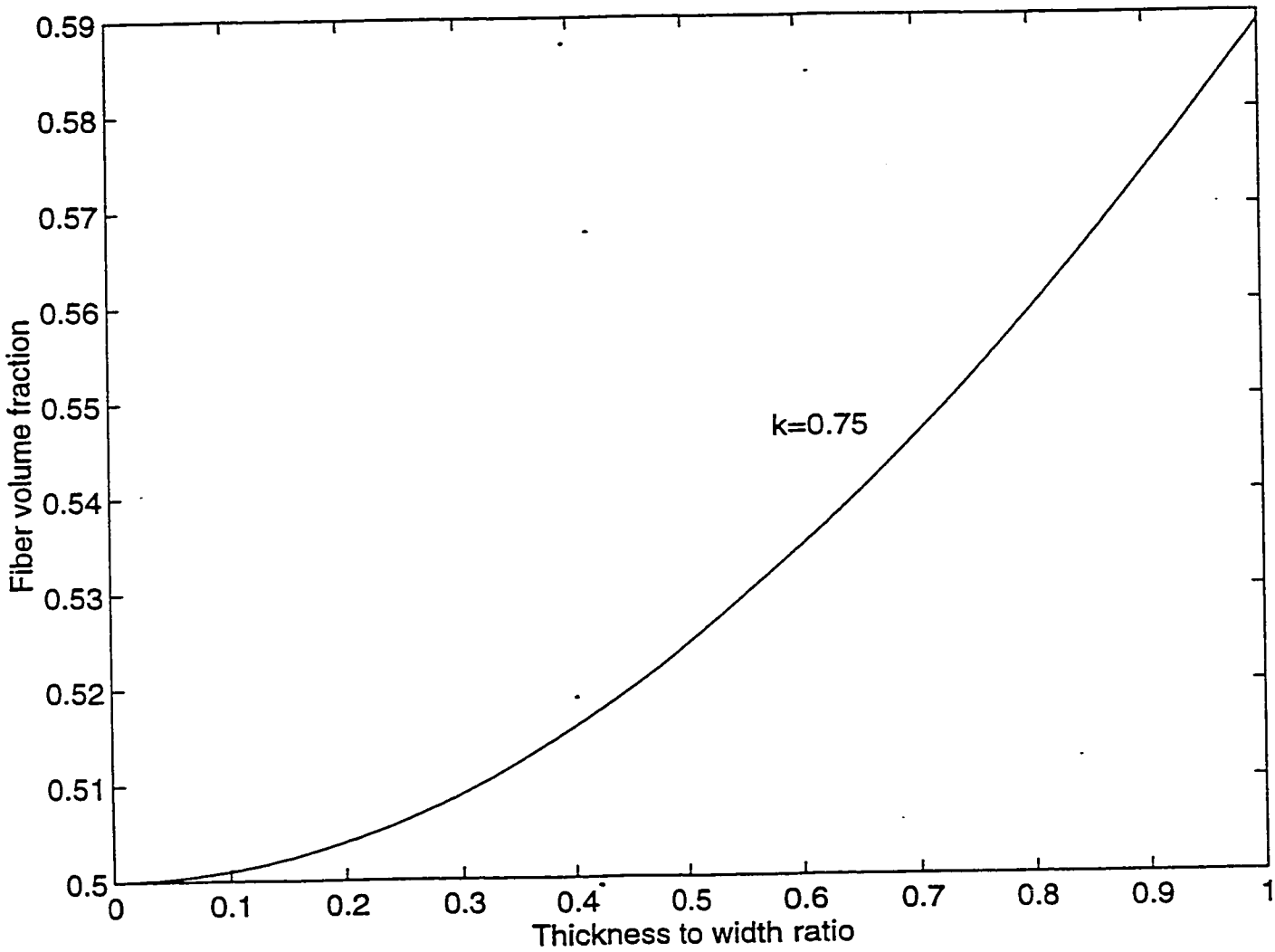

Fig 3.11 Upper limit of fiber volume fraction

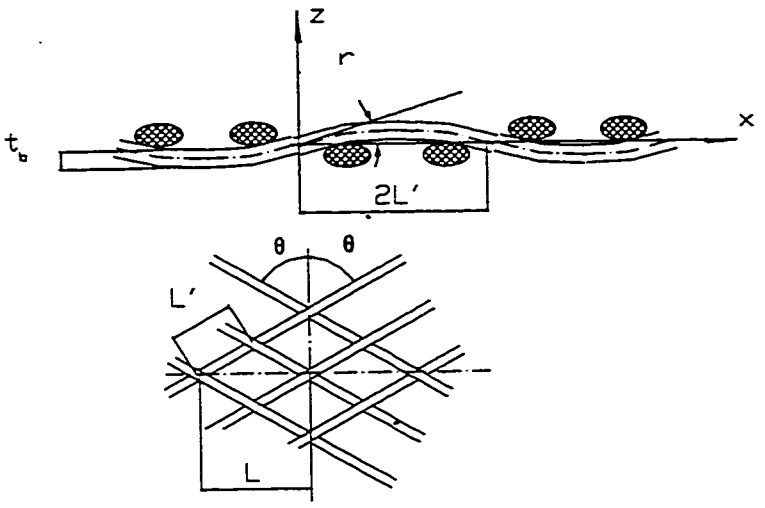

Fig 3.12 The yarn cross section along the braiding yarn direction

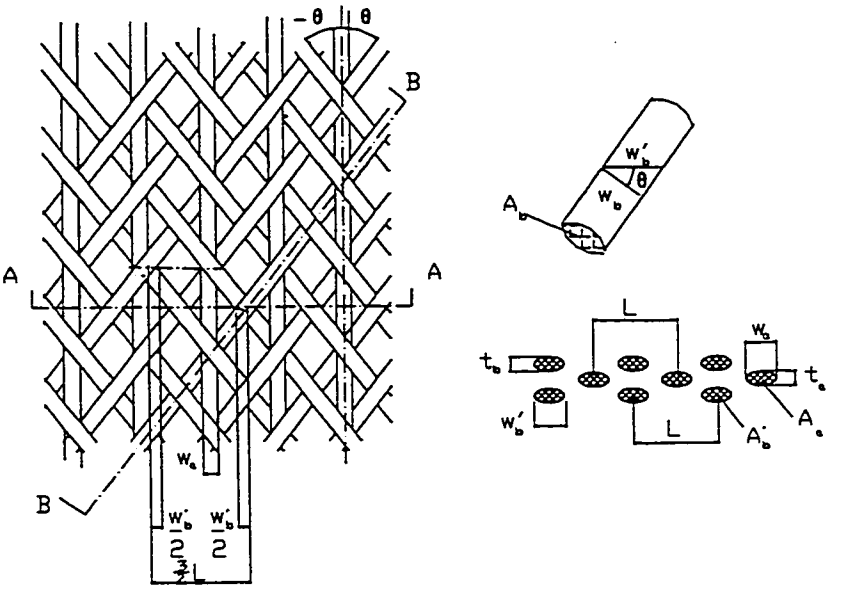

(a) 2×2 Braided preform (b) A-A cross section

Fig 3.13 One layer of triaxial braided preform

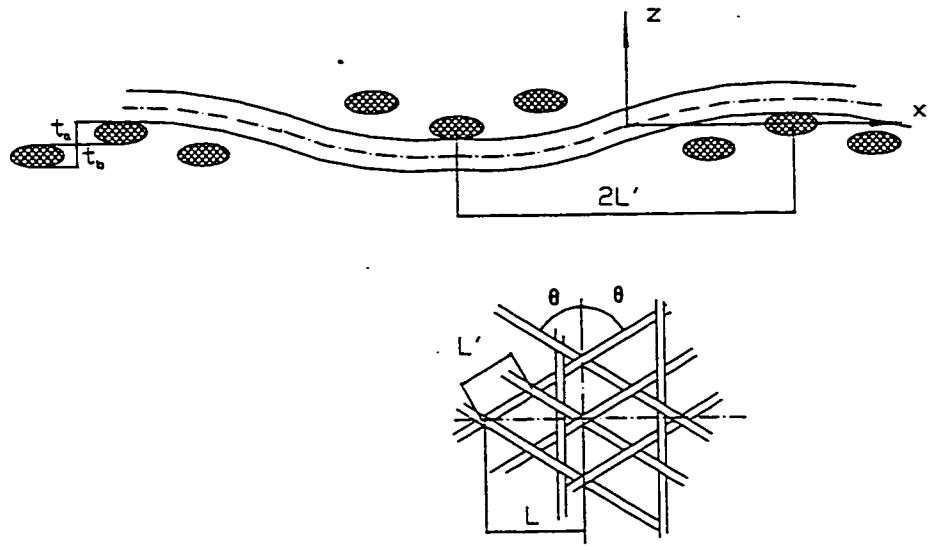

Fig 3.14 The cross section along the braiding yarn direction

Chapter 4 Mechanical behavior of two dimensionally triaxial braided composite materials

As described in chapter 3, the parameters of two dimensional braided composites are numerous. The experimental analysis of mechanical behavior is not so easy. Such analysis can only be performed on limited combinations of braiding parameters. It is necessary to develop a theoretical model to predict the mechanical behavior of braided composites for any kind of combination of braiding parameters.

John E. Masters et al [15], empirically defined the role of the braiding architecture in determining laminate mechanical behavior. A series of braided laminates were investigated in their paper. Their preform architectures were designed to isolate the effect of the braiding parameters on laminate response. A direct comparison with experimental results, therefore provided a measure of sensitivity of the laminate's mechanical properties to changes in the selected braid parameters. The laminates studied in their research are made of AS4 graphite fibers in Shell's 1895 epoxy matrix.

Rajik A. Naik et al [16,17], did many experimental and theoretical analyses for two dimensionally triaxial braided composites. Four different fiber architectures were tested in reference [16]. They were designed to provide a direct comparison of the effects of braid angle, yarn size and axial yarn content. A stress averaging technique [18] based on an iso-strain assumption within the RUC was used by these authors to compute overall composite properties such as three dimensional effective stiffness, coefficients of thermal expansion (CTE). By RUC, it means the repeat unit cell in a braided composite.

In this chapter a method based on energy of elastic deformation in braided composite is proposed for calculating the effective stiffness of 2-D braided composites. The iso-strain assumption is also adopted in our analyses. Seven cases are studied by using this energy method. The results are compared the experimental results given by John E. Master [15]and Rajiv A. Naik et al in paper [16].

4.1 Assumptions and coordinate systems

The braided composites consist of impregnated axial yarns, braiding yarns and matrix material. In the following analysis we assume,

(1) The matrix material is isotropic. Its properties are the same in all directions or are independent of the orientation of reference axes.

(2) Straight impregnated yarn is transversely isotropic material.

(3) The global strain tensor is same in any position of the braided composite (iso-strain assumption).

The reference coordinate system *123* is chosen along the principal direction of impregnated transversely isotropic yarn material. This system is called principal coordinate system. Axis *1* is along the fiber direction as shown in Fig 4-1. Axis *2*, *3* are along the direction of width and thickness respectively. The reference coordinate system *xyz* is the global coordinate system of braided composites. x is along the axial direction of axial yarns. y is perpendicular to x axis and in the plane of the braided composites, Fig 4-2.

The relation of global coordinate system *xyz* and the principal coordinate system *123* of an arbitrary chosen infinitesimal yarn segment is shown in Fig 4-3.

Any point in the braided composites can be represented by vector

$\{x, y, z\}^T$

or

$\{x', y', z'\}^T$

where

subscript ' denotes the principal coordinate system,

x', y', z' correspond to axis *1*, *2*, *3* respectively.

Let the directions of the principal coordinate axes *1*, *2*, *3* specified relative to the old system x, y, z by the table of directional cosines. In Table 4-1 l_{ij} is the cosine of the angle between principal axes *1*, *2*, *3*, and the global axes x, y, z.

Table 4-1 Directional cosines

	x	y	z
x'	l_{11}	l_{12}	l_{13}
y'	l_{21}	l_{22}	l_{23}
z'	l_{31}	l_{32}	l_{33}

Let

$$[l] = \begin{bmatrix} l_{11} & l_{12} & l_{13} \\ l_{21} & l_{22} & l_{23} \\ l_{31} & l_{32} & l_{33} \end{bmatrix}$$

In Fig 4.3, note that y' is always parallel to xy plane. We can easily get all the values of l_{ij} as follows,

$$[l]=\begin{bmatrix} \cos\gamma\cos\theta & \cos\gamma\sin\theta & \sin\gamma \\ -\sin\theta & \cos\theta & 0 \\ -\sin\gamma\cos\theta & -\sin\gamma\sin\theta & \cos\gamma \end{bmatrix} \tag{4-1}$$

So the principal and global coordinate are related by the following equations [19],

$$\begin{Bmatrix} x' \\ y' \\ z' \end{Bmatrix} = [l] \begin{Bmatrix} x \\ y \\ z \end{Bmatrix} \tag{4-2}$$

4.2 Transformation of stress and strain

The components of stress tensor in the principal system are denoted by,

$$\{\sigma'\} = \{\sigma_{11} \quad \sigma_{22} \quad \sigma_{33} \quad \tau_{23} \quad \tau_{31} \quad \tau_{12}\}^T \tag{4-3}$$

where

superscript T means transposition of matrix.

The components of strain tensor in principal coordinate system are represented by,

$$\{e'\} = \{\varepsilon_{11} \quad \varepsilon_{22} \quad \varepsilon_{33} \quad \varepsilon_{23} \quad \varepsilon_{31} \quad \varepsilon_{12}\}^T \tag{4-4}$$

The components of engineering strain have the form as follows,

$$\{\varepsilon'\} = \{\varepsilon_{11} \quad \varepsilon_{22} \quad \varepsilon_{33} \quad \gamma_{23} \quad \gamma_{31} \quad \gamma_{12}\}^T \tag{4-5}$$

As we know, the components of engineering strain and strain tensor have the following relations,

$$\begin{cases} \gamma_{23} = 2\varepsilon_{23} \\ \gamma_{31} = 2\varepsilon_{31} \\ \gamma_{12} = 2\varepsilon_{12} \end{cases} \tag{4-6}$$

So

$$\{\varepsilon'\} = [A]\{e'\} \tag{4-7}$$

Where

$$[A] = \begin{bmatrix} 1 & 0 & 0 & 0 & 0 & 0 \\ 0 & 1 & 0 & 0 & 0 & 0 \\ 0 & 0 & 1 & 0 & 0 & 0 \\ 0 & 0 & 0 & 2 & 0 & 0 \\ 0 & 0 & 0 & 0 & 2 & 0 \\ 0 & 0 & 0 & 0 & 0 & 2 \end{bmatrix} \tag{4-8}$$

The components of stress and strain tensors in global coordinate system are denoted by,

$$\{\sigma\} = \{\sigma_{xx} \quad \sigma_{yy} \quad \sigma_{zz} \quad \tau_{yz} \quad \tau_{zx} \quad \tau_{xy}\}^T \tag{4-9}$$

$$\{e\} = \{\varepsilon_{xx} \quad \varepsilon_{yy} \quad \varepsilon_{zz} \quad \varepsilon_{yz} \quad \varepsilon_{zx} \quad \varepsilon_{xy}\}^T \tag{4-10}$$

respectively, and the components of engineering strain in the global coordinate system are

$$\{\varepsilon\} = \{\varepsilon_{xx} \quad \varepsilon_{yy} \quad \varepsilon_{zz} \quad \gamma_{yz} \quad \gamma_{zx} \quad \gamma_{xy}\}^T \tag{4-11}$$

We can get

$$\{\varepsilon\} = [A]\{e\} \tag{4-12}$$

Where

[A] is given by equation (4-8).

The stress and strain tensors in the global and principal coordinate systems can be related by the following equations given by reference [19],

$$\{\sigma'\} = [T]\{\sigma\} \tag{4-13}$$

$$\{e'\} = [T]\{e\} \tag{4-14}$$

Where

$$[T]=\begin{bmatrix} l_{11}^2 & l_{12}^2 & l_{13}^2 & 2l_{12}l_{13} & 2l_{13}l_{11} & 2l_{11}l_{12} \\ l_{21}^2 & l_{22}^2 & l_{23}^2 & 2l_{22}l_{23} & 2l_{23}l_{21} & 2l_{21}l_{22} \\ l_{31}^2 & l_{32}^2 & l_{33}^2 & 2l_{32}l_{33} & 2l_{33}l_{31} & 2l_{31}l_{32} \\ l_{21}l_{31} & l_{22}l_{32} & l_{23}l_{33} & (l_{22}l_{33}+l_{32}l_{23}) & (l_{23}l_{31}+l_{33}l_{21}) & (l_{21}l_{32}+l_{31}l_{22}) \\ l_{31}l_{11} & l_{32}l_{12} & l_{33}l_{13} & (l_{32}l_{13}+l_{12}l_{33}) & (l_{33}l_{11}+l_{13}l_{31}) & (l_{31}l_{12}+l_{11}l_{32}) \\ l_{11}l_{21} & l_{12}l_{22} & l_{13}l_{23} & (l_{12}l_{23}+l_{22}l_{13}) & (l_{13}l_{21}+l_{23}l_{11}) & (l_{11}l_{22}+l_{21}l_{12}) \end{bmatrix} \quad (4\text{-}15)$$

Substitute (4-12), (4-14) to (4-7),

$$\{\varepsilon'\}=[A][T]\{e\}=[A][T][A]^{-1}\{\varepsilon\}=[B]\{\varepsilon\} \quad (4\text{-}16)$$

where

$$[B]=[A][T][A]^{-1} \quad (4\text{-}17)$$

4.3 The stress-strain relations in the principal coordinate system

4.3.1 Isotropic matrix material

An isotropic material is characterized by an infinite number of planes of material symmetry through a point. Thus, an isotropic material is fully characterized by only two independent constant E and ν, where E is the Young's modulus and ν is the Poisson's ratio. The shear modulus G can obtained by E and ν,

$$G=\frac{E}{2(1+\nu)} \quad (4\text{-}18)$$

The stress-strain relations are represented by Hooke's Law [20],

$$\{\varepsilon'\}=[S_m]\{\sigma'\} \quad (4\text{-}19)$$

or

$$\{\sigma'\}=[C_m]\{\varepsilon'\} \quad (4\text{-}20)$$

Where

subscript m denotes matrix material,

$[C_m]$, $[S_m]$ are the stiffness and compliance matrix of matrix materials respectively.

$$[S_m]=\begin{bmatrix} \frac{1}{E} & \frac{-\nu}{E} & \frac{-\nu}{E} & 0 & 0 & 0 \\ \frac{-\nu}{E} & \frac{1}{E} & \frac{-\nu}{E} & 0 & 0 & 0 \\ \frac{-\nu}{E} & \frac{-\nu}{E} & \frac{1}{E} & 0 & 0 & 0 \\ 0 & 0 & 0 & \frac{1}{G} & 0 & 0 \\ 0 & 0 & 0 & 0 & \frac{1}{G} & 0 \\ 0 & 0 & 0 & 0 & 0 & \frac{1}{G} \end{bmatrix} \tag{4-21}$$

$$[C_m]=[S_m]^{-1} \tag{4-22}$$

4.3.2 Transversely isotropic material of impregnated straight yarn

An orthotropic material is called transversely isotropic when one of its principal planes is a plane of isotropy, i. e. at every point there is a plane on which the mechanical properties are the same in all the directions.

An orthotropic material with transverse isotropy is characterized by only five independent elastic constants, that is E_1, E_2, G_{12}, ν_{12}, ν_{23}. The stress-strain relations are as following [20] ,

$$\{\varepsilon'\}=[S_y]\{\sigma'\} \tag{4-23}$$

or

$$\{\sigma'\}=[C_y]\{\varepsilon'\} \tag{4-24}$$

Where

subscript y denotes straight impregnated yarn,

$[C_y]$, $[S_y]$ are the stiffness and compliance matrix of impregnated straight yarn respectively,

$$[C_y]=[S_y]^{-1} \tag{4-25}$$

$$[S_y]=\begin{bmatrix} S_{11} & S_{12} & S_{12} & 0 & 0 & 0 \\ S_{12} & S_{22} & S_{23} & 0 & 0 & 0 \\ S_{12} & S_{23} & S_{22} & 0 & 0 & 0 \\ 0 & 0 & 0 & 2(S_{22}-S_{23}) & 0 & 0 \\ 0 & 0 & 0 & 0 & S_{66} & 0 \\ 0 & 0 & 0 & 0 & 0 & S_{66} \end{bmatrix} \tag{4-26}$$

Where

$$\begin{cases} S_{11}=\dfrac{1}{E_1} \\ S_{22}=\dfrac{1}{E_2} \\ S_{66}=\dfrac{1}{G_{12}} \\ S_{12}=\dfrac{-\nu_{21}}{E_2}=\dfrac{-\nu_{12}}{E_1} \\ S_{23}=-\dfrac{\nu_{23}}{E_2} \end{cases} \tag{4-27}$$

4.4 The effective stiffness and compliance matrix of braided composites

An energy method is used in this section to deduce the effective stiffness of braided composites. For this, define the effective stress as the average stress over a repeat unit cell.

The effective stresses of braided composite is

$$\{\bar{\sigma}\}=\{\bar{\sigma}_{xx},\bar{\sigma}_{yy},\bar{\sigma}_{zz},\bar{\tau}_{yz},\bar{\tau}_{zx},\bar{\tau}_{xy}\} \tag{4-28}$$

The effective stress-strain relations are as follows,

$$\{\varepsilon\}=[\bar{S}]\{\bar{\sigma}\} \tag{4-29}$$

$$\{\bar{\sigma}\}=[\bar{C}]\{\varepsilon\} \tag{4-30}$$

Where

$[\bar{S}]$, $[\bar{C}]$ are 6×6 effective compliance and effective stiffness matrix of the braided composite respectively,

$$[\bar{S}]=[\bar{C}]^{-1} \tag{4-31}$$

4.4.1 The effective stiffness matrix of braiding yarn

A repeat unit cell (RUC) is shown in Fig 4.4. The whole braided composite consists of many repeat unit cells. The behavior of the RUC can be used to represent the behavior of the whole braided composite.

A braided yarn segment in left half unit cell is shown in Fig 4.5. The effective stress of braiding yarn segment is denoted as,

$$\{\bar{\sigma}_b\}=\{\bar{\sigma}_{bxx},\bar{\sigma}_{byy},\bar{\sigma}_{bzz},\bar{\tau}_{byz},\bar{\tau}_{bzx},\bar{\tau}_{bxy}\} \tag{4-32}$$

Where

subscript b denotes braiding yarn.

So the stress and strain relations of the braiding yarn segment are represented as

$$\{\bar{\sigma}_b\} = [C_b]\{\varepsilon\} \tag{4-33}$$

The energy of elastic deformation stored in the braiding yarn segment is

$$E_b = \frac{1}{2}\int_0^S \{\sigma'\}^T \{\varepsilon'\} A_b ds \tag{4-34}$$

or

$$E_b = \frac{1}{2}\{\bar{\sigma}_b\}^T \{\varepsilon\} A_b S \tag{4-35}$$

Where

A_b is the cross-sectional area of the braiding yarn,

S is the total length of the braiding yarn segment in Fig 4.5,

$$S = \int_{-L'}^{L'} \sqrt{1 + (\frac{dz}{dx})^2}\ dx \tag{4-36}$$

where

z is given by Equation (3-89).

Substitute (4-33) to (4-35)

$$E_b = \frac{1}{2}\{\varepsilon\}^T [C_b]\{\varepsilon\} A_b S \tag{4-37}$$

Substitute (4-24) to (4-34)

$$E_b = \frac{1}{2}\int_{-L'}^{L'} \{\varepsilon'\}^T [C_y]\{\varepsilon'\} A_b \sqrt{1 + (\frac{dz}{dx})^2}\ dx \tag{4-38}$$

Further substitute (4-16) to (4-38)

Then

$$E_b = \frac{1}{2}\{\varepsilon\}^T \left(\int_{-L'}^{L'} [B]^T [C_y][B] \sqrt{1+\left(\frac{dz}{dx}\right)^2}\, dx \right) \{\varepsilon\} A_b \tag{4-39}$$

where

[B] is given by Equation (4-17).

From Equation (4-37), (4-39) and note that the strain $\{\varepsilon\}$ can be arbitrary values,

So

$$[C_b] = \frac{1}{S} \int_{-L'}^{L'} [B]^T [C_y] [B] \sqrt{1+\left(\frac{dz}{dx}\right)^2}\, dx \tag{4-40}$$

4.4.2 The effective stiffness matrix of braided composite

Because the elastic deformation energy of left and right half RUC are same, only the left half RUC are chosen to calculate the energy . The left half RUC is shown in Fig 4.6.

The total elastic deformation energy stored in the half RUC is

$$E = \frac{1}{2}\{\bar{\sigma}\}^T \{\varepsilon\} Ah = \frac{1}{2}\{\varepsilon\}^T [\bar{C}]\, \{\varepsilon\} Ah \tag{4-41}$$

Where

A is the cross-sectional area of the left half RUC

$$A = (t_a + 2t_b)\, L \tag{4-42}$$

and also

$$E = E_b + E_a + E_m \tag{4-43}$$

Where

E_b is the elastic deformation energy stored in the braided yarn segment,

E_a is the elastic deformation energy stored in the axial yarn segment,

E_m is the elastic deformation energy stored in matrix material.

(1) There are two braiding yarn segments with ±θ in the left half RUC, so the elastic deformation energy of braiding yarns is,

$$E_b = \frac{1}{2}\left(\{\bar{\sigma}\}_{+\theta}^T\{\varepsilon\} + \{\bar{\sigma}\}_{-\theta}^T\{\varepsilon\}\right)A_b S \tag{4-44}$$

Where

A_b is the cross-sectional area of the braiding yarn,

S is the total length of the braiding yarn segment in Fig 4.5.

From Fig 4.6 , assume the braiding yarn is straight, then

$$S \approx \frac{h}{\cos\theta\cos\gamma} \tag{4-45}$$

From Equation (3-66)

$A_b = A_b'\cos\delta$

So

$$SA_b \approx \frac{A_b' h}{\cos\gamma} \tag{4-46}$$

Substitute Equation (4-33), (4-46) into (4-44), and note that the subscript ±θ denotes the ±θ braiding yarn respectively,

So

$$E_b = \frac{1}{2}\left(\{\varepsilon\}^T [C_b]_{+\theta} \{\varepsilon\} + \{\varepsilon\}^T [C_b]_{-\theta} \{\varepsilon\}\right) A_b S \approx \frac{1}{2}\{\varepsilon\}^T \left([C_b]_{+\theta} + [C_b]_{-\theta}\right)\{\varepsilon\} \frac{A_b' h}{\cos\gamma}$$

(4-47)

(2) There is only one axial yarn segment in the left half RUC, so the elastic deformation energy is,

$$E_a = \frac{1}{2}\{\varepsilon\}^T [C_y] \{\varepsilon\} A_a h \tag{4-48}$$

(3) The elastic deformation energy stored in matrix material in the left half RUC is,

$$E_m = \frac{1}{2}\{\varepsilon\}^T [C_m] \{\varepsilon\} A_m h \tag{4-49}$$

(4) Effective stiffness of braided composites

From Equation (4-41), (4-43), (4-47) to (4-49), we can get the effective stiffness of braided composites as follows,

$$\begin{aligned}[\bar{C}] &= \left(\frac{[C_b]_{+\theta} + [C_b]_{-\theta}}{2}\right) \frac{2A_b'}{A} \frac{1}{\cos\gamma} + [C_y] \frac{A_a}{A} + [C_m] \frac{A_m}{A} \\ &= \left(\frac{[C_b]_{+\theta} + [C_b]_{-\theta}}{2}\right) \frac{2A_b'}{2A_b' + A_a} \frac{2A_b' + A_a}{A} \frac{1}{\cos\gamma} + [C_y] \frac{A_a}{2A_b' + A_a} \frac{2A_b' + A_a}{A} \\ &\quad + [C_m] \frac{A_m}{A}\end{aligned}$$

(4-50)

From Equation (3-36), (3-67), (4-42)

$$V_f = \frac{k(2A_b^{'} + A_a)}{\frac{\pi D}{N/2}(2t_b + t_a)} = \frac{k(2A_b^{'} + A_a)}{L\,(2t_b + t_a)} = \frac{k(2A_b^{'} + A_a)}{A}$$

So

$$\frac{2A_b^{'} + A_a}{A} = \frac{V_f}{k} \tag{4-51}$$

From Equation (3-93)

$$\chi = \frac{A_a}{2A_b^{'} + A_a} \tag{4-52}$$

Substitute Equation (4-51), (4-52) into (4-50),

Finally we get,

$$[\overline{C}] = \left(\frac{[C_b]_{+\theta} + [C_b]_{-\theta}}{2}\right)\frac{(1-\chi)}{\cos\gamma}\frac{V_f}{k} + [C_y]\,\chi\frac{V_f}{k} + [C_m]\,(1-\frac{V_f}{k}) \tag{4-53}$$

where

$[C_b]$ is given by Equation (4-40),

$[\chi]$ is given by Equation (3-94),

V_f is given by Equation (3-68),

$[C_y]$ is given by Equation (4-25),

$[C_m]$ is given by Equation (4-22),

γ is given by Equation (3-92).

Generally, $\gamma < 20°$, so $\cos\gamma \approx 1$, thus Equation (4-53) can be simplified to

$$[\overline{C}] = \left\{ \left(\frac{[C_b]_{+\theta} + [C_b]_{-\theta}}{2} \right) (1-\chi) + [C_y]\chi \right\} \frac{V_f}{k} + [C_m]\left(1 - \frac{V_f}{k}\right) \tag{4-54}$$

The above Equation has an obviously physical meaning. It is an average by volume fraction of all components. The effective stiffness consists of contributions of overall yarn stiffness and matrix material stiffness. The yarn volume fraction is $\frac{V_f}{k}$, so the contribution of yarn material is $\frac{V_f}{k}$, the contribution of matrix material is $\left(1 - \frac{V_f}{k}\right)$. There are two different kinds of impregnated yarns in braided composites, braiding yarns and axial yarns. Each of them contributes a part of stiffness to the overall yarn stiffness. Because the percentage by volume of axial yarns in a braided preform is χ, so the contribution of axial yarns is χ while the contribution of braiding yarns is $(1-\chi)$.

4.5 The discrete equations for numerical analysis

We use Equation (4-53) to design Matlab program of effective stiffness matrix. If we discretize the braiding yarn into small segments, then the discrete form of Equation (4-36) is as follows,

$$S = \sum_{i=-n}^{n-1}\left(\sqrt{1+\left(\frac{dz}{dx}\right)^2}\right)\Delta x \tag{4-55}$$

From Equation (3-89)

$$\frac{dz}{dx} = \frac{(t_a + t_b)\,\pi}{4L'}\cos\left(\frac{\pi x}{2L'}\right) \tag{4-56}$$

Substitute Equation (4-56) to (4-55)

$$S = \sum_{i=-n}^{n-1}\left(\sqrt{1+\left(\frac{(t_a + t_b)\pi}{4L'}\cos\left(\frac{\pi x}{2L'}\right)\right)^2}\right)\Delta x \tag{4-57}$$

where

L' is given by Equation (3-90)

$$\Delta x = \frac{L'}{n} \tag{4-58}$$

$$\begin{cases} x_{i+1} = x_i + \Delta x \\ x_{-n} = -L' \end{cases} \quad (i = -n, -(n-1), \ldots\ldots, (n-1)) \tag{4-59}$$

The discrete form of Equation (4-40) is as follows,

$$[C_b] = \frac{1}{S}\sum_{i=-n}^{n-1}[B]^T[C_y][B]\sqrt{1+\left(\frac{dz}{dx}\right)^2}\,\Delta x \tag{4-60}$$

4.6 The comparison of effective stiffness between the experimental results [15], [16] and the theoretical results

The values of fiber volume fraction V_f and braiding yarn thickness t_b from our theoretical analyses are used to calculate the effective stiffness of braided composites. These values are listed in Tables 3-2, and 3-4. The elastic constants of impregnated yarn and resin are chosen from reference [15], and listed in Table 4-2. The yarns are made of AS4 graphite fibers impregnated with Shell's 1895 epoxy matrix.

When the theoretical results are compared with experimental results of reference [15] in Table 4-3, the maximum relative errors of E_{xx}, E_{yy}, G_{xy}, ν_{xy} are 19.1 %, 12.5 %, 13.8 %, 11.7 % respectively.

When the theoretical results are compared with experimental results of reference [16] in table 4-4, the maximum relative errors of E_{xx}, E_{yy}, G_{xy}, ν_{xy} are 5.17%. 7.4 %, 7.23 %, 1.53 % respectively.

Table 4-2 Elastic constants of impregnated yarn and resin [15]

Material	E_{11}, GPa	E_{22}, GPa	G_{12}, GPa	ν_{12}	ν_{23}
Yarn	144.80	11.73	5.52	0.23	0.3
Resin	3.45	3.45	1.28	0.35	0.35

Table 4-3 Effective stiffness of experiment [15] and proposed theory

Material type	Axial Modulus Exx, GPa		Transverse Modulus Eyy, GPa		Shear Modulus Gxy, GPa		Poisson's ratio ν_{xy}	
	Exp.[15]	Theory	Exp.[15]	Theory	Exp.[15]	Theory	Exp.[15]	Theory
$[0_{18k}/\pm 66.5_{6k}]$ 37.6% Axial (6.10mm)	53.3	45.2	56.5	49.4	12.8	11.2	0.223	0.197
$[0_{18k}/\pm 66.5_{6k}]$ 37.6% Axial (5.25mm)	55.4	44.8	53.4	48.6	13.8	11.9	0.197	0.196
$[0_{18k}/\pm 66.5_{6k}]$ 37.6% Axial (4.8mm)	53.5	44.8	47.6	48.2	13.5	11.8	0.199	0.195

Table 4-4 Effective stiffness of experiment [16] and proposed theory

Material type	Axial Modulus Exx, GPa		Transverse Modulus Eyy, GPa		Shear Modulus Gxy, GPa		Poisson's ratio ν_{xy}	
	Exp.[16]	Theory	Exp.[16]	Theory	Exp.[16]	Theory	Exp.[16]	Theory
$[0_{30k}/\pm70_{6k}]$ 46% Axial (6.05mm)	55.67	58.55	49.3	52.85	9.68	10.38	0.15	0.152
$[0_{75k}/\pm70_{15k}]$ 46% Axial (11.04mm)	59.63	58.54	53.38	53.31	10.38	10.43	0.15	0.152
$[0_{36k}/\pm45_{15k}]$ 46% Axial (5.52mm)	62.67	62.68	20.78	21.47	18.40	18.25	0.65	0.642
$[0_{6k}/\pm45_{15k}]$ 12% Axial (5.52mm)	27.92	28.87	20.13	21.16	26.00	26.99	0.73	0.724

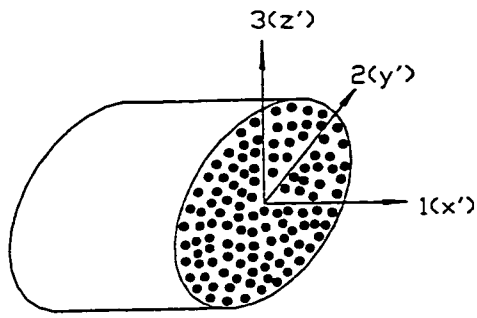

Fig 4.1 The principal coordinate system

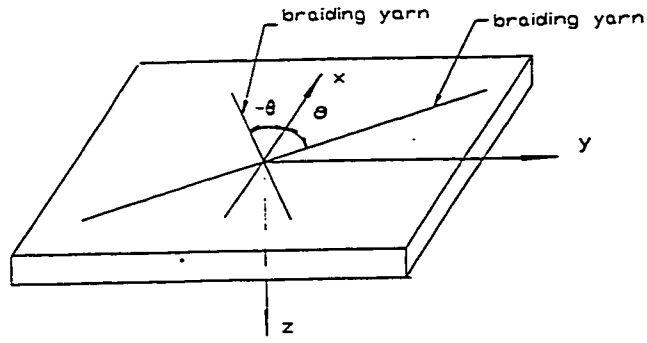

Fig 4.2 The global coordinate system

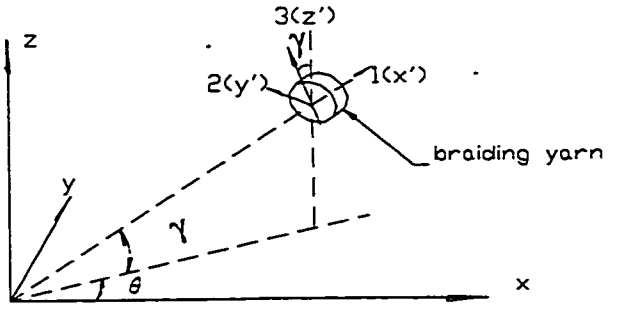

Fig 4.3 The transformation between principal and global coordinate system

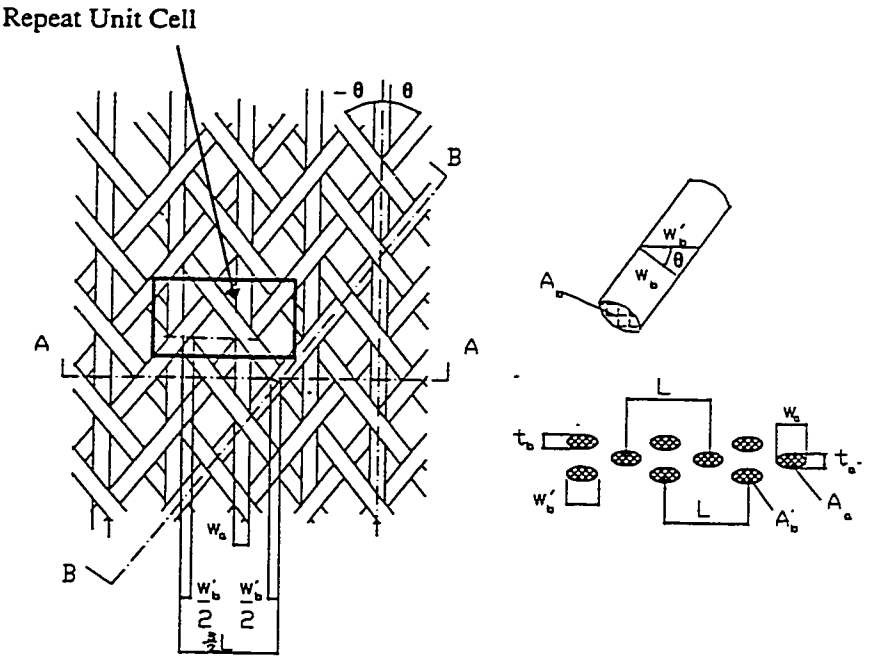

(a) 2×2 Braided Composite (b) A-A cross section

Fig 4-4 The repeat unit cell in a triaxial braided composite

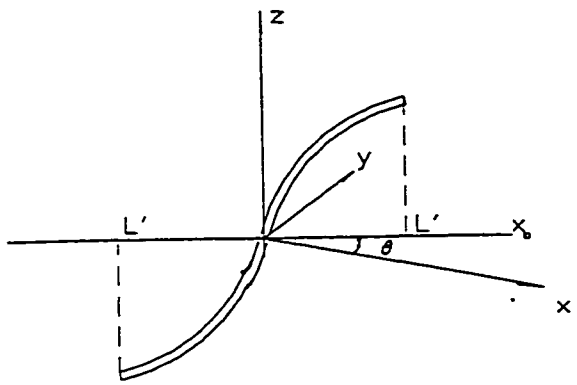

Fig 4.5 The length of a braiding yarn segment

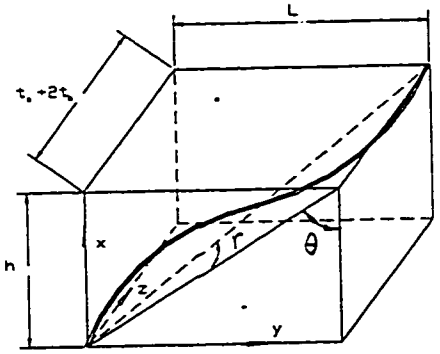

Fig 4.6 The left haft RUC (-θ braiding yarn and axial yarn segment are not plotted)

Chapter 5 Hygrothermal behavior of 2-D braided composites

After fabrication, composite structures operate in a variety of thermal and moisture environments that may have a pronounced impact on their performance. These hygrothermal effects are a result of the temperature and moisture content variations and are related to the difference in thermal and hygro properties of the constituents. Analysis of the processing and hygrothermal effects is an important component of the overall structural design and analysis. The performance of a composite structure is a function of its environment history, temperature and moisture distributions, processing and hygrothermal stresses, and property variations with temperature and moisture [20].

In this chapter, we use the virtual work method to deduce the effective coefficients of thermal expansion and hygro expansion.

5.1 The virtual work method

Let us consider the RUC in Fig 5.1, which is cut out from Fig4.4. assume there are initial strains in the RUC, which may be thermal strains, hygro strains, plastic strains, or any other strains caused by some reasons, or a combination of them. The residual stresses caused by initial strains are in self-equilibrium, so the resultant force of surface traction of the RUC equals to zero.

As shown in Fig 5.2, the surface traction vector on the top edge of the RUC is

$$\{F\} = \left\{F_x, F_y, F_z\right\}^T \tag{5-1}$$

So

$$\iint_{\Omega} \{F\} d\Omega = 0 \tag{5-2}$$

Where

Ω is the total surface area of the top edge of the RUC.

If we give a constant virtual deflection vector along the top edge

$$\{\delta^*\} = \{\delta^*_x, \delta^*_y, \delta^*_z\}^T \tag{5-3}$$

The corresponding virtual strain vector is

$$\{\varepsilon^*\} = \{\varepsilon^*_{xx}, \varepsilon^*_{yy}, \varepsilon^*_{zz}, \varepsilon^*_{yz}, \varepsilon^*_{zx}, \varepsilon^*_{xy}\}^T \tag{5-4}$$

which is same at any point of the RUC.

From Equation (5-2) , we get

$$\left\{\iint_{\Omega} \{F\}^T d\Omega\right\} \{\delta^*\} = 0 \tag{5-5}$$

The virtual work done by $\{F\}$ is

$$W^* = \iint_{\Omega} \{F\}^T \{\delta^*\} d\Omega = \left\{\iint_{\Omega} \{F\}^T d\Omega\right\} \{\delta^*\} = 0 \tag{5-6}$$

As we know, the virtual work done by the surface traction of a RUC should be equal to the virtual elastic deformation energy stored in the RUC,

thus

$$E^* = W^* = 0 \tag{5-7}$$

The virtual energy consists of three components, E_b^*, E_a^*, E_m^*,

$$E^* = E_b^* + E_a^* + E_m^* \tag{5-8}$$

where

E_b^* is the virtual energy of elastic deformation stored in braiding yarn segments,

E_a^* is the virtual energy of elastic deformation stored in axial yarn segments,

E_m^* is the virtual energy of elastic deformation stored in matrix material.

5.2 The residual stress vectors in the principal coordinate system

The residual stress vector in the principal coordinate system is

$$\{\sigma'\} = [C]\{\varepsilon_e'\} \tag{5-9}$$

For impregnated straight yarn,

$$[C] = [C_y] \tag{5-10}$$

For matrix material

$$[C] = [C_m] \tag{5-11}$$

where

$[C_y]$ is the stiffness matrix of impregnated straight yarn, which is given by Equation (4-25),

$[C_m]$ is the stiffness matrix of matrix material, which is given by Equation (4-22),

$\{\varepsilon_e'\}$ is the elastic strain vector, subscript e denotes elastic deformation.

The total strain vector is as follows,

$$\{\varepsilon'\} = \{\varepsilon_e'\} + \{\varepsilon_0'\} \tag{5-12}$$

Where $\{\varepsilon_0'\}$ is the initial strain vector.

So

$$\{\varepsilon_e'\} = \{\varepsilon'\} - \{\varepsilon_0'\} \tag{5-13}$$

Substitute Equation (5-13), (4-16) into Equation (5-9),

$$\{\sigma'\} = [C]\{\varepsilon'\} - [C]\{\varepsilon_0'\} = [C][B]\{\varepsilon\} - [C]\{\varepsilon_0'\} \tag{5-14}$$

Thus, for the impregnated straight yarn,

$$\{\sigma'\} = [C_y][B]\{\varepsilon\} - [C_y]\{\varepsilon_{0y}'\} \tag{5-15}$$

The matrix material is isotropic,

so

$$\{\sigma'\} = [C_m]\{\varepsilon\} - [C_m]\{\varepsilon_{0m}'\} \tag{5-16}$$

5.3 The analysis of virtual energy of elastic deformation

(1) The virtual energy E_b^*

In Fig 5.1, there are four braiding yarn segments, two of them with +θ braiding angle, and another two with -θ braiding angle. The virtual energy is as following,

$$E_b^* = 2\left(\frac{1}{2}\int_0^s \{\sigma'\}^T \{\varepsilon^{*'}\} A_b dS\right)_{+\theta} + 2\left(\frac{1}{2}\int_0^s \{\sigma'\}^T \{\varepsilon^{*'}\} A_b dS\right)_{-\theta} \tag{5-17}$$

Where

A_b is the cross-sectional area of the braiding yarns,

S is the length of braiding yarn segment, which is given by Equation (4-36),

$\{\sigma'\}$ is the residual stress vector caused by initial strain vector $\{\varepsilon_0'\}$, given in Equation (5-15),

$\{\varepsilon^{*'}\}$ is the virtual strain vector in the principal coordinate system,

Superscript ' denotes the principal coordinate system,

Subscripts +θ, -θ denote the directions of braiding yarns.

The virtual strain vector in the principal coordinate system is

$$\{\varepsilon^{*'}\} = \{\varepsilon^{*'}_{xx}, \varepsilon^{*'}_{yy}, \varepsilon^{*'}_{zz}, \varepsilon^{*'}_{yz}, \varepsilon^{*'}_{zx}, \varepsilon^{*'}_{xy}\}^T \tag{5-18}$$

From Equation (4-16), we get the relation between the virtual strain vector in the global coordinate system and that in the principal coordinate system as follows,

$$\{\varepsilon^{*'}\} = [B]\{\varepsilon^{*}\} \tag{5-19}$$

Where

$[B]$ is given by Equation (4-17)

Substitute Equation (5-15), (5-19) into Equation (5-17), we get the virtual energy as follows,

$$\begin{aligned}
E_b^* &= \left(\int_0^s \{\varepsilon\}^T [B]^T [C_y][B]\{\varepsilon^*\} A_b ds - \int_0^s \{\varepsilon_{0y}\}^T [C_y][B]\{\varepsilon^*\} A_b ds\right)_{+\theta} \\
&+ \left(\int_0^s \{\varepsilon\}^T [B]^T [C_y][B]\{\varepsilon^*\} A_b ds - \int_0^s \{\varepsilon_{0y}\}^T [C_y][B]\{\varepsilon^*\} A_b ds\right)_{-\theta} \\
&= \{\varepsilon\}^T \left(\frac{1}{S}\int_0^s [B]^T [C_y][B] ds\right)_{+\theta} \{\varepsilon^*\} S A_b + \{\varepsilon\}^T \left(\frac{1}{S}\int_0^s [B]^T [C_y][B] ds\right)_{-\theta} \{\varepsilon^*\} S A_b \\
&- \left\{\frac{1}{S}\int_0^s \{\varepsilon_{0y}\}^T [C_y][B] ds\right\}_{+\theta} \{\varepsilon^*\} S A_b - \left\{\frac{1}{S}\int_0^s \{\varepsilon_{0y}\}^T [C_y][B] ds\right\}_{-\theta} \{\varepsilon^*\} S A_b
\end{aligned} \tag{5-20}$$

Let

$$\{\sigma_{0b}\}^T = \frac{1}{S}\int_0^s \{\varepsilon_{0y}\}^T [C_y][B] dS \tag{5-21}$$

Where

Subscript b denotes braiding yarn segment.

Substitute Equation (5-21), (4-40), into Equation (5-20)

We get,

$$E_b^* = \{\varepsilon\}^T \left([C_b]_{+\theta} + [C_b]_{-\theta} \right) \{\varepsilon^*\} SA_b - \left(\{\bar{\sigma}_\infty\}_{+\theta}^T + \{\bar{\sigma}_\infty\}_{-\theta}^T \right) \{\varepsilon^*\} SA_b \qquad (5\text{-}22)$$

(2) The virtual energy E_a^*

In Fig 5.1 , there are two axial yarn segments, so the virtual energy of elastic deformation stored in axial yarn segments is,

$$E_a^* = 2\left(\frac{1}{2} \{\sigma'\}^T \{\varepsilon^{*'}\} A_a h \right) \qquad (5\text{-}23)$$

Substitute Equation (5-15), (5-19) into Equation (5-23), and note that the principal coordinate system coincides with the global system for axial yarns, then get

$$E_a^* = \{\varepsilon\}^T [C_y] \{\varepsilon^*\} A_a h - \{\varepsilon_{oy}'\}^T [C_y] \{\varepsilon^*\} A_a h \qquad (5\text{-}24)$$

(3) The virtual energy E_m^*

By using Equations (5-16), (5-19), we get the virtual energy of matrix material,

$$E_m^* = \frac{1}{2} \{\sigma'\}^T \{\varepsilon^*\} (2A_m) h = \{\varepsilon\}^T [C_m] \{\varepsilon^*\} A_m h - \{\varepsilon_{0m}'\}^T [C_m] \{\varepsilon^*\} A_m h \qquad (5\text{-}25)$$

Where

A_m is one half of the cross sectional area of the resin in the RUC,

Subscript m denotes the matrix material.

(4) The total virtual energy E^*

Substitute Equation (5-22), (5-24), (5-25) into (5-8), we get the totally virtual energy,

$$E^* = \{\varepsilon\}^T \Big(\left([C_b]_{+\theta} + [C_b]_{-\theta}\right) A_b S + [C_y] A_a h + [C_m] A_m h \Big) \{\varepsilon^*\}$$
$$- \Big(\left(\{\bar{\sigma}_\infty\}^T_{+\theta} + \{\bar{\sigma}_\infty\}^T_{-\theta} \right) A_b S + \{\varepsilon_{0y}'\}^T [C_y] A_a h + \{\varepsilon_{0m}'\}^T [C_m] A_m h \Big) \{\varepsilon^*\} \quad (5\text{-}26)$$

Substitute Equation (4-46) into (5-26),

get

$$E^* = \{\varepsilon\}^T \Big(\frac{\left([C_b]_{+\theta} + [C_b]_{-\theta}\right)}{2} \frac{2A_b'}{2A_b' + A_a} \frac{2A_b' + A_a}{A} \frac{1}{\cos\gamma}$$
$$+ [C_y] \frac{A_a}{2A_b' + A_a} \frac{2A_b' + A_a}{A} + [C_m] \frac{A_m}{A} \Big) \{\varepsilon^*\} Ah$$
$$- \Big(\frac{\left(\{\bar{\sigma}_\infty\}^T_{+\theta} + \{\bar{\sigma}_\infty\}^T_{-\theta} \right)}{2} \frac{2A_b'}{2A_b' + A_a} \frac{2A_b' + A_a}{A} \frac{1}{\cos\gamma}$$
$$+ \{\varepsilon_{0y}'\}^T [C_y] \frac{A_a}{2A_b' + A_a} \frac{2A_b' + A_a}{A} + \{\varepsilon_{0m}'\}^T [C_m] \frac{A_m}{A} \Big) \{\varepsilon^*\} Ah \quad (5\text{-}27)$$

Further substitute Equation (4-50), (4-51), (4-52) into Equation (5-27),

$$E^* = \{\varepsilon\}^T [\bar{C}] \{\varepsilon^*\} Ah - \{\bar{\sigma}_0\}^T \{\varepsilon^*\} Ah \quad (5\text{-}28)$$

Where

$[\bar{C}]$ is given in Equation (4-53).

$$\{\bar{\sigma}_0\}^T = \frac{\left(\{\bar{\sigma}_\infty\}^T_{+\theta} + \{\bar{\sigma}_\infty\}^T_{-\theta} \right)}{2} \frac{(1-\chi) V_f}{\cos\gamma} \frac{V_f}{k} + \{\varepsilon_{0y}'\}^T [C_y] \chi \frac{V_f}{k} + \{\varepsilon_{0m}'\}^T [C_m] (1 - \frac{V_f}{k}) \quad (5\text{-}29)$$

Where

$\{\bar{\sigma}_\infty\}^T$ is given in Equation (5-21),

$+\theta$ and $-\theta$ denote the directions of braiding yarns,

χ is given in Equation (3-94),

V_f is given in Equation (3-68),

$[C_y]$ is given in Equation (4-25),

$[C_m]$ is given in Equation (4-22),

γ is given in Equation (3-92),

k is the filament packing fraction.

5.4 The total strain vector caused by initial strain vector

From Equations (5-7), (5-28),

get

$$\{\varepsilon\}^T[\overline{C}]\{\varepsilon^*\}Ah - \{\overline{\sigma}_0\}^T\{\varepsilon^*\}Ah = 0 \tag{5-30}$$

The virtual strain vector can be chosen arbitrarily,

so

$$\{\varepsilon\}^T[\overline{C}] - \{\overline{\sigma}_0\}^T = 0 \tag{5-31}$$

That is

$$\{\varepsilon\} = [\overline{C}]^{-1}\{\overline{\sigma}_0\} \tag{5-32}$$

Where

$\{\overline{\sigma}_0\}$ is given in Equation (5-29),

$[\overline{C}]$ is given in Equation (4-53).

5.5 The effective coefficients of thermal expansion

(1) The thermal strain vectors

In this case, the thermal strain vectors are the initial strain vectors.

The thermal strain vector of impregnated straight yarn is ,

$$\{\varepsilon_{0y}'\} = \{\alpha_y\}\Delta T \tag{5-33}$$

where

$$\{\alpha_y\} = \{\alpha_1, \alpha_2, \alpha_2, 0, 0, 0\}^T \tag{5-34}$$

Subscript y denotes yarn,

α_1 is the coefficient of thermal expansion of impregnated straight yarn material along the fiber direction,

α_2 is the coefficient of thermal expansion of impregnated straight yarn material along the direction vertically to fiber direction,

ΔT is the uniform change in temperature.

The thermal strain vector of matrix material is

$$\{\varepsilon_{0m}'\} = \{\alpha_m\}\Delta T \tag{5-35}$$

where

$$\{\alpha_m\} = \{\alpha, \alpha, \alpha, 0, 0, 0\}^T \tag{5-36}$$

Subscript m denotes the matrix material,

α is the coefficient of thermal expansion of matrix material.

(2) The effective coefficients of thermal expansion

The effective coefficients of thermal expansion are denoted by,

$$\{\bar{\alpha}\}=\left\{\bar{\alpha}_{xx},\bar{\alpha}_{yy},\bar{\alpha}_{zz},\bar{\alpha}_{yz},\bar{\alpha}_{zx},\bar{\alpha}_{xy}\right\}^T \tag{5-37}$$

So the total strain vector caused by the thermal expansion can be represented by,

$$\{\varepsilon\}=\{\bar{\alpha}\}\Delta T \tag{5-38}$$

Substitute (5-38) into (5-32),

$$\{\bar{\alpha}\}=[\bar{C}]^{-1}\{\bar{\sigma}_0\}\frac{1}{\Delta T} \tag{5-39}$$

Substitute (5-33) into (5-21),

$$\{\bar{\sigma}_{0b}\}^T=\left(\frac{1}{S}\int_0^s\{\alpha_y\}^T[C_y][B]dS\right)\Delta T=\{\bar{\sigma}_{0b}{}^{UT}\}^T\Delta T \tag{5-40}$$

where

$$\{\bar{\sigma}_{0b}{}^{UT}\}^T=\left(\frac{1}{S}\int_0^s\{\alpha_y\}^T[C_y][B]dS\right) \tag{5-41}$$

Superscript UT denotes the unit change in temperature.

Substitute (5-40), (5-33), (5-35) into Equation (5-29),

we get

$$\frac{1}{\Delta T}\{\bar{\sigma}_0\}^T=\frac{\left(\{\bar{\sigma}_{0b}{}^{UT}\}_{+\theta}^T+\{\bar{\sigma}_{0b}{}^{UT}\}_{-\theta}^T\right)}{2}\frac{(1-\chi)}{\cos\gamma}\frac{V_f}{k}+\{\alpha_y\}^T[C_y]\chi\frac{V_f}{k}+\{\alpha_m\}^T[C_m](1-\frac{V_f}{k}) \tag{5-42}$$

Substitute (5-42) into (5-39), we get the effective coefficients of thermal expansion,

$$\{\bar{\alpha}\}=[\bar{C}]^{-1}\left(\frac{\left(\{\bar{\sigma}_{0b}{}^{UT}\}_{+\theta}+\{\bar{\sigma}_{0b}{}^{UT}\}_{-\theta}\right)}{2}\frac{(1-\chi)}{\cos\gamma}\frac{V_f}{k}+[C_y]\{\alpha_y\}\chi\frac{V_f}{k}+[C_m]\{\alpha_m\}(1-\frac{V_f}{k})\right) \tag{5-43}$$

5.6 The effective coefficients of hygro expansion

(1) The hygro strain vectors

In this case, the hygro strain vectors are the initial strain vectors.

The hygro strain vector of impregnated straight yarn is ,

$$\{\varepsilon_{0y}'\} = \{\beta_y\}\Delta H \tag{5-44}$$

where

$$\{\beta_y\} = \{\beta_1, \beta_2, \beta_2, 0, 0, 0\}^T \tag{5-45}$$

Subscript y denotes yarn,

β_1 is the coefficient of hygro expansion of impregnated straight yarn material along the fiber direction,

β_2 is the coefficient of hygro expansion of impregnated straight yarn material along the direction vertically to fiber direction,

ΔH is the uniform change in moisture.

The hygro strain vector of matrix material is

$$\{\varepsilon_{0m}'\} = \{\beta_m\}\Delta H \tag{5-46}$$

where

$$\{\beta_m\} = \{\beta, \beta, \beta, 0, 0, 0\}^T \tag{5-47}$$

Subscript m denotes the matrix material,

β is the coefficient of hygro expansion of matrix material.

(2) The effective coefficients of hygro expansion

The effective coefficients of hygro expansion are denoted by,

$$\{\overline{\beta}\} = \{\overline{\beta}_{xx}, \overline{\beta}_{yy}, \overline{\beta}_{zz}, \overline{\beta}_{yz}, \overline{\beta}_{zx}, \overline{\beta}_{xy}\}^T \tag{5-48}$$

So the total strain vector caused by the hygro expansion can be represented by,

$$\{\varepsilon\} = \{\overline{\beta}\}\Delta H \tag{5-49}$$

Substitute (5-49) into (5-32),

$$\{\overline{\beta}\} = [\overline{C}]^{-1}\{\overline{\sigma}_0\}\frac{1}{\Delta H} \tag{5-50}$$

Substitute (5-44) into (5-21),

$$\{\overline{\sigma}_{0b}\}^T = \left(\frac{1}{S}\int_0^s \{\beta_y\}^T [C_y][B]dS\right)\Delta H = \{\overline{\sigma}_{0b}{}^{UH}\}^T \Delta H \tag{5-51}$$

where

$$\{\overline{\sigma}_{0b}{}^{UH}\}^T = \left(\frac{1}{S}\int_0^s \{\beta_y\}^T [C_y][B]dS\right) \tag{5-52}$$

Superscript UH denotes the unit change in moisture.

Substitute (5-51), (5-44), (5-46) into Equation (5-29),

we get

$$\frac{1}{\Delta H}\{\overline{\sigma}_0\}^T = \frac{\left(\{\overline{\sigma}_{0b}{}^{UH}\}_{+\theta}^T + \{\overline{\sigma}_{0b}{}^{UH}\}_{-\theta}^T\right)}{2}\frac{(1-\chi)}{\cos\gamma}\frac{V_f}{k} + \{\beta_y\}^T[C_y]\chi\frac{V_f}{k} + \{\beta_m\}^T[C_m](1-\frac{V_f}{k}) \tag{5-53}$$

Substitute (5-53) into (5-50), we get the effective coefficients of hygro expansion,

$$\{\overline{\beta}\} = [\overline{C}]^{-1}\left(\frac{\left(\{\overline{\sigma}_{0b}{}^{UH}\}_{+\theta} + \{\overline{\sigma}_{0b}{}^{UH}\}_{-\theta}\right)}{2}\frac{(1-\chi)}{\cos\gamma}\frac{V_f}{k} + [C_y]\{\beta_y\}\chi\frac{V_f}{k} + [C_m]\{\beta_m\}(1-\frac{V_f}{k})\right) \tag{5-54}$$

5.7 The discrete Equations for numerical analysis

The discrete forms of Equation (5-41), (5-52) are as follows,

$$\left\{\overline{\sigma}_{0b}{}^{UT}\right\}^T = \frac{1}{S}\sum_{i=-n}^{n-1}\left\{\alpha_y\right\}^T\left[C_y\right][B]\sqrt{1+\left(\frac{dz}{dx}\right)^2}\,\Delta x \tag{5-55}$$

$$\left\{\overline{\sigma}_{0b}{}^{UH}\right\}^T = \frac{1}{S}\sum_{i=-n}^{n-1}\left\{\beta_y\right\}^T\left[C_y\right][B]\sqrt{1+\left(\frac{dz}{dx}\right)^2}\,\Delta x \tag{5-56}$$

Where

$\Delta x = \frac{L'}{n}$ (Equation (4-58)),

S is given in Equation (4-57).

5.8 The predicted effective coefficients of thermal expansion

The effective coefficients of thermal expansion are predicted in this section. The elastic constants, coefficients of thermal expansion that are used for this prediction are listed in Tables 4-2, 5-1 respectively. Four cases are studied. The known parameters of the four cases are given in Table 3-3. The predicted effective coefficients of thermal expansion are shown in Table 5-2. Because no experiment results are available, the predicted results need to be verified further.

Table 5-1 Coefficients of thermal expansion of matrix material and impregnated straight yarn [17]

Material	α_{11}	α_{22}
Yarn	-0.324	14.000
Resin	40.000	40.000

Table 5-2 Effective coefficients of thermal expansion

Material type	α_{xx} (10^{-6}/°C)	α_{yy} (10^{-6}/°C)	α_{zz} (10^{-6}/°C)
$[0_{30k}/\pm70_{6k}]$ 46% Axial (6.05mm)	2.520	2.750	28.150
$[0_{75k}/\pm70_{15k}]$ 46% Axial (11.04mm)	2.480	2.790	28.090
$[0_{36k}/\pm45_{15k}]$ 46% Axial (5.52mm)	0.170	8.000	27.20
$[0_{6k}/\pm45_{15k}]$ 12% Axial (5.52mm)	1.170	4.410	27.99

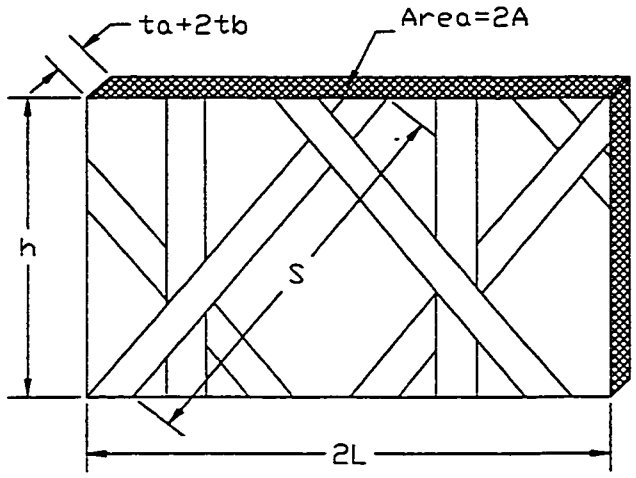

Fig 5.1 The repeat unit cell (RUC)

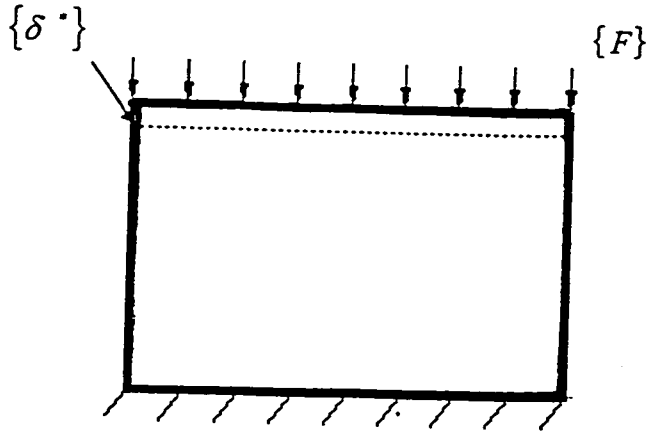

Fig 5.2 The virtual defection on the top edge of RUC

Chapter 6 The parameter analysis of 2-D braided composites

As the theoretical analysis of 2-D braided composite is developed so far, there are so many parameters in 2-D braiding process , such as filament packing fraction k, filament diameter d_f, count number of braiding and axial yarn m_b, m_a, thickness of braiding yarn and axial yarn t_b, t_a, cross sectional areas of braiding and axial yarn A_b, A_a , braiding angle θ, yarn space L, fiber volume fraction V_f, yarn crimp angle γ, axial yarn content in a braided preform χ, material constants of yarns and resin. All these parameters have more or less some effect on the behavior and properties of 2-D braided composites. Although the number of parameters for braided composites is huge, there is a limited number of independent parameters in our theoretical analysis and these independent parameters can be classified into three different groups. All other parameters are only functions of these independent parameters. The objective of this chapter is to find out the independent parameters in theoretical analysis of 2-D braided composites and their effects on behavior and properties of braided composite materials .

6.1 The independent parameters of a 2-D braided composite

For simplifying the problem of finding independent parameters of a braided composite, all the relative equations in previous chapters are listed in following simplified notation:

From Equation (3-57), (3-58), the cross sectional areas of axial yarn and braiding yarn A_a and A_b are

$$A_a = f(k, m_a, d_f) \tag{6-1}$$

$$A_b = f(k, m_b, d_f) \tag{6-2}$$

From Equation (3-26)

$$\lambda = f(\xi) \tag{6-3}$$

From Equations (3-60), (3-61) and note the Equations (6-1), (6-2), (6-3), the thicknesses of axial and braiding yarn are

$$t_a = f(k, m_a, d_f, \xi) \tag{6-4}$$

$$t_b = f(k, m_b, d_f, \xi) \tag{6-5}$$

From Equation (3-55), (3-56), note Equation (6-4), (6-5) and the assumption of $\xi_a=\xi_b=\xi$ in our analysis, so the widths of axial and braiding yarn are,

$$w_a = f(k, m_a, d_f, \xi) \tag{6-6}$$

$$w_b = f(k, m_b, d_f, \xi) \tag{6-7}$$

From Equation (3-68) and note the Equation (6-3), (6-5), the fiber volume fraction is

$$V_f = f(k, m_a, m_b, d_f, \xi, \theta, L) \tag{6-8}$$

From Equation (3-92) and note Equation (6-4), (6-5), the yarn crimp angle is

$$\gamma = f(k, m_a, m_b, d_f, \xi, \theta, L) \tag{6-9}$$

From Equation (3-94), the axial yarn content in a braided preform is

$$\chi = f(m_a, m_b, 6) \tag{6-10}$$

From Equation (4-22), (4-21), (4-18), the stiffness matrix of matrix material is,

$$[C_m] = [f(E, \upsilon)]_{6\times6} \tag{6-11}$$

From Equation (4-25), (4-26), (4-27), the stiffness matrix of impregnated straight yarn is,

$$[C_y] = [f(E_1, E_2, G_{12}, \upsilon_{12}, \upsilon_{23})]_{6\times6} \tag{6-12}$$

From Equation (4-40), (3-89), (3-90), and note the Equation (6-4), (6-5), (6-9),(6-12)

$$[C_b] = [f(k, m_a, m_b, d_f, \xi, \theta, L, E_1, E_2, G_{12}, \upsilon_{12}, \upsilon_{23})]_{6\times6} \tag{6-13}$$

From Equation (4-53), the effective stiffness matrix of braided composite is,

$$[\overline{C}] = [f(k, m_a, m_b, d_f, \xi, \theta, L, E, \upsilon, E_1, E_2, G_{12}, \upsilon_{12}, \upsilon_{23})]_{6\times6} \tag{6-14}$$

From Equation (5-43), the effective coefficient matrix of thermal expansion is,

$$\{\overline{\alpha}\} = \{f(k, m_a, m_b, d_f, \xi, \theta, L, E, \upsilon, E_1, E_2, G_{12}, \upsilon_{12}, \upsilon_{23}, \alpha, \alpha_1, \alpha_2)\}_{6\times1} \tag{6-15}$$

From Equation (5-54), the effective coefficient matrix of hygric expansion is,

$$\{\overline{\beta}\} = \{f(k, m_a, m_b, d_f, \xi, \theta, L, E, \upsilon, E_1, E_2, G_{12}, \upsilon_{12}, \upsilon_{23}, \beta, \beta_1, \beta_2)\}_{6\times1} \tag{6-16}$$

So from Equations (6-1) to (6-16), we know that k, m_a, m_b, d_f, ξ, θ, L, E, υ, E_1, E_2, G_{12}, υ_{12}, υ_{23}, α, α_1, α_2, β, β_1, β_2 are the independent parameters in our theoretical analysis. They can be classified into three groups (1) yarn geometric parameters (k, m_a, m_b, d_f, ξ,), (2) composite geometric parameter (θ, L), (3) material constants (E, υ, E_1, E_2, G_{12}, υ_{12}, υ_{23}, α, α_1, α_2, β, β_1, β_2). The relations between the independent parameters and other parameters are shown in Fig 6.1.

The value of ξ is not easy to be found without the microscopic examination of braided composite. So the thickness of braiding yarn t_b is chosen as independent parameter, then ξ is dependent on t_b. The thickness of braiding yarn t_b can be obtained easily by measuring the thickness of a braided composite. If the thickness of a braided composite is H and the number of layer is n. Then t_b equals to H/n.

Further more, the relations between machine parameters (speed ratio ω, diameter of mandrel D) and the independent preform geometric parameters (θ , L) can be simplified as follows:

From (3-36),and note that the number of braiding yarn carriers is considered as constant, so the mandrel diameter is

$$D = f(L) \tag{6-17}$$

From Equation (3-5), and note Equation (6-17), the speed ratio is,

$$\omega = f(\theta, L) \tag{6-18}$$

Thus the relations between independent parameters and other parameters are redrawn in Fig 6.2 .

All the independent parameters used for parameter analysis in our research are listed in Table 6-1 with their definitions.

A braided composite of $[0_{30k}/\pm 70_{6k}]$ 46% Axial yarn (yarn space L=6.05mm) in second row of Table 3-3 is chosen for our parameter analysis. The values of its independent parameters are listed in Table 6-1. When we do the parameter analysis, each time only two of the independent parameters θ, L, m_a are changed in certain range. All other independent parameters are kept unchanged. Thus the distributions of mechanical behavior of a braided composite according to the variation of L, m_a, θ can be plotted in 3 dimensional diagram from Figs 6.5 to 6.22. The distributions of V_f and χ are shown in Figure 6.3. The distributions of crimp angle γ are shown in Fig 6.4 .

6.2 The parameter analysis of fiber volume fraction, crimp angle and axial yarn content

6.2.1 Fiber volume fraction

In Fig 6.3 (a), the braiding angle θ changes from 0 to 89 degrees, the count number of axial yarn m_a changes from 0 to $20m_b$. The fiber volume increases with the increases of θ, and decrease first at small m_a and then increase with the increase of m_a until yarn jamming happens. After that, the fiber volume fraction keeps unchanged.

In Fig 6.3 (b), the yarn space L changes from 1mm to 40mm, the count number of axial yarn m_a changes from 0 to $20m_b$. The fiber volume fraction increases with the

the decrease of the yarn space L until the yarn jamming happens. With the increase of m_a, V_f decreases first at small m_a and then increases till yarn jamming happens.

In Fig 6.3(c), the yarn space L changes from 1mm o 40mm and the braiding angle θ changes from 0 to 89 degrees. The fiber volume increases with the decrease of yarn space L and with the increase of braiding angle θ until the yarn jamming happens.

6.2.2 Axial yarn content in a braided preform

The distribution of axial yarn content is shown in Fig 6.3 (d), the axial yarn content increases both with the increase of the axial yarn count number and with the decrease of the braiding angle. It is the function only of independent parameters m_a and θ.

6.2.3 Yarn crimp angle

In Fig 6.4 (a), the braiding angle θ changes from 0 to 90 degrees, m_a changes from 0 to 20 m_b. The crimp angle increases both with the increases of the braiding angle θ and the count number of axial yarn m_a.

In Fig 6.4 (b), the braiding angle θ changes from 0 to 90 degrees, the yarn space L changes from 0 to 5mm. The crimp angle increases with the increase of the braiding angle and the decrease of the yarn space L.

In Fig 6.4(c), the m_a changes from 0 to 20 m_b, the yarn space L changes from 1mm to 10 mm. The crimp angle increases with the increase of m_a and the decrease of yarn space L.

6.3 The parameter analysis of effective stiffness of braided composite

In this study , each time only two of the independent parameters L, θ, m_a are chosen as variables, while other independent parameters are kept constant values as listed in Table 6-1. The relative dependent parameters and their definition are listed in Table 6-2.

6.3.1 Change the values of θ and m_a

θ varies in the range of 1 to 89 degrees, m_a varies from 0 to $20m_b$.

(1) Effective *Exx*

In Fig 6.5(a), *Exx* decreases with the increase of θ. *Exx* drops greatly when θ is near 45 degrees . *Exx* increases with the increase of m_a until yarn jamming happens. After that, *Exx* almost has no change with the variation of m_a

(2) Effective *Eyy*

In Fig 6.5 (b), Eyy increases with the increase of braiding angle. It goes up quickly when θ is greater than 45 degrees. The increase of m_a has no significant effect on *Eyy* when θ is less than 45 degrees. But the increase of m_a does reduce the value of *Eyy* slowly when θ is greater than 45 degrees.

(3) Effective *Ezz*

In Fig 6.5 (c), *Ezz* increases with the increase of θ and m_a until yarn jamming happens. After that, the value of *Ezz* has not much change.

(4) Effective *Gxy*

In Fig 6.5 (d), *Gxy* attains to its local maximum values when θ is near 45 degrees. The smaller is the m_a, the higher is the maximum values, especially when m_a is very small.

Gxy is much more sensitive to θ than to m_a.

(5) Effective *Gyz*

In Fig 6.6 (a), *Gyz* keeps increasing both with increase of m_a and θ until yarn jamming happens. After that, *Gyz* does not change very much.

(6) Effective *Gzx*

In Fig 6.6 (b), *Gzx* increases with the increase of m_a and θ. There is a abrupt change of the slope of *Gzx* curve surface when yarn jamming happens.

(7) Effective ν_{xy}

In Fig 6.6 (c), ν_{xy} attains to its local maximum values when θ is near 30 degrees. The smaller the value of m_a, the higher the maximum values. ν_{xy} is more sensitive to θ than to m_a

The distributions of above mechanical behaviors can also be plotted as function of V_f and χ, as shown in Fig 6.7 and Fig 6.8. V_f and χ themselves are functions of θ and m_a and are not independent parameters. It should be noted that the increase of V_f reduces the effective *Exx*, as shown in Fig 6.7 (a). Also the maximum *Gxy* is not obtained when V_f is at its maximum value, as shown in Fig 6.7 (d) . The reason is that the increase of V_f comes from the increase of θ. The larger the θ, the smaller the effective *Exx* . Also *Gxy* gets its local maximum values when θ is near 45 degrees which does not correspond the maximum fiber volume fraction.

Table 6-1 Definition and values of independent parameters [17]

Independent parameters	Definition	Values
k	filament packing fraction	0.75
m_a	the count number of axial yarn	30000
m_b	the count number of braiding yarn	6000
d_f	the diameter of filament	0.007mm
t_b	the thickness of braiding yarn	0.167mm
θ	the braiding angle	70°
L	the yarn space	6.05mm
E_1	the young's modulus along axis 1 (axial direction) of straight yarn	144.8GPa
E_2	the young's modulus along axis 2 (transverse direction) of straight yarn	11.73GPa
G_{12}	the shear modulus according to 1,2 direction of straight yarn	5.52GPa
v_{12}	possion ratio according to 1,2 direction	0.23
v_{23}	possion ratio according to 2,3 direction	0.3
E	young's modulus of resin	3.45GPa
v	possion ratio of resin	0.35
α	coefficient of thermal expansion of resin	40.0e-6
α_1	coefficient of thermal expansion of yarn along 1 direction	-0.324e-6
α_2	coefficient of thermal expansion of yarn along 2 direction	14.0e-6
β	coefficient of hygric expansion of resin	----------
β_1	coefficient of hydric expansion of yarn along 1 direction	----------
β_2	coefficient of hydric expansion of yarn along 2 direction	----------

Table 6-2 Relative dependent parameters

dependent parameters	Definition
A_a	cross sectional area of axial yarn
A_b	cross sectional area of braiding yarn
W_a	width of axial yarn
W_b	width of braiding yarn
t_a	thickness of axial yarn
ξ	thickness to width ratio
ω	speed ratio of braiding machine
D	diameter of mandrel
V_f	fiber volume fraction
χ	axial yarn content of braided preform
γ	yarn crimp angle
$[\overline{C}]$	effective stiffness matrix of braided composite
$[\overline{\alpha}]$	effective coefficients of thermal expansion of braided composite.
$[\overline{\beta}]$	effective coefficients of hydric expansion of braided composite.

6.3.2 Change the value of θ and *L*

θ varies in the range of 1 to 89 degrees. *L* varies in the range of 0 to 40 mm. All other independent parameters are kept unchanged.

(1) Effective *Exx*

In Fig 6.9 (a), *Exx* increases with the decrease of *L* and θ until yarn jamming happens. After that, *Exx* has no much change.

(2) Effective *Eyy*

In Fig 6.9 (b), when θ is less than 45 degrees *Eyy* is not sensitive to the change of *L*. When θ is greater than 45 degrees, *Eyy* increase with the decrease of L until yarn jamming happens. Then *Eyy* almost has no change until *L* becomes very

small which corresponds to very large crimp angle γ. After that, *Eyy* drops again. *Eyy* increase with the braiding angle and is very sensitive to it.

(3) Effective *Ezz*

In Fig 6.9 (c), *Ezz* increases both with the increase of θ and the decrease of L until yarn jamming happens. After that, *Ezz* keeps unchanged. Then *Ezz* jumps to high values when θ is very large and L is very small that correspond to very large crimp angle.

(4) Effective *Gxy*

In Fig 6.9 (d), *Gxy* attains to its local maximum value when θ is near 45 degrees. *Gxy* increases with the decrease of L until yarn jamming happens. Then *Gyz* keeps unchanged. The less the yarn space L, the higher the local maximum of *Gxy*.

(5) Effective *Gyz*

In Fig 6.10 (a), *Gyz* increase with the decrease of L until yarn jamming happens. After that, *Gyz* keeps unchanged till L becomes very small which corresponds to very large crimp angle. Then *Gyz* increases again. *Gyz* also increase with the increase of θ.

(6) Effective *Gzx*

In Fig 6.10 (b), *Gzx* increases with the increase of θ and the decrease of L. At small θ, *Gzx* increases rapidly because of the rapidly increased crimp angle.

(7) Effective ν_{xy}

In Fig 6.10 (c), ν_{xy} attains to its local maximum values when θ is near 30 degrees. ν_{xy} is most sensitive to θ, but not so sensitive to yarn space L.

The corresponding distributions of *Exx*, *Eyy*, *Ezz*, *Gxy*, *Gyz*, *Gzx*, ν_{xy} according to V_f and χ are shown in Fig 6.11 and Fig 6.12.

6.3.3 Change the values of m_a and L

L varies from 1 mm to 20 mm, m_a varies from 0 to 20 m_b, all other independent parameters are kept unchanged.

(1) Effective *Exx*

In Fig 6.13 (a), *Exx* increases with the decrease of L until yarn jamming happens. After that, *Exx* has no change. *Exx* also increases with the increase of m_a.

(2) Effective *Eyy*

In Fig 6.13 (b), *Eyy* increases with the decrease of yarn space L until yarn jamming happens.Then *Eyy* has no change until L becomes very small which corresponds to very large crimp angle. After that, *Eyy* drops. Although *Eyy* decreases slowly with the increase of m_a , it is not sensitive to m_a.

(3) Effective *Ezz*

In Fig 6.13 (c), *Ezz* increases slowly with the decrease of L and the increase of m_a until yarn jamming happens, then it keeps unchanged. When L becomes very small and m_a very large, the crimp angle becomes very large. So *Ezz* increases very fast again.

(4) Effective *Gxy*

In Fig 6.13 (d), *Gxy* increases with the decrease of L until yarn jamming happens. Then it keeps unchanged . When L is very small that corresponds to very

large crimp angle, *Gxy* increases greatly again. *Gxy* also increase with the decrease of m_a.

(5) Effective *Gyz*

In Fig 6.14 (a), *Gyz* increases slowly with the decrease of *L* until yarn jamming happens. Then it keeps unchanged. When *L* becomes very small that corresponds to very large crimp angle γ, *Gyz* again increases rapidly with the decrease of *L*. *Gyz* also increases slowly with the increase of m_a. *Gyz* is a matrix dominate property. *Gyz* is not sensitive to *L* and m_a, before yarn jamming happens.

(6) Effective *Gzx*

In Fig 6.14 (b), *Gzx* increases slowly with the decrease of *L* until yarn jamming happens. Then it keeps unchanged. When L becomes very small that corresponds to very large crimp angle, *Gzx* increases rapidly again with the decrease of *L*. *Gzx* is a matrix dominate property , it is not sensitive to m_a and *L* before yarn jamming happens.

(7) Effective ν_{xy}

In Fig 6.14 (c) , although ν_{xy} increases slowly with the increase of L and m_a, it is not sensitive to *L* and m_a

The corresponding distributions of *Exx*, *Eyy*, *Ezz*, *Gxy*, *Gyz*, *Gzx*, ν_{xy} according to V_f and χ are shown in Fig 6.15 and 6.16.

6.4 The parameter analysis of coefficients of thermal expansion.

6.4.1 Change the values of θ and m_a

Braiding angle θ changes from 1 to 89 degrees, m_a changes from 0 to $20m_b$. All other independent parameters are kept unchanged.

(1) Effective α_{xx}

In Fig 6.17(a), α_{xx} is not sensitive to θ and m_a when θ is less than 45 degrees. α_{xx} increases rapidly with the increase of θ and decrease of m_a when θ is greater than 45 degrees.

(2) Effective α_{yy}

In Fig 6.17(b), α_{yy} is not sensitive to m_a. It decreases with the increase of θ. Especially it drops greatly when θ is near 45 degrees.

(3) Effective α_{zz}

In Fig 6.17 (c), α_{zz} gets its local maximum when θ is near 45 degrees and at small m_a. At larger value of m_a, α_{zz} is not sensitive to ma and θ, although it increases slowly with the increase of θ.

The corresponding distributions of α_{xx} α_{yy} α_{zz} according to V_f and χ are shown in Fig 6.18 .

6.4.2 Change the values of braiding angle θ and yarn space L

In Fig 6.19, θ is in the range of 1 to 89 degrees. L is in the range of 1 to 40mm. All other independent parameters are kept unchanged.

(1) Effective α_{xx}

In Fig 6.19 (a), α_{xx} increases both with the increase of L and θ.

(2) Effective α_{yy}

In Fig 6.19 (b), α_{yy} increases with the increase of L , but it decreases with the increases of θ.

(3) Effective α_{zz}

In Fig 6.19 (c), α_{zz} increases with the increase of L. α_{zz} increases first and then decreases with the increase of θ.

The corresponding distributions of α_{xx} α_{yy} α_{zz} according to V_f and χ are shown in Fig 6.20.

6.4.3 Change the values of count number of axial yarn m_a and yarn space L

In Fig 6.21, L changes from 1mmto 40mm, m_a changes from 0 to 20 m_b. All other independent parameters are kept unchanged.

(1) Effective α_{xx}

In Fig 6.21 (a,), α_{xx} increases with the increase of L and the decrease of m_a.

(2) Effective α_{yy}

In Fig 6.21(b), α_{yy} increases with the increase of L and m_a before yarn jamming happens.

(3) Effective α_{zz}

In Fig 6.21(c), α_{zz} increases with the increase of L . α_{zz} increases rapidly first and then decrease slowly with the increase of m_a.

The corresponding distributions of α_{xx}, α_{yy}, α_{zz} according to V_f and χ are shown in Fig 6.22 .

6.5 The conclusion of parameter analysis

If there is no yarn jamming in a braided composite, then the conclusion can be obtained as follows,

(1) Increase of braiding angle or decrease of yarn space will increase the fiber volume fraction. Increase of the count number of axial yarn will decrease fiber volume fraction first when m_a is very small, and then increase fiber volume fraction when m_a becomes larger.

(2) Increase of braiding angle, count number of axial yarn, or decrease of yarn space will increase the crimp angle.

(3) Increase of fiber volume fraction does not always increase the effective *Exx* and *Gxy*. If the increase of fiber volume only comes from the increase of braiding angle, the more the fiber volume fraction the less the effective *Exx*.

(4) Increase of count number of axial yarn and decrease of braiding angle and yarn space will increase the effective *Exx*.

(5) Increase of braiding angle and decrease of yarn space will increase effective *Eyy*. *Eyy* is not sensitive to the variation of the count number of axial yarn.

(6) Increase of braiding angle, the count number of axial yarn and decrease of yarn space will increase the values of, *Ezz*, *Gyz*, *Gzx*.

(7) Gxy and ν_{xy} attain to their local maximum values when braiding angle are near 45 and degrees respectively. The lower are the yarn space and the count number of axial yarn, the higher is the local maximum.

(8) Increase of braiding angle, yarn space and decrease of the count number of axial yarn will increase the effective coefficient of thermal expansion α_{xx}.

(9) Increase of braiding angle and decrease of yarn space will decrease the effective coefficient of thermal expansion α_{yy}.

(10) α_{zz} attains to its local maximum value when the count number of axial yarn is very small and braiding angle is near 45 degrees. Increase of the count number of axial yarn and decrease of yarn space will decrease α_{zz}.

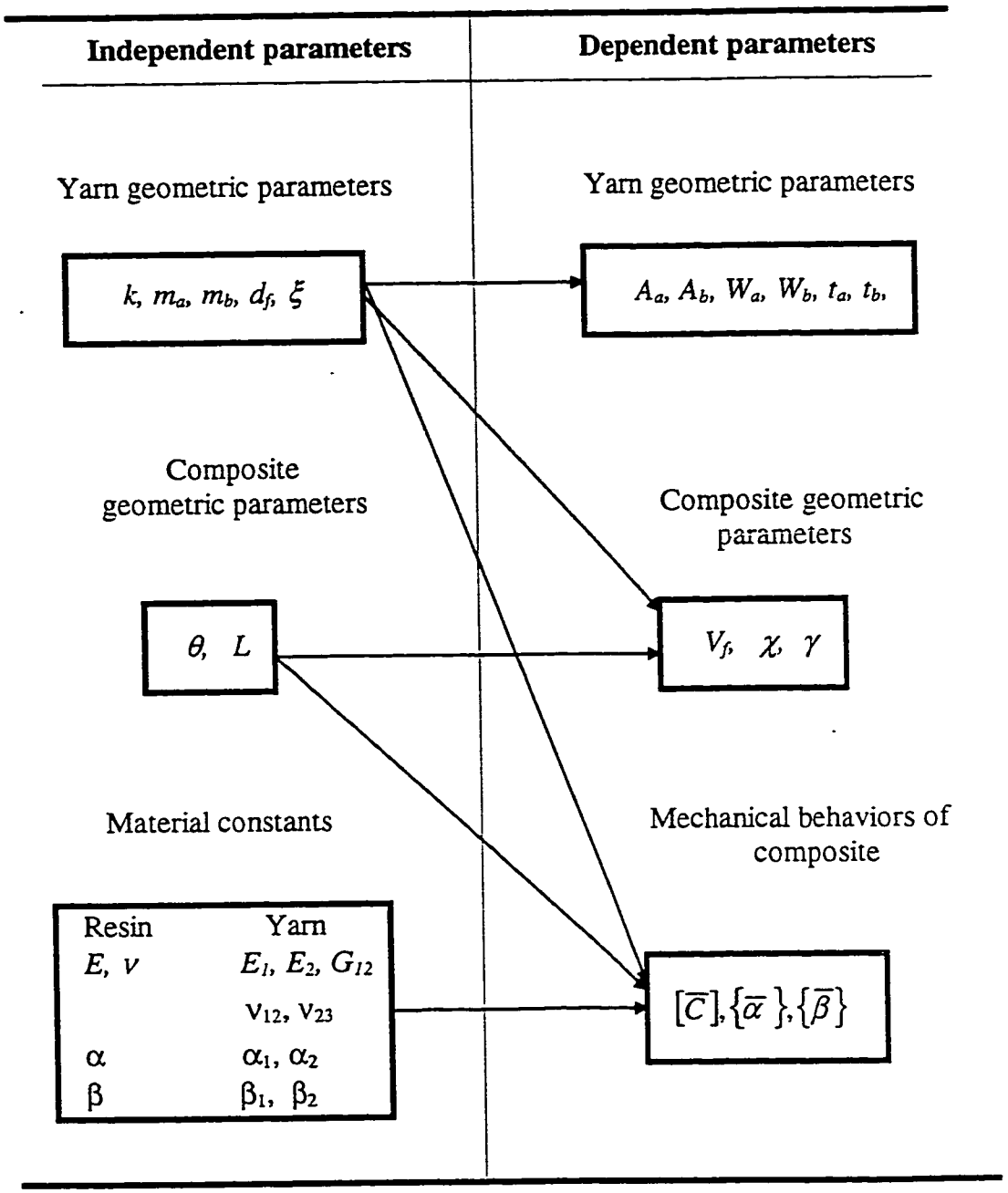

Fig 6.1 The parameters in the theoretical analysis of 2-D braided composite. ξ is chosen as independent parameter.

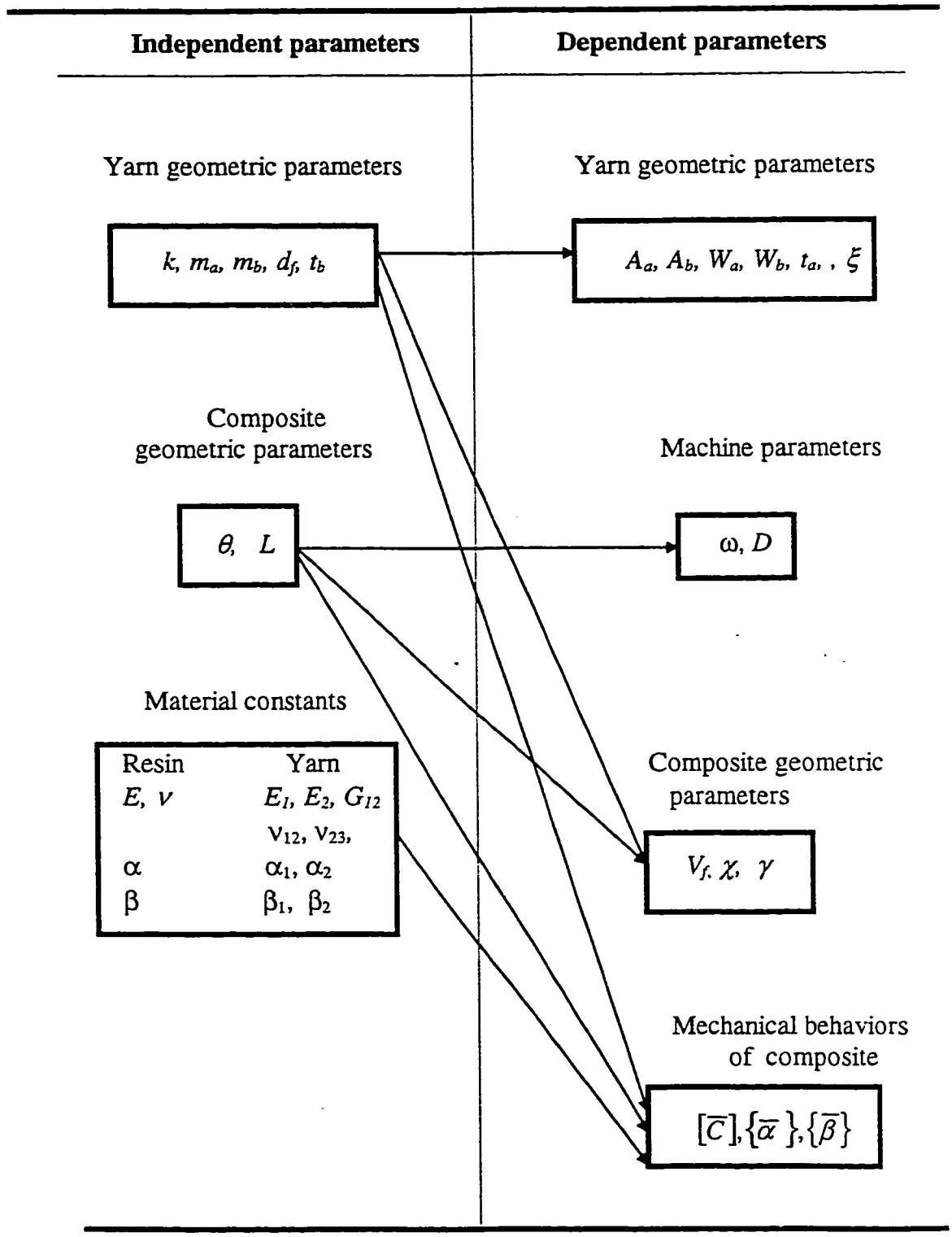

Fig 6.2 The parameters in the theoretical analysis of 2-D braided composite. t_b is chosen as independent parameter.

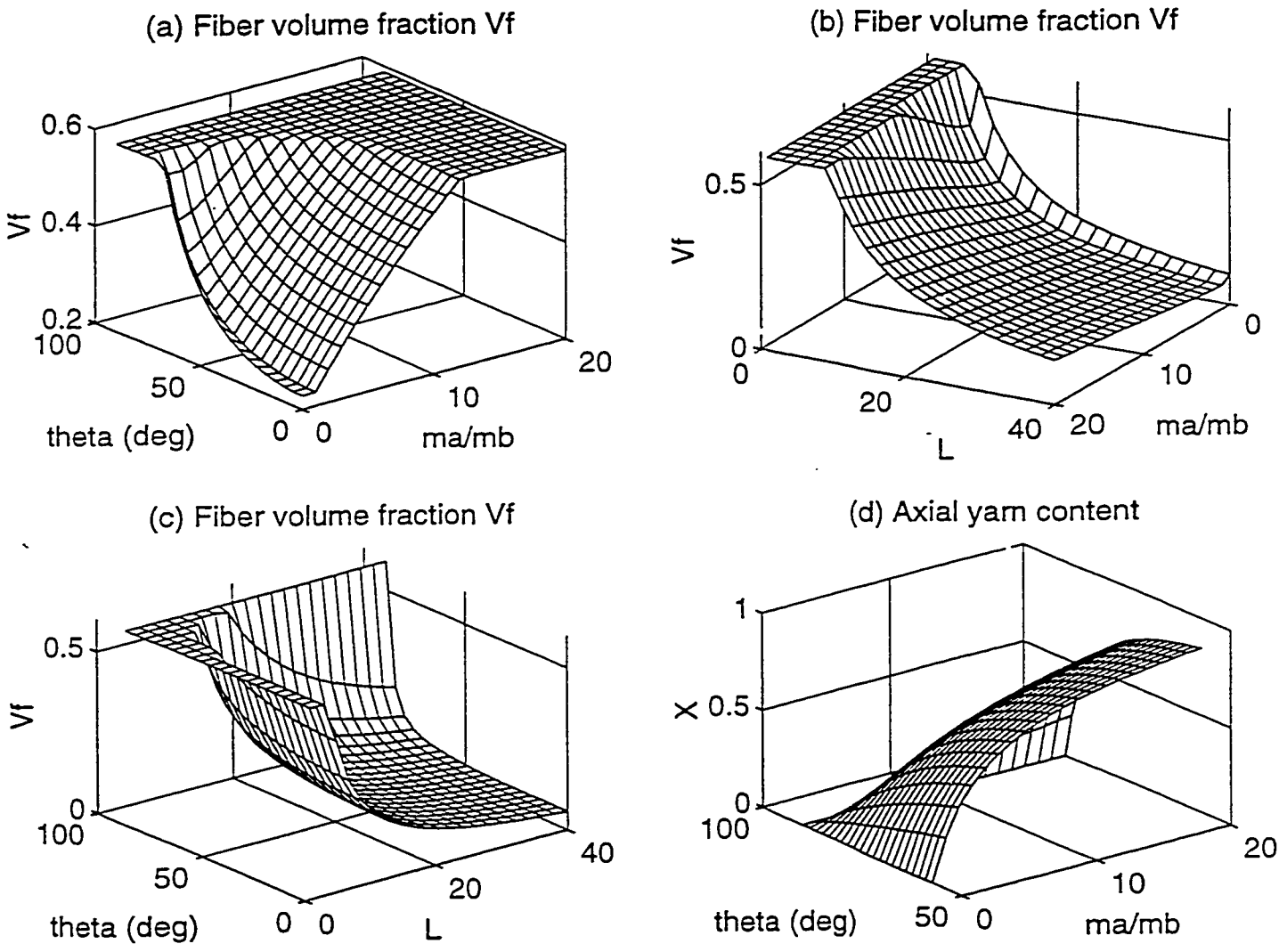

Fig 6.3 Distribution of fiber volume fraction and axial yarn content

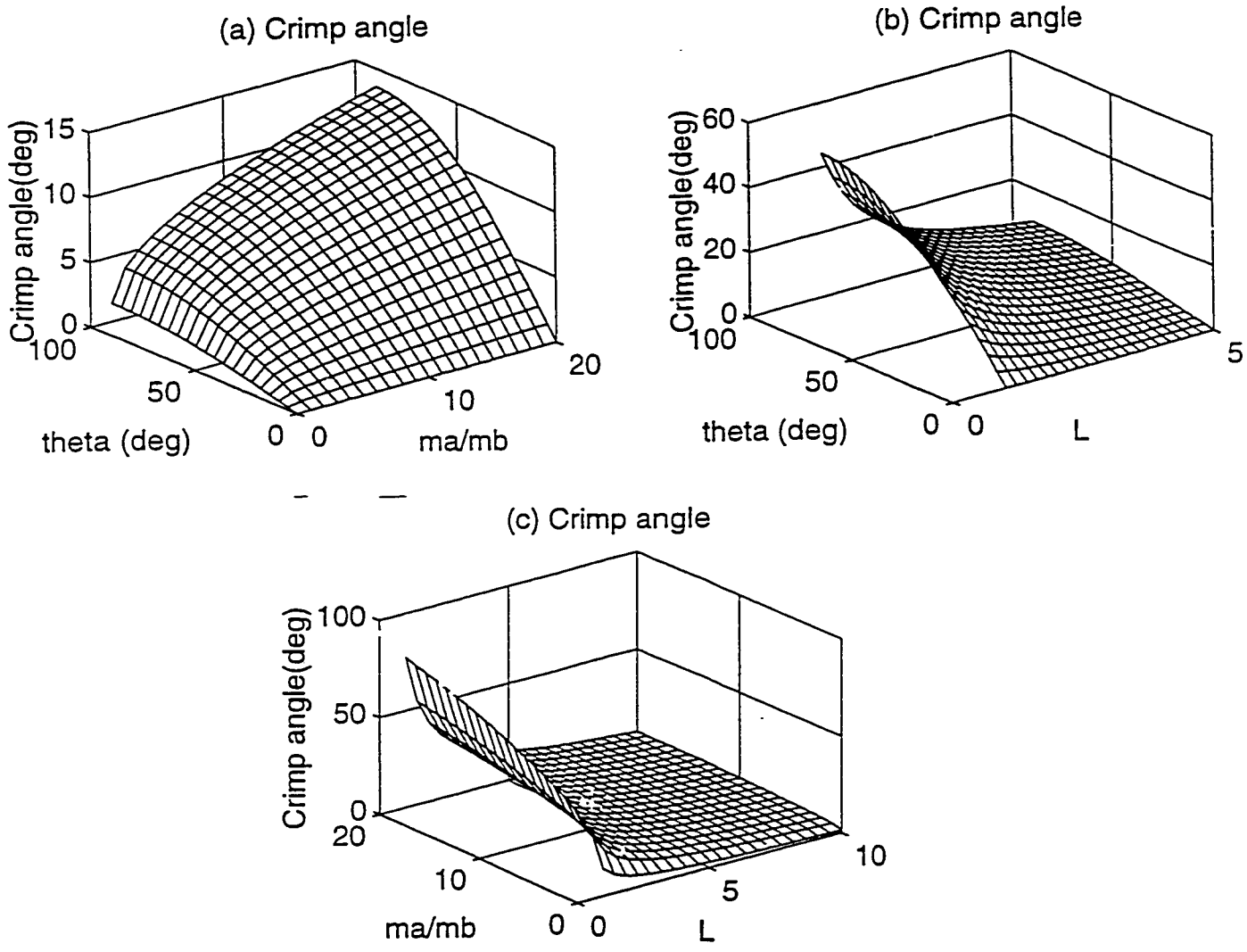

Fig 6.4 Distribution of yarn crimp angle

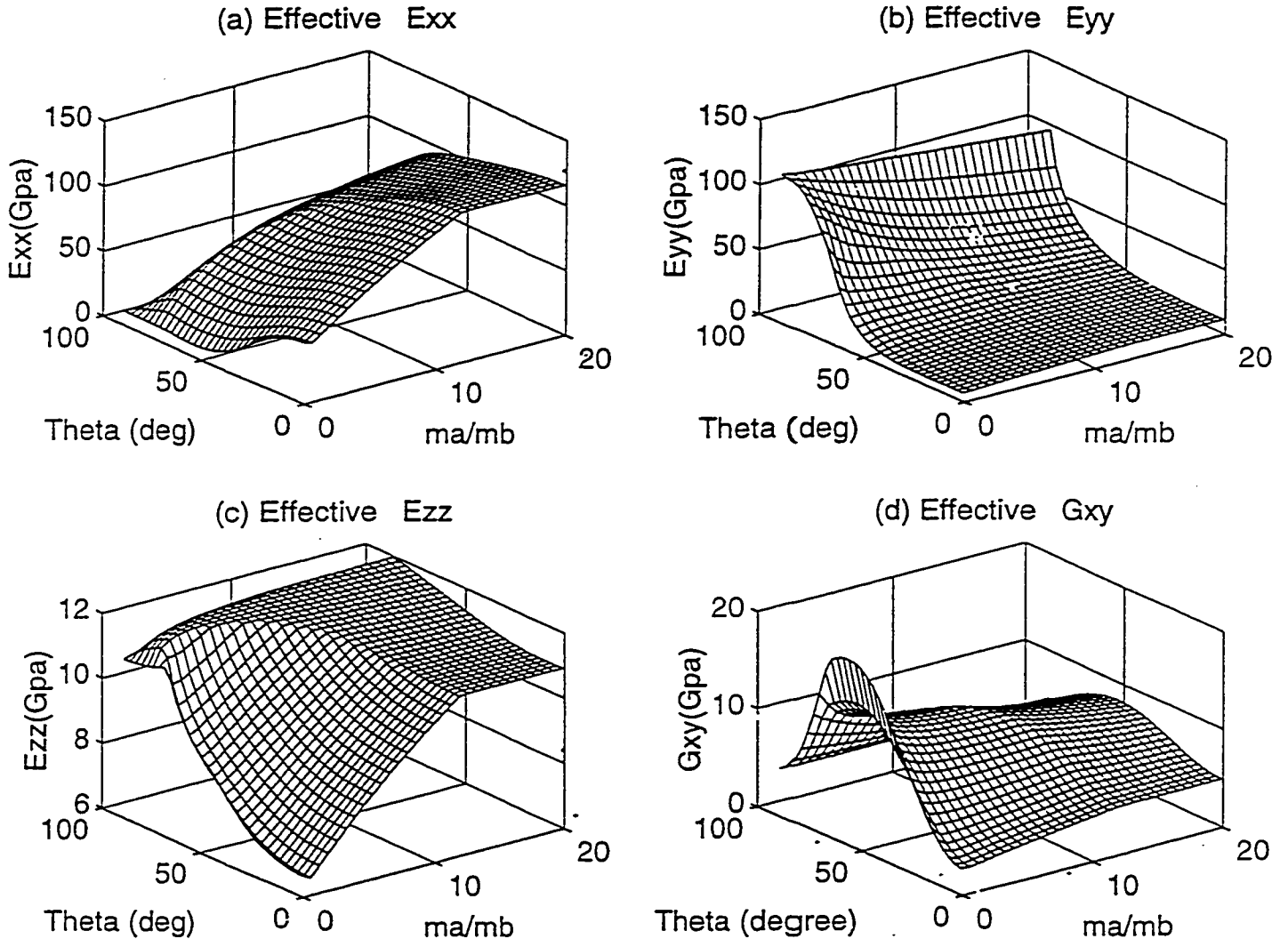

Fig 6.5 Distribution of effective *Exx, Eyy, Ezz, Gxy* with the variation of θ, m_a

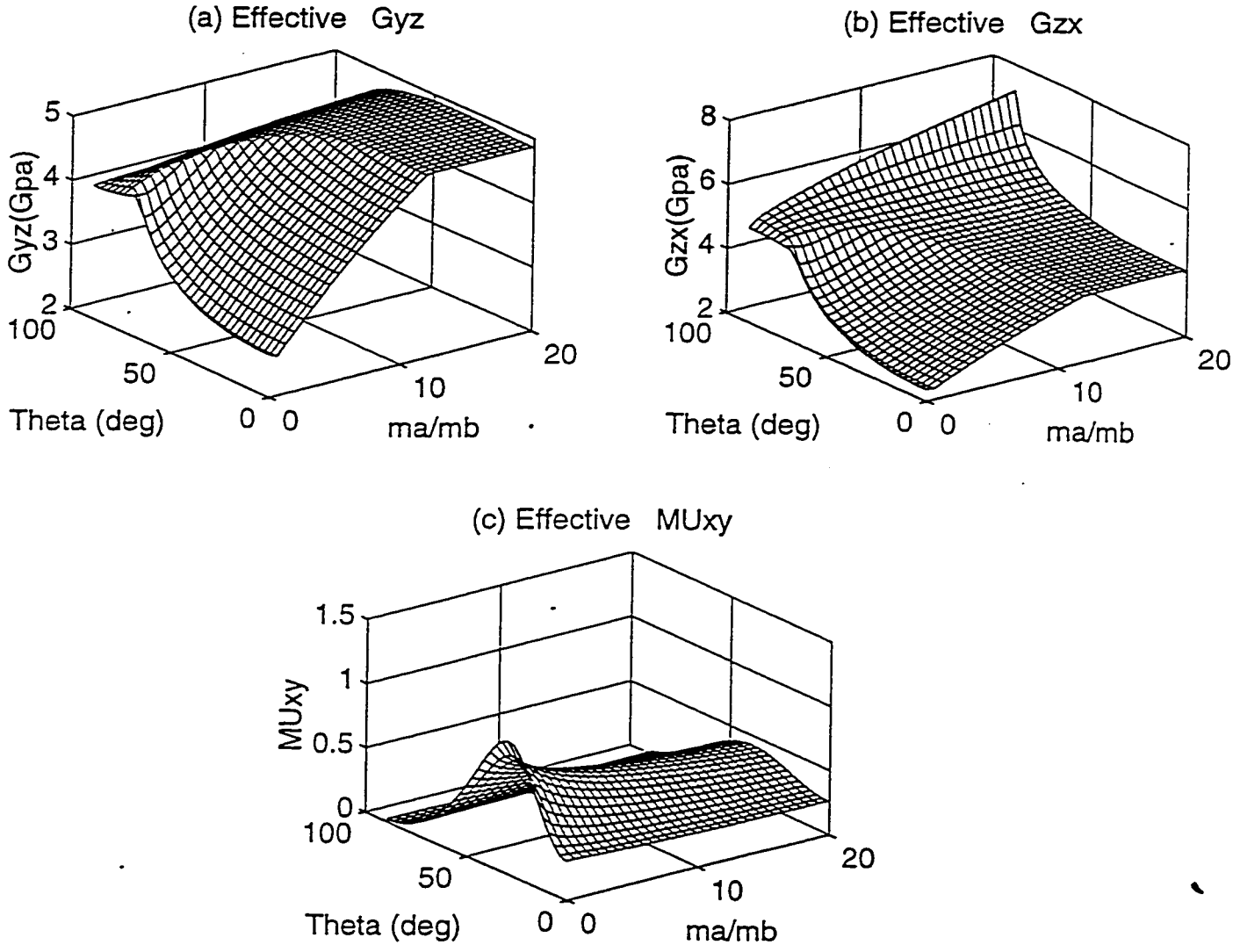

Fig 6.6 Distribution of effective *Gyz*, *Gzx*, ν_{xy} with the variation of θ, m_a

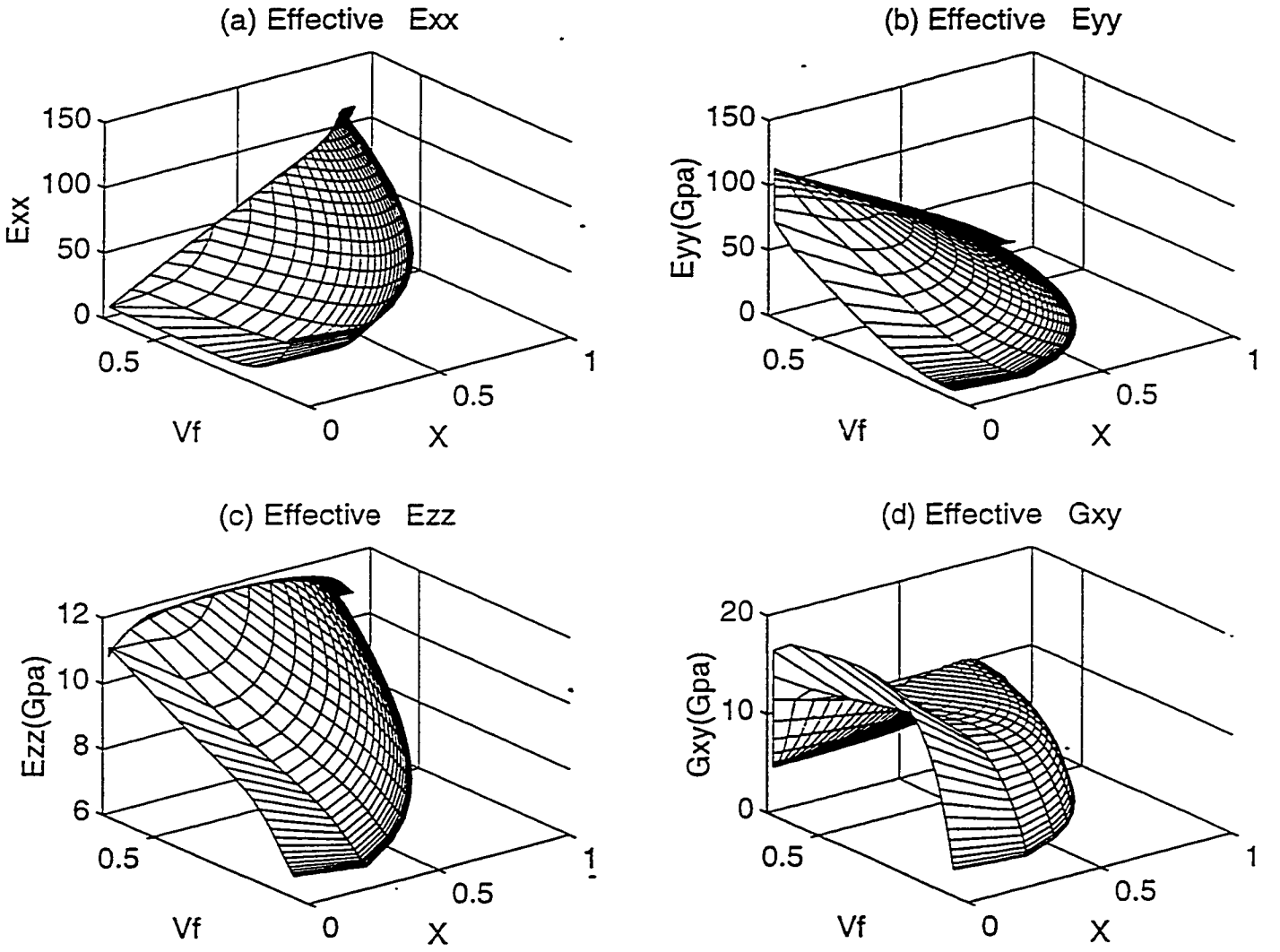

Fig 6.7 Distribution of effective *Exx, Eyy, Ezz, Gxy* with the variation of θ, m_a Choose χ as x axis, V_f as y axis.

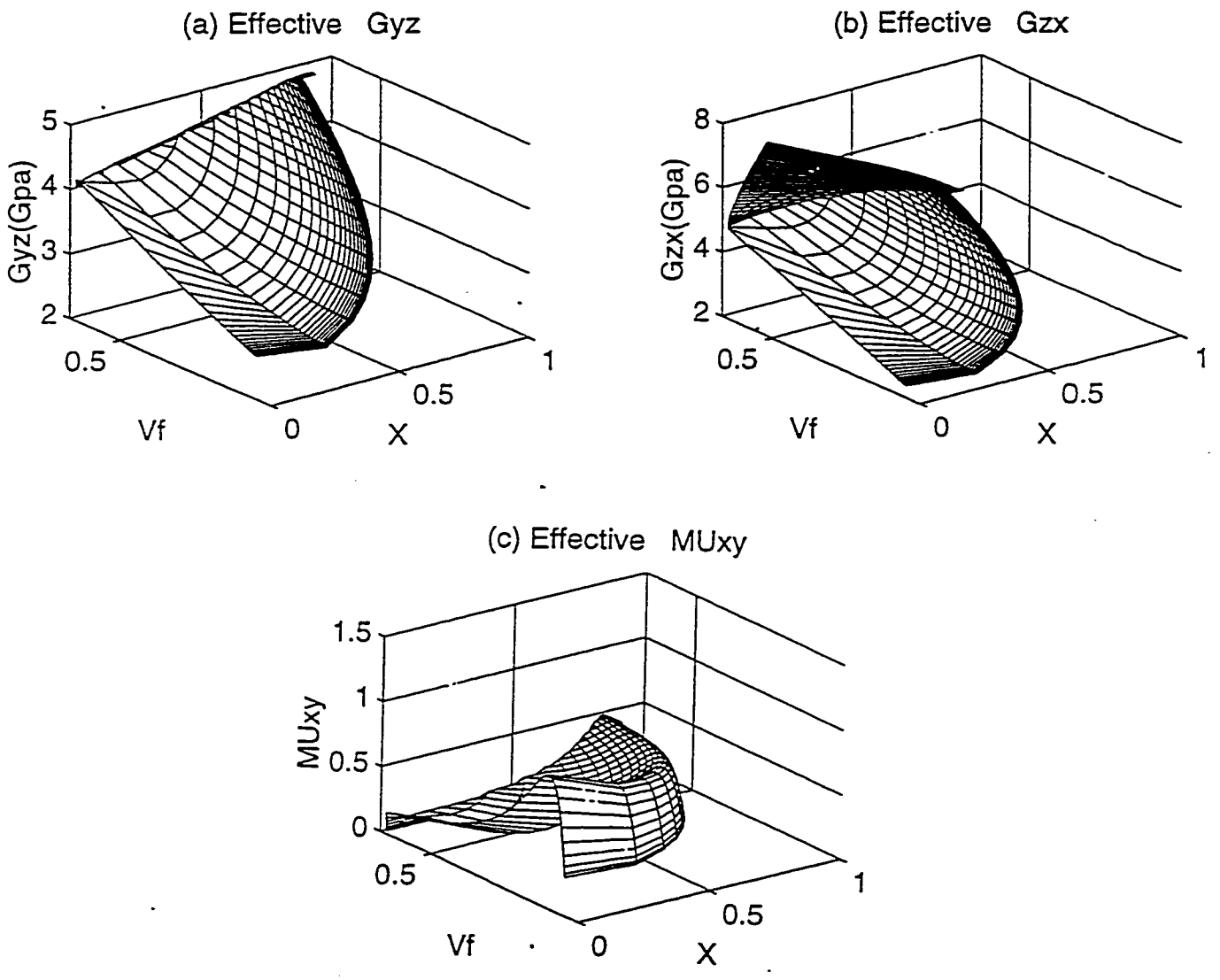

Fig 6.8 Distribution of effective *Gyz*, *Gzx*, ν_{xy} with the variation of θ, m_a. Choose χ as x axis, V_f as y axis.

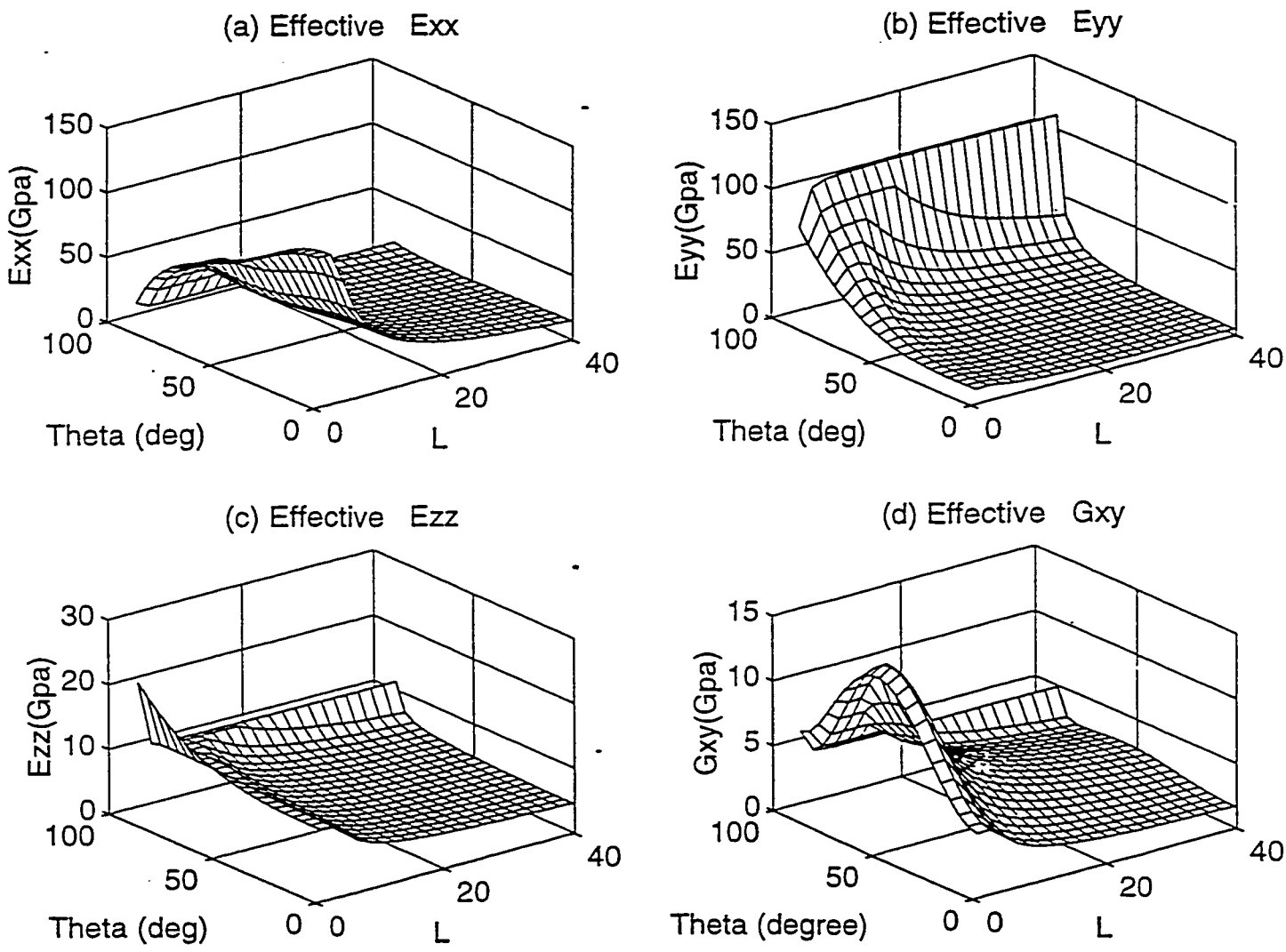

Fig 6.9 Distribution of effective *Exx, Eyy, Ezz, Gxy* with the variation of θ, *L*

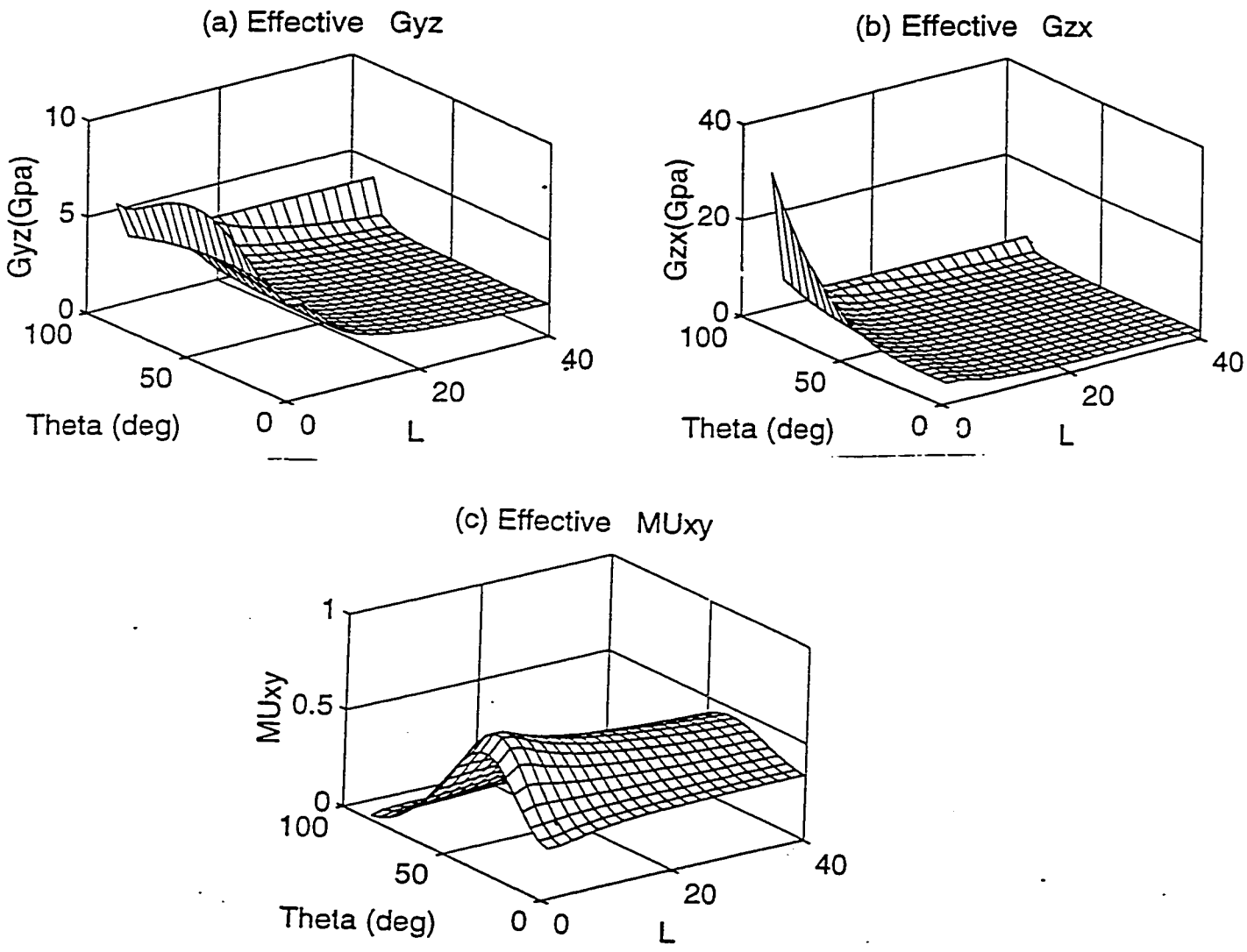

Fig 6.10 Distribution of effective *Gyz*, *Gzx*, ν_{xy} with the variation of θ, *L*

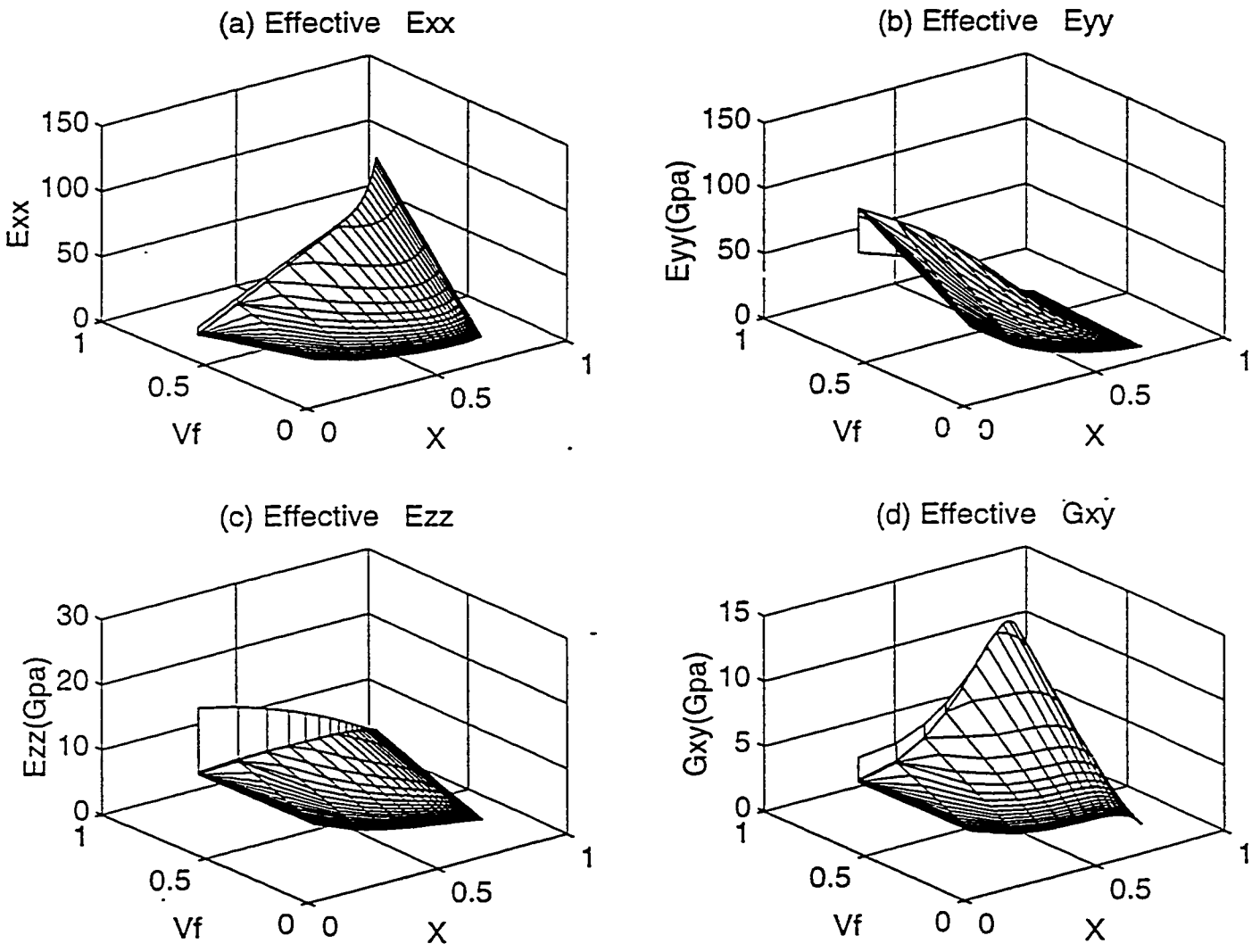

Fig 6.11 Distribution of effective *Exx, Eyy, Ezz, Gxy* with the variation of θ, *L*. Choose χ as x axis, V_f as y axis.

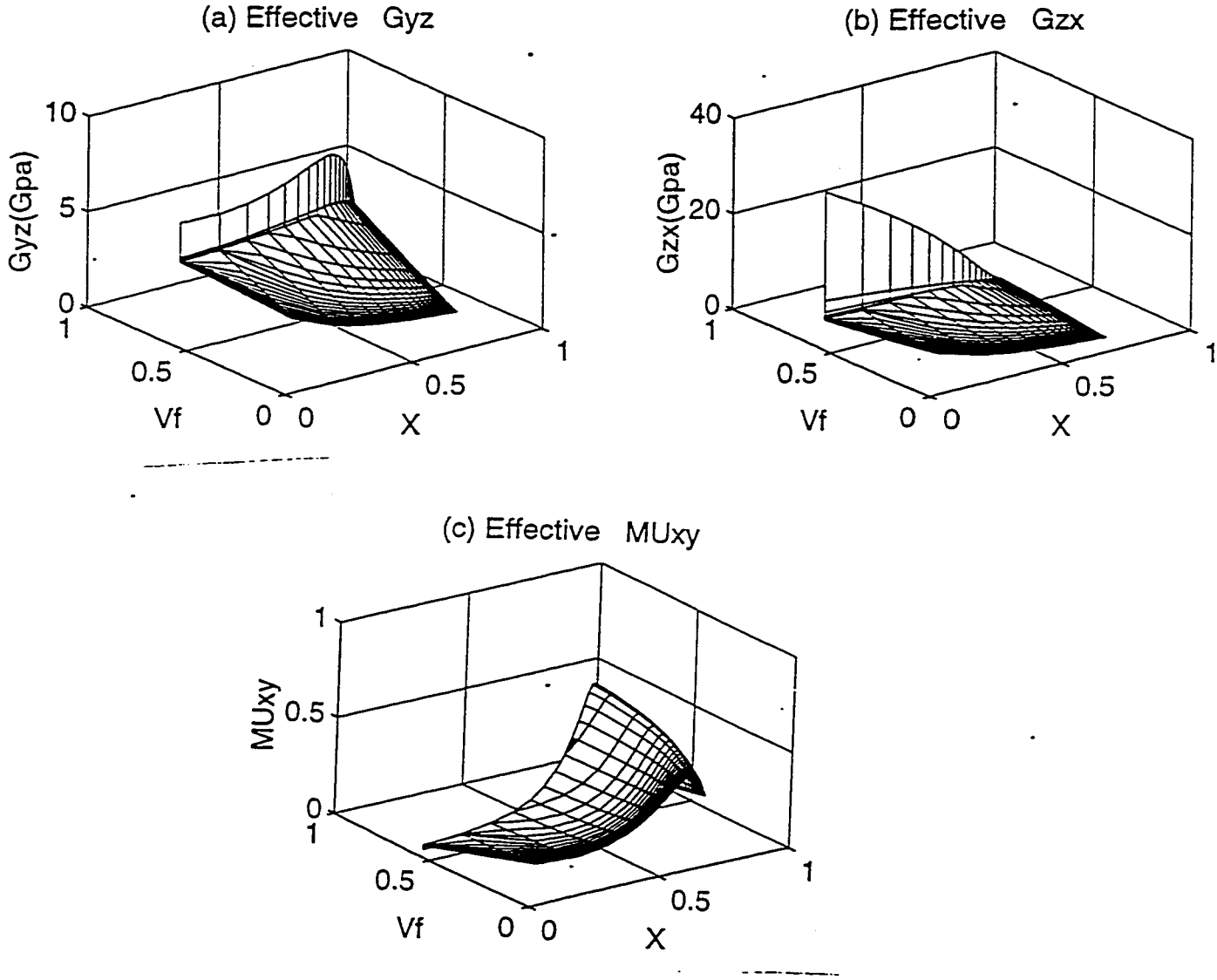

Fig 6.12 Distribution of effective *Gyz*, *Gzx*, ν_{xy} with the variation of $\theta, \overline{L_i}$. Choose χ as x axis, V_f as y axis.

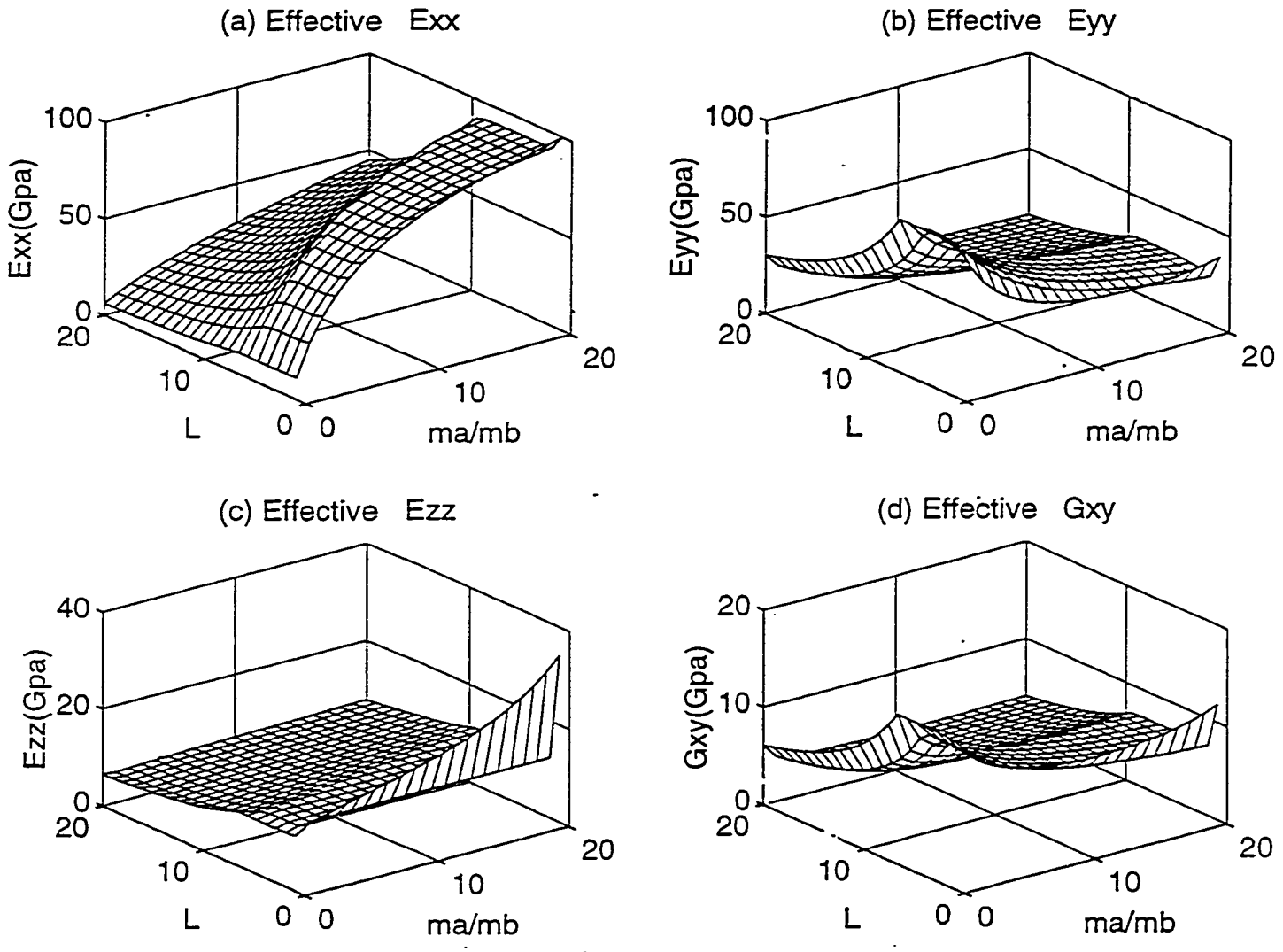

Fig 6.13 Distribution of effective *Exx, Eyy, Ezz, Gxy* with the variation of m_a, L

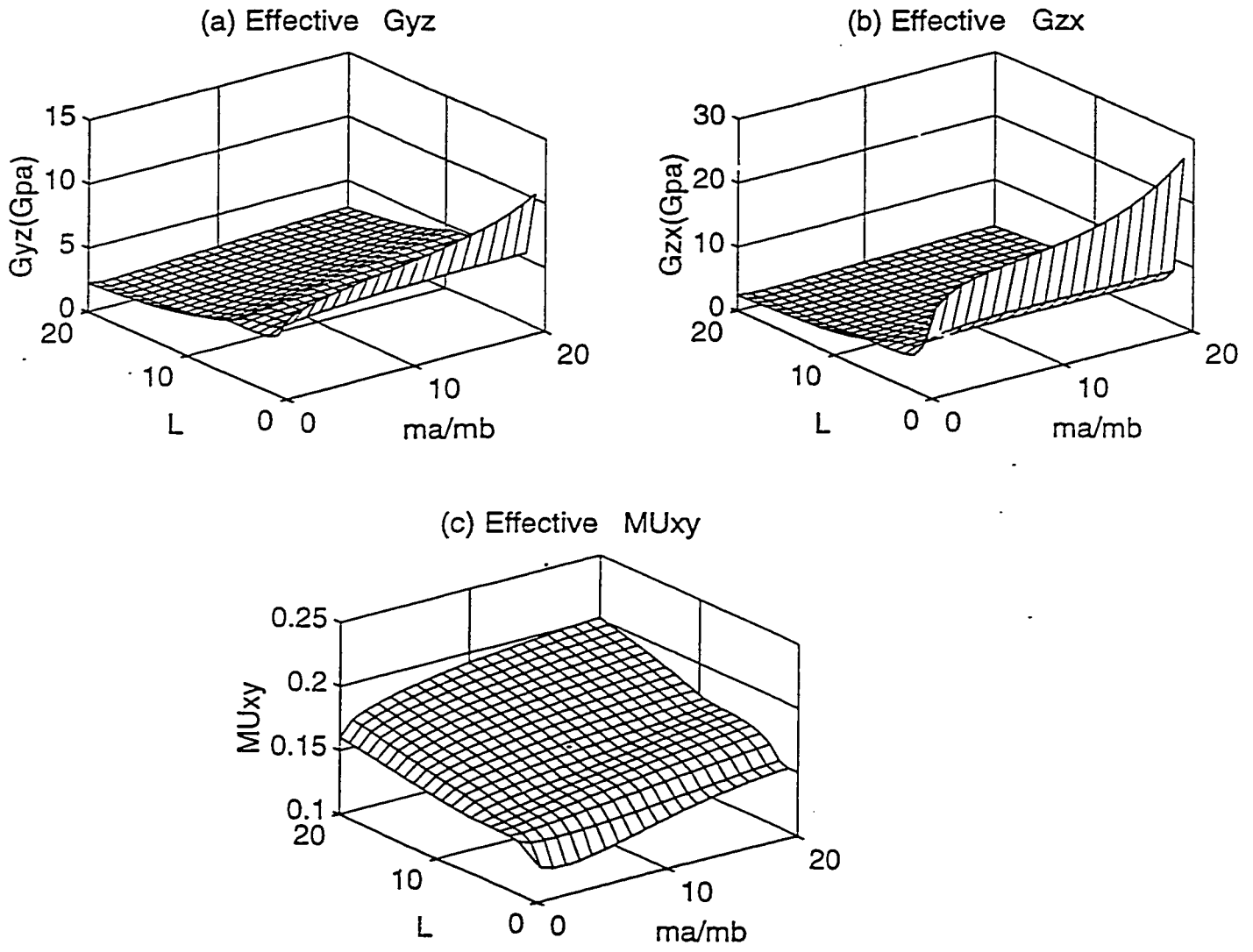

Fig 6.14 Distribution of effective Gyz, $\bar{G}zx$, ν_{xy} with the variation of m_a, L

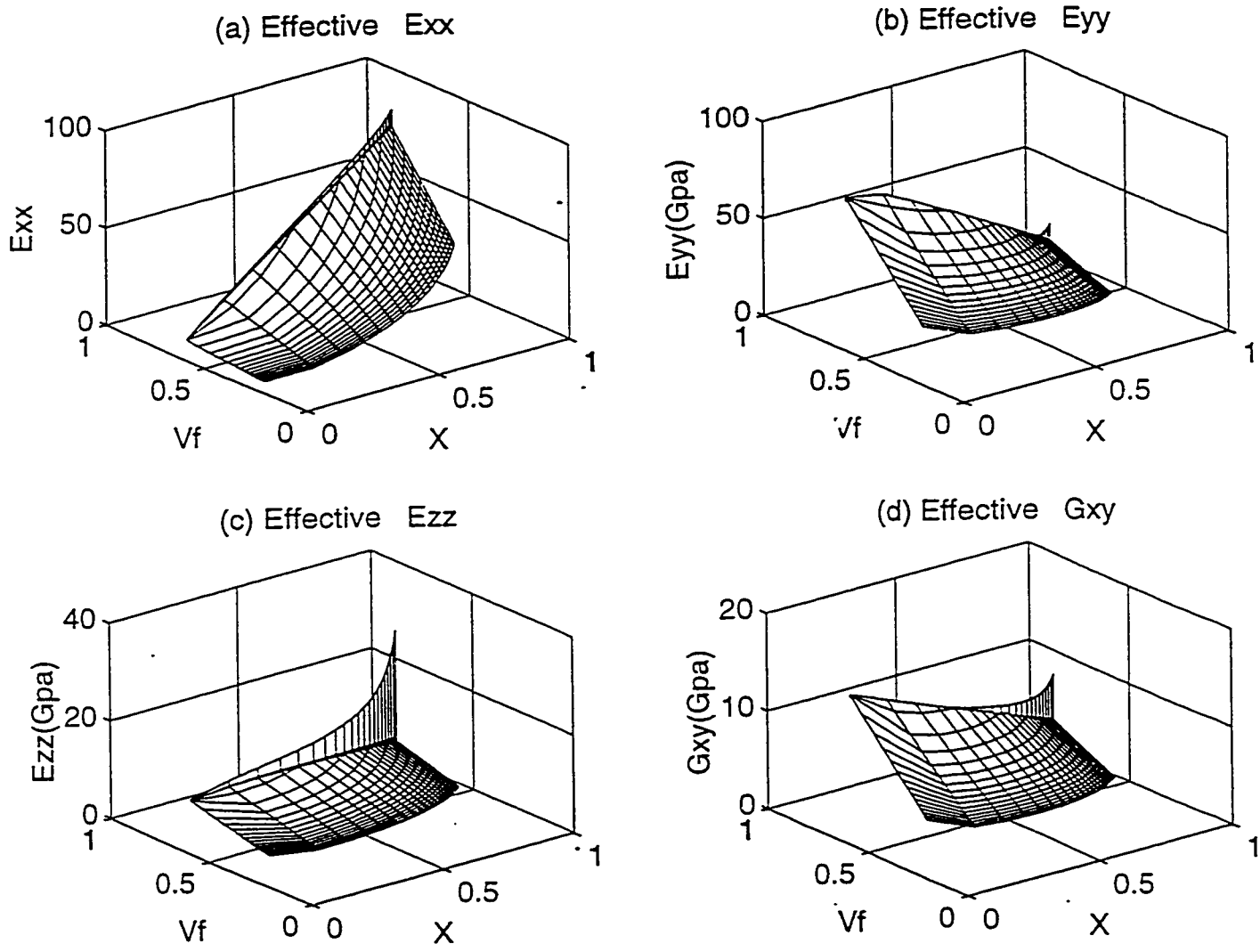

Fig 6.15 Distribution of effective *Exx, Eyy, Ezz, Gxy* with the variation of m_a, L. Choose χ as x axis, V_f as y axis.

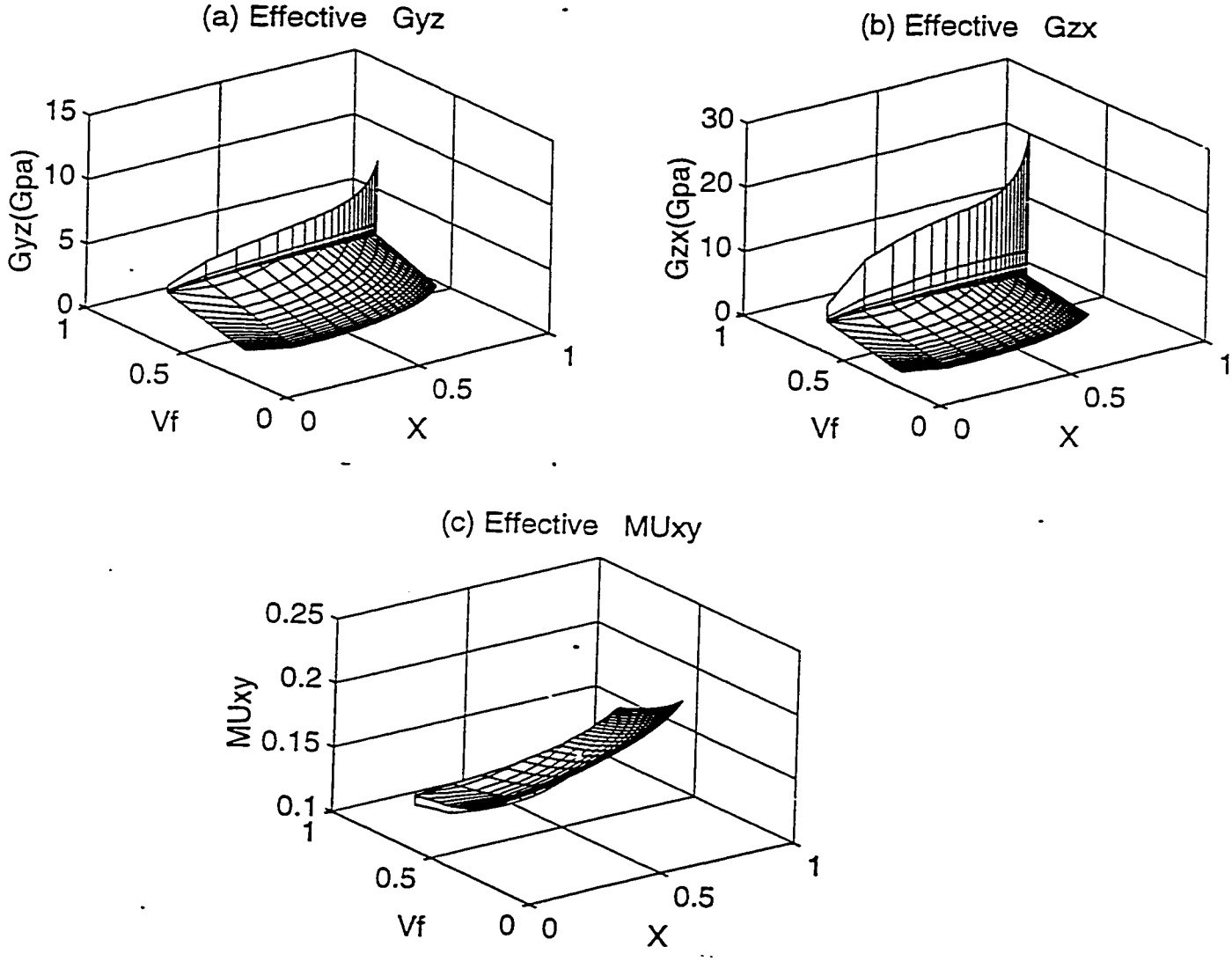

Fig 6.16 Distribution of effective *Gyz*, *Gzx*, ν_{xy} with the variation of m_a, L. Choose χ as x axis, V_f as y axis.

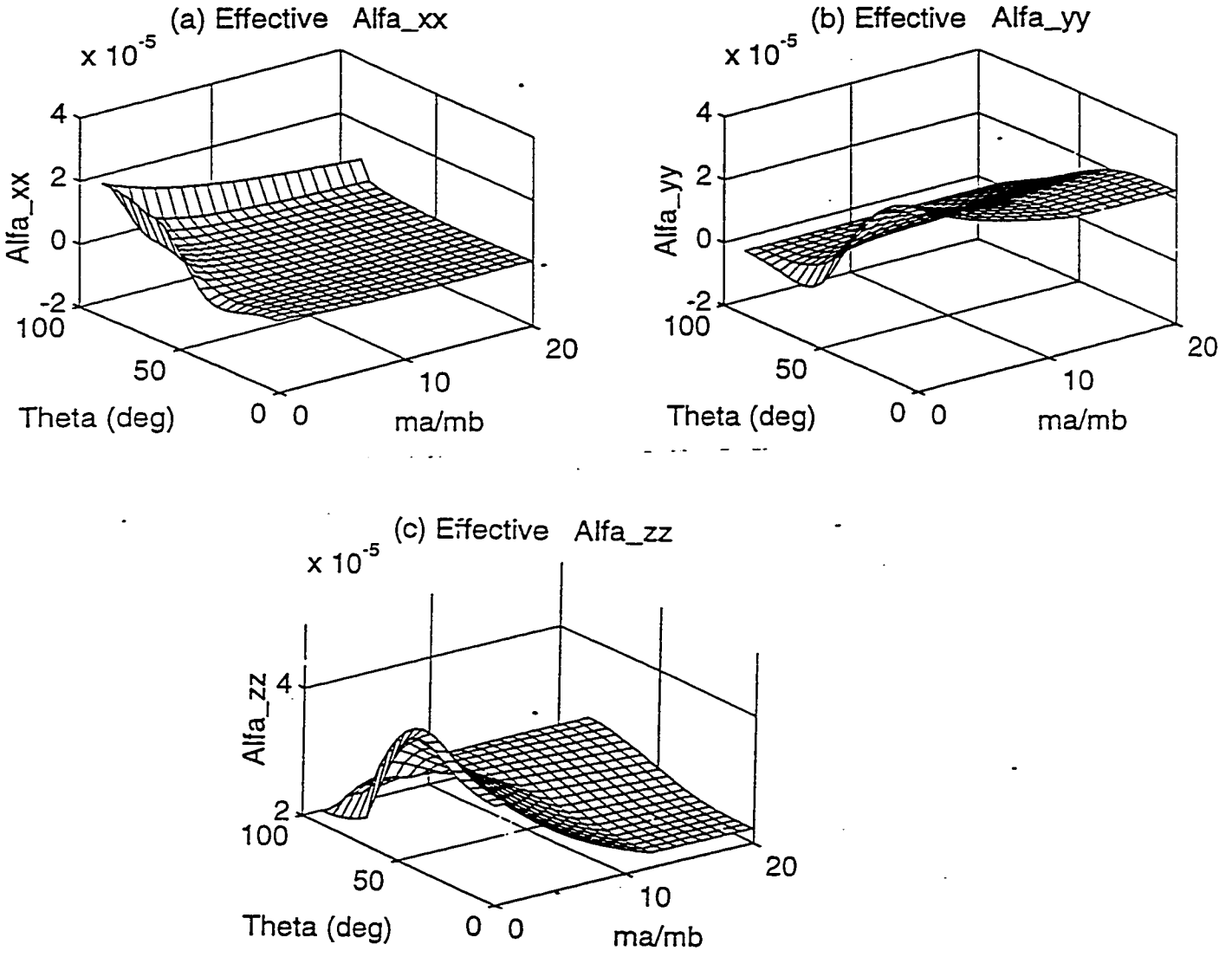

Fig 6.17 Distribution of effective coefficient of thermal expansion $\alpha_{xx}, \alpha_{yy}, \alpha_{zz}$ with the variation of θ, m_a

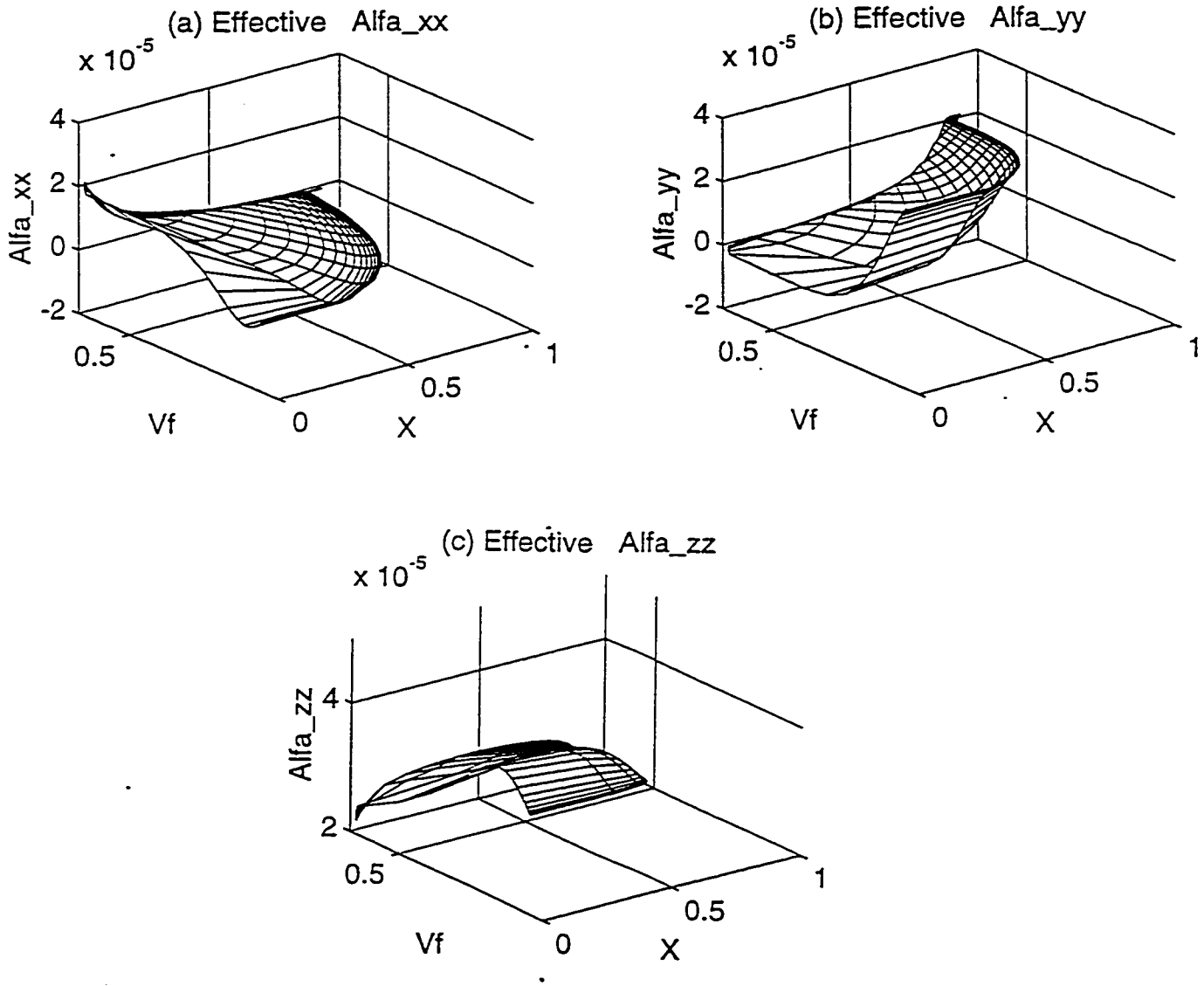

Fig 6.18 Distribution of effective coefficient of thermal expansion $\alpha_{xx}, \alpha_{yy}, \alpha_{zz}$ with the variation of θ, m_a. Choose χ as x axis, V_f as y axis.

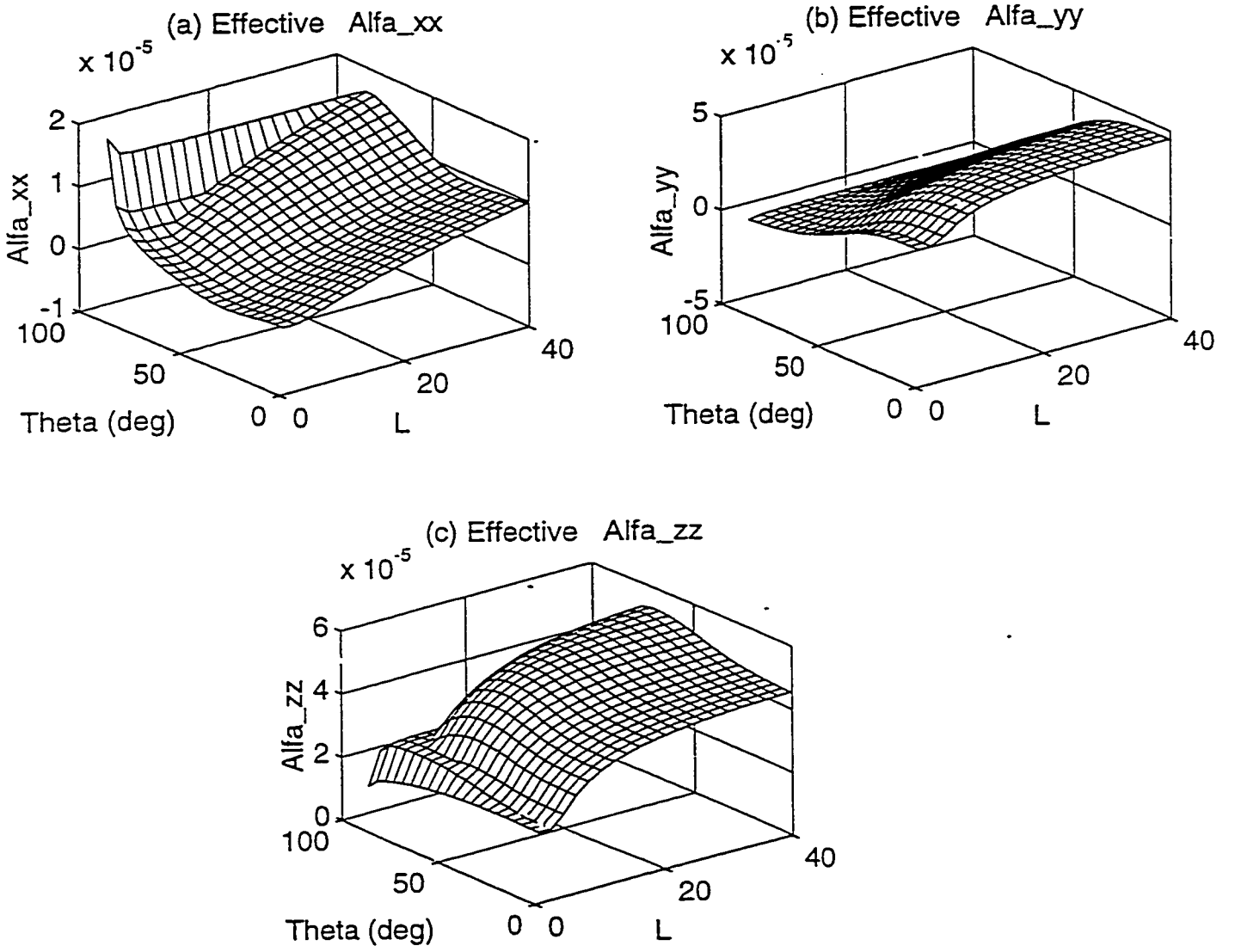

Fig 6.19 Distribution of effective coefficient of thermal expansion $\alpha_{xx}, \alpha_{yy}, \alpha_{zz}$ with the variation of θ, L.

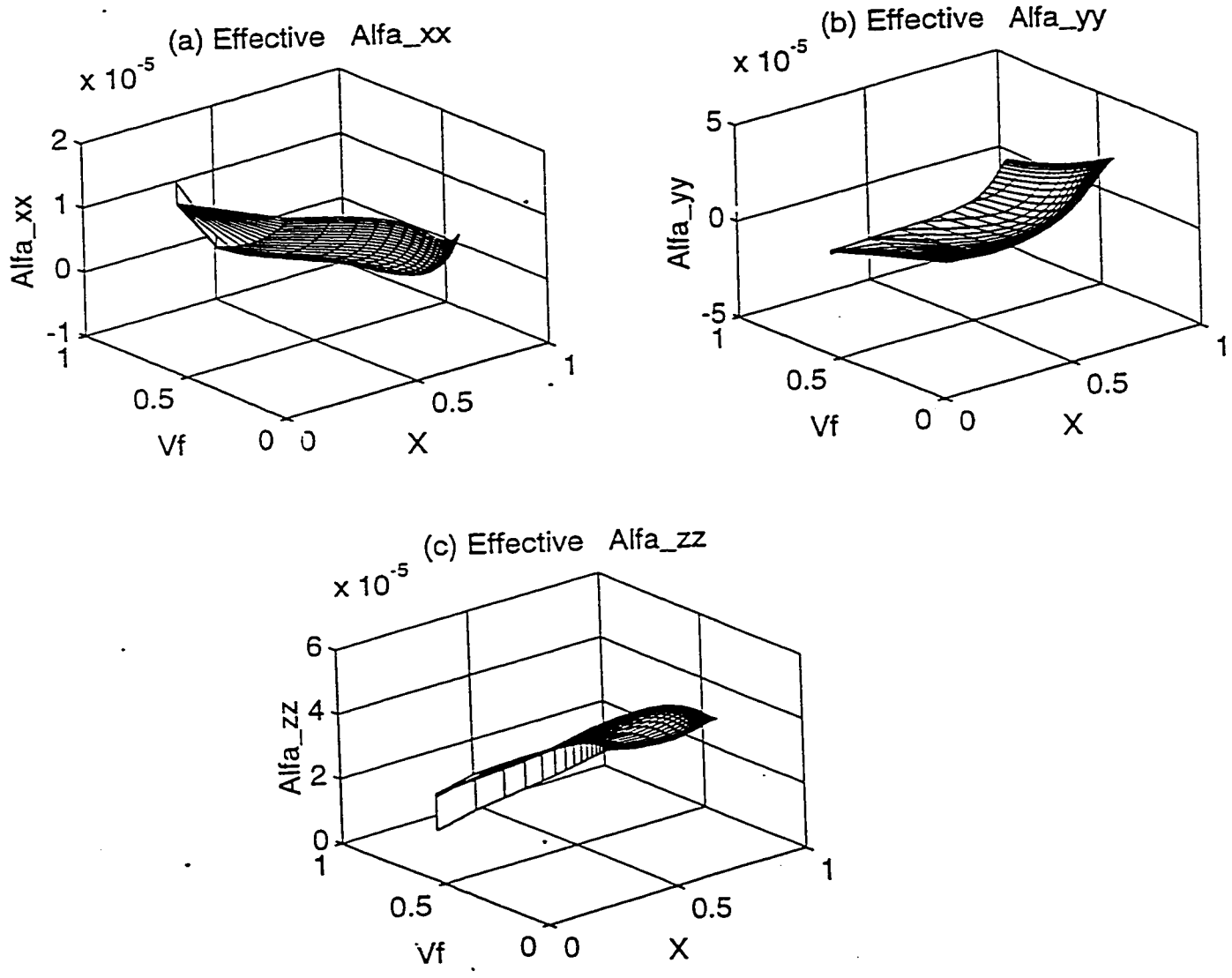

Fig 6.20 Distribution of effective coefficient of thermal expansion $\alpha_{xx}, \alpha_{yy}, \alpha_{zz}$ with the variation of θ, L. Choose χ as x axis, V_f as y axis.

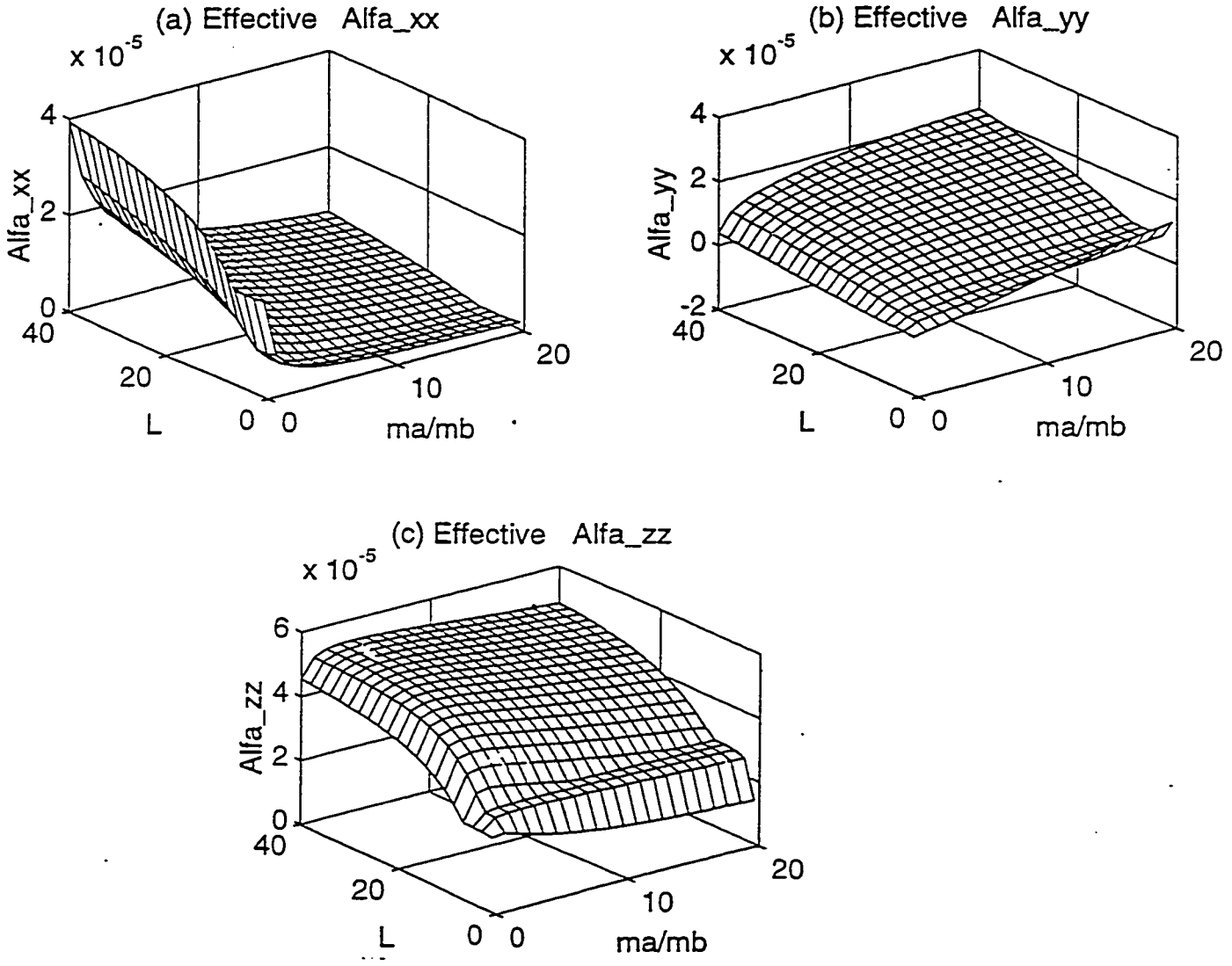

Fig 6.21 Distribution of effective coefficient of thermal expansion $\alpha_{xx}, \alpha_{yy}, \alpha_{zz}$ with the variation of m_a, L.

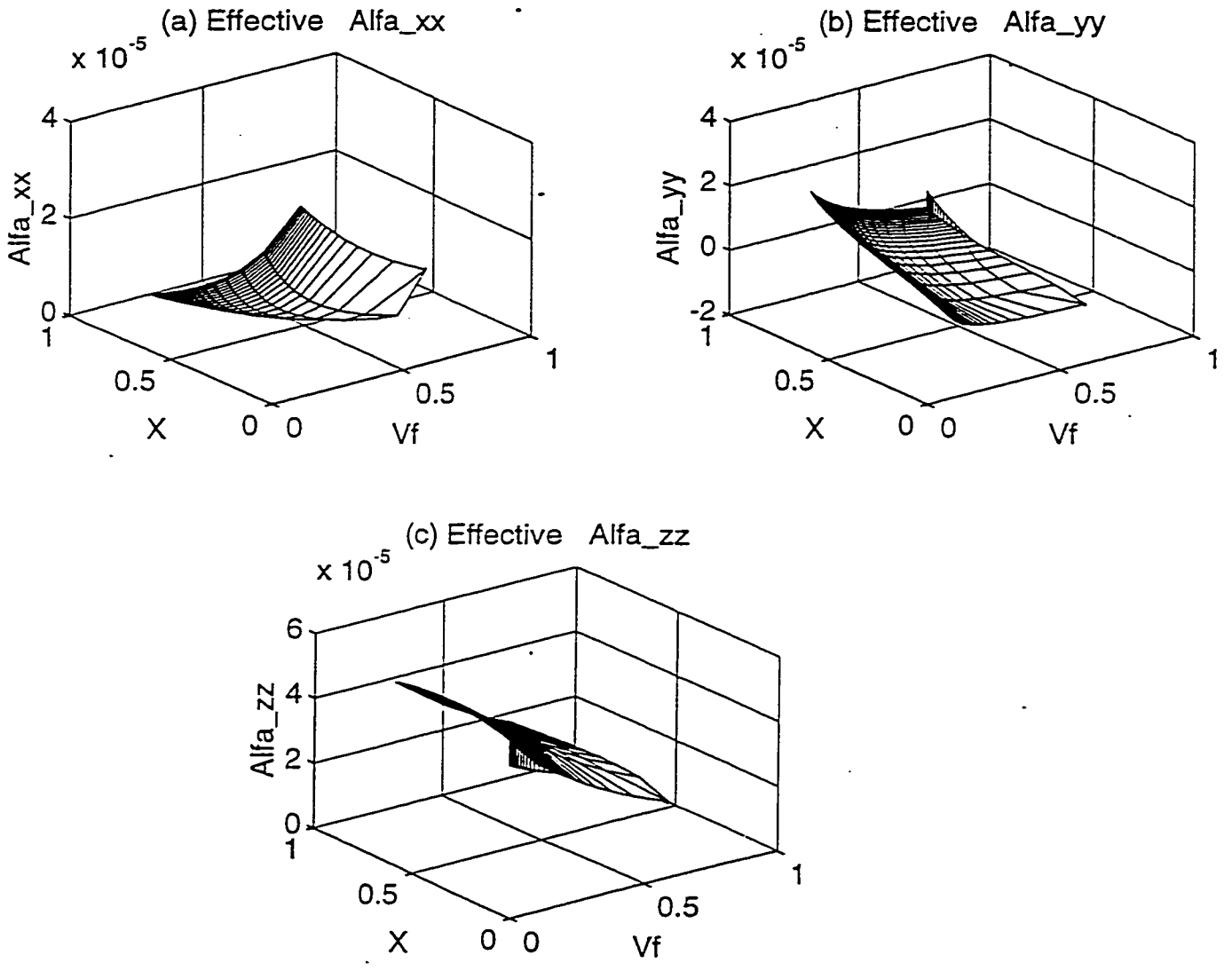

Fig 6.22 Distribution of effective coefficient of thermal expansion $\alpha_{xx}, \alpha_{yy}, \alpha_{zz}$ with the variation of m_a, L. Choose χ as x axis, V_f as y axis.

Chapter 7 Conclusion and suggestion for future work

A microstructure model of 2-D braided composite is built in this study. Fiber volume and crimp angle are evaluated by this model and are compared with experimental results. Maximum fiber volume fraction is also obtained by theoretical analysis. Effective stiffness matrix of 2-D braided composite is obtained in a close form by the analysis of elastic deformation energy in a repeat-unit-cell of braided composites. The effective stiffness consists of contributions of axial yarn, braiding yarn, and matrix material. Each of them takes a different weight in the effective stiffness. The weights of contribution of axial yarn, braiding yarn, and matrix material are $\chi V_f/k$, $(1-\chi)V_f/k$, and $(1-V_f/k)$ respectively, where V_f is the fiber volume fraction. χ is the axial yarn content in a braided composite, and k is the filament packing fraction. The results of effective stiffness from theoretical prediction are very good as compared with test data from experiments. Independent parameters in design and analysis of braided composites are successfully separated from all other parameters. This greatly reduces the difficulties of design and analysis of 2-D braided composites. Objected-oriented Matlab programs are built for the parameter analysis. The conclusions obtained from parameter analysis are as follows:

(1) Increase of braiding angle or decrease of yarn space will increase the fiber volume fraction until yarn jamming happens.

(2) Increase of braiding angle, count number of axial yarn, or decrease of yarn space will increase the crimp angle.

(3) Increase of fiber volume fraction does not always increase the effective E_{xx} and G_{xy}. If the increase of fiber volume only comes from the increase of braiding angle, the more is the fiber volume fraction the less is the effective E_{xx}.

(4) Increase of count number of axial yarn and decrease of braiding angle and yarn space will increase the effective E_{xx}.

(5) Increase of braiding angle and decrease of yarn space will increase effective E_{yy}. E_{yy} is not sensitive to the variation of the count number of axial yarn.

(6) Increase of braiding angle, the count number of axial yarn and decrease of yarn space will increase the values of E_{zz}, G_{yz}, G_{zx}.

(7) G_{xy} attains to its local maximum values when braiding angle is near 45 degrees. The lower are the yarn space and the count number of axial yarn, the higher is the local maximum.

(8) Increase of braiding angle, yarn space and decrease of the count number of axial yarn will increase the effective coefficient of thermal expansion α_{xx}.

(9) Increase of braiding angle and decrease of yarn space will decrease the effective coefficient of thermal expansion α_{yy}.

(10) α_{zz} attains to its local maximum value when the count number of axial yarn is very small and braiding angle is near 45 degrees, Increase of the count number of axial yarn and decrease of yarn space will decrease α_{zz}.

The energy approach proposed here has several advantages as compared with other theories.

(1) The equation of effective stiffness is in close form and has obviously physical meaning. Each contribution of axial yarn, braiding yarn, and matrix material can be separated clearly.

(2) The independent parameters in the design and analysis of 2-D braided composites can be separated from all other parameters. Fiber volume fraction and axial yarn content are not independent parameters. So they can not be change independently.

(3) Three dimensional diagrams of variation of effective stiffness are obtained by changing any two of the three parameters that are braiding angle, yarn space. and the count number of axial yarn.

(4) The theoretical results obtained by this energy approach are good as compared with test results .

Suggestions for future work:

(1) More theoretical and experimental research should be done to find parameters to control the thickness of braiding yarn.

In Table 3-1, the material type and the number of layers are same for the three specimen, but the thickesses of them are different.

(2) Large number of experiment should be done further to verify the distribution of effective stiffness and effective hygrothermal coefficient of expansion.

In this study, only limited experimental data from other authors are used to compare with proposed theory. That is not sufficient.

(3) Proper geometric parameters of yarn and parameters of machine should be find to obtain high quality braided preform.

We failed to braid good quality preform by using fiberglass. The reason is that the type of fiberglass and the spring force of the braiding machine are not proper.

(4) Graphic software interface should be developed to help user to design braided composite easily.

A large number of software languages can be used to build such interface. Matlab and Visual Basic are suggested here.

Reference:

[1] Avva V. S., ect., "Through-the-Thickness Tension Strength of 3-D Braided Composites", Journal of Composite Materials, Vol. 30(1) 1996, pp. 51-68.

[2] Du Guang-Wu, Tsu-Wei Chou, "Analysis of Three-Dimensional Textile Preforms for Miltidirectional Reinforcement of Composites", Journal of Materials Science 26,1996, pp. 3438-3446.

[3] Popper P. and R. F. McNNELL, US Pat. 4719837, January 1988.

[4] Weller R. D., "AYPEX: A New Method of Composite Reinforcement Braiding". 3-D Composite Materials, NASA Conference Publication 2420, November 1985.

[5] Cole P. M., US Pat. 4737 399, 1988.

[6] Li W. and A. El. Shiekh, SAMPE Q. 19(22),1922.

[7] Kostar T. D., T-W. Chou, "Process Simulation and Fabrication of Advanced Multi-Step Three- Dimensional Braided Preforms". Journal of Materials Science 29,1994. pp.2159-2167.

[8] Kostar T. D.,T-W. Chou, "Microstructural Design of Advanced Multi-Step Three-Dimensional Braided Preforms", Journal of Composite Materials, Vol. 28(13) 1994, pp. 1180-1201.

[9] Hamada Hiroyuki, et al., "CAE in Integrated Braided Composite" Science and Engineering of Composite Material", Vol. 4(2),1995, pp. 109-120.

[10] Du, G-W., et al., "Analysis and Automation of Two-Step Braiding", Fiber-Tex Conference, September 13-15,1988.

[11] Pastore, C. M. and F. K. Ko. 1988. "A processing Science model for Three - Dimensional Braiding," SAMPE Quarterly, 19(4):22-28.

[12] Camponeschi, E. T., Jr. And R.M. Crane "A model for the Fiber Geometry and Stiffness of Mutidirectional Braided Composites", Journal of Composite Materials. 11,1987, pp. 285-289.

[13] Yang, J-M, C-L. Ma and T-W. Chou, "Fiber Inclination Model of Three-Dimensional Textile Structural Composites". Journal of Composite Materials. 29,1986, pp. 472-483.

[14] HEARLE J. W. S., P. GROSBERG and S.BACKER, "Structural Mechanics of Fibers, Yarns, and Fabrics", Vol. 1(Wiley-Interscience,1969) p. 80.

[15] Master John E. and Pieere J. Minguet, "Effect of Preform Architecture on Modulus and Strength of Two - Dimensional, Triaxially Braided, Textile Composite Materials", Composite Material: Testing and Design(Twelfth Volume), ASTM STP 1274, R. B. Deo and C. R. Staff, Eds., American Society for Testing and Material. 1996, PP. 201-217.

[16] Naik Rajiv A., et al, "Effect of Fiber Architecture Parameters on Deformation Fields and Elastic Moduli of 2-D Braided Composites", Journal of Composite Materials, Vol. 28, No. 7, 1994, PP656-681.

[17] Naik Rajiv A., "Analysis of Woven and Braided Fabric-Reinforced Composites", Composite Materials: Testing and Design(Twelfth Volume), ASTM STP 1274, R. B. Deo and C. R. Saff, Eds., American Society for Testing and Materials, 1996, PP.239-263.

[18] Rosen, R. W., S. N. Chatterjee and J. J. Kibler, "An Analysis Model for Spatially Oriented Fiber Composites", Composite Materials: Testing and Design (Fourth Conference), ASTM STP 617, American Society for Testing and Materials, 1977. PP.243-254.

[19] Muskhelishvili, N. I., "Some Basic Problems of the Mathematical Theory of Elasticity", Forth, Corrected and Augmented Edition Moscow, 1954, Translated from the Russian by J. R. M. Radok, P. Noordhoff Ltd., Groningen - the Netherland, PP 15.

[20] Daniel Isaac M., Ori Ishai, "Engineering Mechanics of Composite Materials". Oxford University Press, 1994.